ENGINEERED BIOMATERIAL DRUG DELIVERY SYSTEMS FOR ENHANCED DELIVERY TO LYMPH NODES

A Dissertation
Presented to
The Academic Faculty

By

Alex Schudel

In Partial Fulfillment
Of the Requirements for the Degree
Doctor of Philosophy in Bioengineering

Georgia Institute of Technology

August 2018

ENGINEERED BIOMATERIAL DRUG DELIVERY SYSTEMS FOR ENHANCED DELIVERY TO LYMPH NODES

Approved by:

Dr. Susan N. Thomas, Advisor
School of Mechanical Engineering
Georgia Institute of Technology

Dr. M.G. Finn
School of Chemistry
Georgia Institute of Technology

Dr. Brandon Dixon
School of Mechanical Engineering
Georgia Institute of Technology

Dr. Michael Davis
Department of Biomedical Engineering
Georgia Institute of Technology

Dr. Valeria Milam
School of Materials Science
Georgia Institute of Technology

Date Approved: May 7, 2018

DEDICATION

To my undergraduate advisor, Dr. Gillis, for his guidance and direct impact on my scientific career.

To my parents, Carol and Gregg, and brother, Gary, for their enduring support all these years.

To my partner and soulmate, Emma, for everything she has done for me; I wouldn't be the man I am without her in my life.

ACKNOWLEDGEMENTS

First and foremost, I would like to thank my advisor, Dr. Susan Thomas, who has been my mentor and friend for the past six years of my life. I have absolutely loved my time in grad school and can largely attribute this to my overall experience in the Thomas lab. Susan possesses a deep understanding of scientific literature, has a compassionate, competent managerial style, and fun-loving personality, which is emulated throughout our lab culture.

Next, I would like to thank both current and past members of the Thomas lab whom I've had the distinct pleasure of working with on a daily basis and now call friends. As one of the first graduate students to join the Thomas lab, I am continually impressed with Susan's ability to recruit the highest quality students to join her lab, and can say that I have grown considerably, both intellectually and personally, due to their influences.

Finally, I would like to thank all of those that I have had the honor of directly collaborating with on the various projects I have worked on: Dr. Timothy Kassis (Dixon lab) whose infectious curiosity and steadfastness helped me through the production of my first paper; Lauren Sestito (Thomas lab) for enduring my "style" of experiments and for her partnership with me on my second paper; Dr. Cody Higginson (Finn lab) whose admirable enthusiasm for creative chemistry made for a successful collaboration; Dr. Annika Yao (Finn lab) whose unbreakable determination and ability to problem solve helped overcome the many challenges we faced on my third paper and; David Francis

(Thomas lab) for his friendship and stimulating discussions, his always-interesting points of view, and for his help and encouragement on many of my projects.

TABLE OF CONTENTS

LIST OF FIGURES

SUMMARY

State-of-the-art drug delivery currently focuses on delivery vehicle size, surface chemistry, and/or receptor interactions, all with the hope of improving drug accumulation within the tissue target. This work seeks to alter this paradigm by recognizing that tissue targets are not black boxes to which simply achieving accumulation is sufficient, but instead, complex microenvironments that house the cells that actually produce the function of the tissue and are the real targets of drug delivery. For example, while tissues critically involved in the regulation of immune processes, such as the lymphatics and lymph nodes, possess delivery barriers to getting drugs to their anatomical location, due to the complex spatial and temporal regulations of adaptive immune responses, these tissues, more importantly, possess delivery barriers to specific cells within them that must be overcome to achieve the desired immune response. The main innovation of this work, therefore, is that it addresses all drug delivery barriers, from site of injection to site of action, for the lymphatics and lymph nodes. This work has produced two novel nanoparticle-based delivery systems: one which proposes nitric oxide as a therapeutic for lymphatic-related therapies including direct delivery of nitric oxide to the lymphatics to regulate pumping function, and delivery of nitric oxide to lymph node-resident antigen presenting cells to increasing nanoparticle uptake as well as possibly promote tolerance; and the second which proposes a novel mechanism for the delivery of small molecules to deep lymph node cells for enhanced immune responses. Both of these systems while being nanoparticle-based, however, have engineered through either endogenous or synthetic chemistry the ability to release their small molecule payload, and thus are the first multi-stage lymphatic and lymph node drug delivery systems.

CHAPTER 1. Introduction

1.1 Motivation

The targeting of lymph nodes (LN), tissues where organized lymphocyte accumulation in the body occurs, has the potential to improve the treatment of a variety of pathologies, such as B and T cell malignancies as well as sentinel LN metastasis, and is the primary site of action for immunotherapeutic treatments.[1] In addition to facilitating LN targeting, delivery of therapeutic or imaging agents directly to the lymphatic endothelium is also of interest, since the lymphatics are involved in a wide variety of diseases either as the primary tissue of interest or as an accessory to the pathologies of other diseases.[2-5] Due to the integral role lymphatics play in tissue fluid regulation,[6, 7] lipid transport, and immune cell functions,[8-10] and the importance of the LN in generating adaptive immune responses,[9] there is thus, a clear need to develop a biomaterials approach to improving the efficacy of delivery of molecules within these deep tissues,[11] and to expound upon the rich cellular diversity within these tissues for eliciting more targeted immune responses.

The therapeutic efficacy of administered drug, however, is restricted by several delivery barriers that reduce drug bioavailability and lifetime of action within the target site, with deleterious off-target effects and toxicities reducing the maximum tolerable dose.[11] Immunotherapy, which is of resurgent interest due to its potential to provide benefit in the treatment of a broad array of pathologies, primarily employs clinically approved small molecules or biologic agents, and thus requires strategies that enhance the

delivery of these drugs to tissues such as lymphoid tissues, and more specifically to the immune cells important in the initiation and regulation of immune response.[12] Hence, formulation approaches that improve immunotherapeutic drug bioactivity while minimizing off-target effects and toxicities are of high interest and include novel co-formulation, targeting, and release schemes. Despite recent advances in drug formulation improving circulation times and targeting, however, efficacy is stymied by inadequate penetration into and retention within the lymphatics and LN, and there are currently no delivery strategies for providing cellular targeting that could dramatically improve drug efficacy.[11, 13]

The overall goal of this work is, therefore, to address these technological needs by rationally designing a biomaterial platform capable of delivering therapeutics to immune cells within deep tissues such as the lymphatics and LN. To this end, such an approach would possess the following characteristics: 1) be in the critical size range for lymphatic uptake; 2) be able to deliver a wide variety of therapeutic agents; and 3) employ mechanisms to be able to modulate the targeting of specific lymphoid cells and tissues. We addressed this technological need by developing a lymphatic-draining nanoparticle (NP) system designed with either a physiological or engineered cargo release mechanism to deliver nitric oxide (NO) or immunotherapeutics, respectively, to LN-resident cells. Through the use of these multi-stage systems we have demonstrated that we can design for both improved tissue delivery as well as increased cellular access, and showed *in vivo* that multi-stage NP-based delivery produced both potent local tissue and systemic immune responses.

1.2 Specific Aims

1.2.1 Specific Aim 1: S-nitrosated poly(propylene sulfide) NP for enhanced NO delivery to lymphatic tissues.

The *working hypothesis* was that poly(propylene sulfide) NP are uniquely suited for creating a lymphatic/lymph node targeting NO-donor NP (SNO-NP) because they hold several advantages over existing NO donors: 1) by virtue of their unique size properties, the SNO-NP have significantly enhanced lymphatic uptake efficiency; 2) they are based on a chemistry that is physiologically compatible and bioavailable; and 3) they preserve the drug delivery benefits of micelle technology to enable precise and controlled delivery of encapsulated NO. Through the use of an *ex vivo* lymphatic-resident filarial worm model and an *in vivo* mouse lymphatic transport model, we were able to assess the biological activity and cellular distribution of these SNO-NP. We demonstrated the synthesis and modification of NP with NO in order to harness the physiological S-nitrosothiol chemistry for NO delivery and bioactivity. These SNO-NP stably encapsulated high levels of NO and facilitated its controlled release. In particular, we demonstrated that the bioactive form of released NO from SNO-NP, either NO_2^- or SNO-cysteine, depended on the ratio of free cysteine (CYS), a common endogenous low molecular weight thiol important in transnitrosation reactions, to SNO-NP. Furthermore, we demonstrated the cytotoxic activity of SNO-NP against lymphatic-resident *B. malayi* adult female filarial worms, for which there is no existing treatment. *In vivo* we showed that donation of NO from SNO-NP, which scaled in proportion to the total administered dose, enhanced LN accumulation by two orders of magnitude, compared to standard small molecule NO donor, without substantially reducing the lymphatic transport of NP or the viability and extent of NP uptake by LN-resident cells. Additionally, NO delivery

by SNO-NP was accompanied by low-to-negligible NO accumulation in systemic tissues with no apparent inflammation. These results suggest the utility and selectivity of SNO-NP for the targeted treatment of NO-regulated diseases that afflict lymphatic tissues.

1.2.2 Specific Aim 2: Multi-stage lymphatic-targeting NP delivery system augments lymphoma immunotherapy.

The *working hypothesis* was that despite nanoformulations of an intermediate nanoscale size being ideal for lymphatic partitioning and LN accumulation after injection in the periphery, small molecules have increased potential to penetrate deeply within the LN cortex, therefore a controlled release strategy of co-formulated drug could be utilized to optimally target LN-resident cells via enhanced drug penetration. By conjugating our drug cargo to our lymphatic-targeting NP with oxanorbornadiene (OND) linkers, which undergo retro-Diels Alder fragmentation to release cargo with predefined half-lives, we demonstrated a versatile lymphatic-targeting NP system that was able to precisely tune the release profile of conjugated cargo within the lymphatic tissues. Through the use of *in vivo* lymphatic-transport and mouse tumor models we were able to assess the improvement in LN-resident cell targeting and immunotherapeutic response elicited by releasing small molecule cargo from lymphatic-draining NP. Using confocal imaging and flow cytometry we showed increased accumulation of released cargo and access to deep LN-resident cells. We were able to conjugate the TLR9 ligand CpG through our OND linkage to lymphatic-draining NP and demonstrated that these OND-CpG-NP dramatically altered the abundance and type of lymphocytes within the treated LN, producing a large increase in total lymphocytes and a greater maturation of resident antigen presenting cells (APCs). We further demonstrated that this delivery strategy afforded a substantial immunotherapeutic response shown by a dramatic reduction in LN

tumor size compared to other CpG delivery strategies, and a slowing of primary tumor growth. These results suggest the utility of the multi-stage OND-NP approach for the delivery of immunotherapeutics to LN-resident cells for the treatment of LN and primary tumors.

1.3 Significance

The work presented herein provides innovation in carrier design by improving the penetration of delivered agents deeply to within healthy and diseased tissues, as well as to tissue targets of emerging interest for their diagnostic and therapeutic utility – lymphatic vessels and the LN to which they drain. First, this work is important because it identifies NO as a therapeutic of particular interest for the treatment of lymphatic-related diseases, and has resulted in a novel NP-based delivery system that is able to enhance the delivery of NO to lymphatics and LN-resident cells; something that to our knowledge no other NP system or NO donor described to date can accomplish. Second, this work has refocused LN drug delivery to the cells within the LN instead of the tissue itself through the use of a multi-stage NP-based delivery system; something that to our knowledge has never been attempted for LN drug delivery. Overall, the significance of this work is the idea that accumulation within tissues such as the lymphatics and LNs is not a sufficient metric, instead, drug delivery design should take into account the spatial, temporal, and cellular regulation of the processes within the tissue targets that are trying to be achieved.

Specific Aim 1. Diseases involving lymphatic tissues range from infectious and cardiovascular diseases to cancer and are estimated to afflict more than 40 million people worldwide. NO is a therapeutic implicated for the treatment of these diseases, however existing technologies available for NO therapy provide poor bioactivity within lymphatic

tissues. Our platform, SNO-NP, provides a solution to this significant technology gap by enabling facile delivery of NO to lymphatic tissues through an innovative NP formulation that encapsulates high levels of NO for its controlled release. Advantages of this technology for therapeutic applications in lymphatic tissue targeting include: a >100-fold increase in drug exposure in LN relative to small molecule NO donors to dramatically improve drug bioactivity; improved lymphatic tissue targeting to facilitate dose sparing and reduction of off-target side effects with minimal systemic and local inflammation; encapsulation of high per NP levels of NO, far surpassing those of existing NO donors; and biological activity of delivered NO including cytotoxicity against lymphatic-resident filarial worms. Furthermore, the ease of NP synthesis and NO loading, formulation stability, and composition make this technology highly amenable for therapeutic use.

Specific Aim 2. Since LN are bathed in lymph drained from the periphery in a steady state fashion, design principles optimizing drug targeting for penetration through the interstitium and lymphatics to reach lymph using more conventional and less intrusive drug administration techniques, such as subcutaneous injection, are attractive for LN delivery. However, within the LN, solutes and particulates are filtered based on size, with smaller molecules penetrating more deeply into LN cortex than large particulates by virtue of uptake within LN conduits. Drug and macromolecular formulation therefore have the potential to play a significant role in regulating the distribution within the LN as a function of macromolecular size. To achieve localized delivery to LN-resident cells for immunotherapeutic responses, we have created a NP system that combines lymphatic-targeting NP with time-released cargo linker optimized to increase accumulation and access to deep LN-resident cells, as well as improve immunotherapeutic responses

against LN and primary tumors. Advantages of this system include: a >100-fold increase in T and B cell targeting relative to conventional drug delivery; improved immunotherapeutic efficacy requiring lower doses of potent adjuvants with minimal potential for systemic off-target effects; multi-valency that allows for unique co-formulation delivery; and a tunable release mechanism for altering cargo release profiles that has the potential to tune the cell types targeted within the LN.

CHAPTER 2. Background and Literature Review

2.1 Introduction

Drug efficacy after administration is restricted by its capacity to appreciably accumulate at the desired site of action at bioactive doses in order to mediate its effect(s).[11] The concept of drug targeting to enhance therapeutic benefit and minimize toxicities largely brings to mind the directed retention of drugs or imaging agents at and within cells and tissues of interest using affinity-based molecular interactions or, in the case of solid tumors, exploiting the leaky vasculature to facilitate their preferential accumulation. Hence, as in these situations, formulation approaches that improve lymphatic and LN drug bioactivity while minimizing systemic delivery are of high interest.[13] This background will discuss the relevant concepts pertinent to drug delivery to the lymphatics and LN, how formulation design and delivery schemes have facilitated advances in effective targeting and improved immunological outcomes for a variety of lymphatic/LN-related therapeutic purposes, explore novel treatment strategies for lymphatic/LN-related diseases, and discuss what challenges and opportunities remain.

2.2 Drug Delivery for Lymphatics

2.2.1 Lymphatic physiology

Within the interstitium, which constitutes the extracellular space, solutes, matrix, and space between cells, exchange of solutes between the capillary plexus and the cells occurs. Due to differences in oncotic pressure between the arterial and venous sides of the capillary plexus as a result of permanent protein extravasation, not all of the fluid

makes its way back to the venous side, resulting in a putative net loss of up to 10% of circulation volume.[6] This volume loss would result in fluid accumulation if not for the lymphatic system, which drains the excess fluid and returns it to the circulation. Unlike the circulatory system, which contains a central pump, the lymphatics operate on a more local level. Within the interstitium, fluid uptake and transport by the initial lymphatics is thought to be driven by expansion and compression of the initial lymphatics, with expansion resulting in percolation of the interstitial fluid through the endothelial microvalves, resulting in filling of the initial lymphatics, which then get compressed by the surrounding tissue, sending the lymph out in the direction of the large collecting lymphatics.[14] The initial lymphatics are blind-ended and composed of non-fenestrated overlapped endothelial cells with anchoring filaments to the surrounding extracellular matrix in order to provide mechanical support against the low pressure inside the initial lymphatic vessel lumen.[15] Because of the relatively large fluid reabsorption rate difference between the vascular capillaries and the lymphatic, only a certain size range of molecules is preferentially taken up by the lymphatics,[16] which has major ramifications on drug formulation and delivery to the lymphatics following intradermal injection and will be discussed in more detail later.[11] Following initial lymphatic uptake the interstitial fluid moves to larger collecting lymphatics where it is termed lymph. Within the collecting lymphatic vessels, the lymph is propelled by a synchronized movement of lymphatic vessel compartments called lymphangions, which contain one-way valves to propel the lymph in a unidirectional manner. Surrounding the lymphatic vessels are a series of lymphatic smooth muscle cells which contract autonomically, squeezing the

lymphangions and propelling the lymph through the vessels, and eventually through the LN before returning the collected fluid to circulation.[6]

While the main function of the lymphatics is the transport of interstitial fluid from the extracellular space to the circulation, the lymphatics are also involved in other important processes including facilitating immune cell homing and immune responses due to their distribution of fluid to the LN.[17] However, stagnation of lymph flow has been shown to disrupt these processes, making lymphatic pumping of lymph one of the lymphatics' most critical functions.[7] Furthermore, the loss of pumping function can lead to pathologies such as edema, characterized by accumulation of fluid within the interstitial space. Consequently, the restoration of pumping function is an important aspect of lymphatic therapy relevant to many pathologies including myocardial infarction[18] and parasitic infection,[19] where expansion of the accumulating fluid causes damage to the surrounding tissue.

2.2.2 Lymphatic diseases and current treatments

Due to the integral role the lymphatics play in tissue fluid regulation,[6] lipid transport,[7] and immune cell functions,[8] the lymphatics are involved in a wide variety of diseases either as the primary tissue of interest, such as with lymphedema[2] or lymphatic filariasis,[3] or as an accessory to the pathologies of other diseases, such as with myocardial infarction[4, 5] and cancer.[10] The combined effect of all diseases in which the lymphatics are directly affected is staggering at an estimated 40M worldwide.[20, 21] Despite the high prevalence of lymphatic-associated diseases, treatment methods, especially for diseases where the lymphatics are the primary tissue of interest, remain stagnated or in some cases non-existent. As one example, the current

gold standard for the treatment of lymphatic filariasis, an infection of the lymphatics by parasitic worms, is the use of antibiotic cocktails that are administered systemically and do not result in appreciable drug accumulation within the lymphatics where the worms reside.[3] Moreover, lymphedema, one of the resulting diseases of lymphatic filariasis and sentinel LN removal following breast tumor resection, only employs a combination of compression and physical therapy.[22] For diseases where the lymphatics are not the primary target but are critically involved in the disease pathology or may be useful therapeutically, there exist few approved treatments that are specifically formulated to target the lymphatics, producing a range of undesired consequences from increased toxicity as a result of higher dosing to inefficient immune responses such as inhibited antigen uptake.[13] Thus, there is a clear need to develop effective therapies that specifically target the lymphatics and restore lymphatic function.

2.2.3 Role of NO in lymphatic function

NO is an extremely promiscuous biological molecule that takes part in a variety of physiological processes ranging from vasodilation, to neural signaling, to immune cell cytotoxic defenses. This small, semi-hydrophobic nonelectrolyte diffuses rapidly, accumulating preferentially in the lipid phases of cells.[23] Similar to blood vessel physiology, the vessels of the lymphatics are sensitive to shear stress and dilate accordingly to compensate for changes in lymph flow.[24, 25] NO is the signaling molecule responsible for facilitating this dilation.[26, 27] Under increased shear rates membrane-bound inducible nitric oxide synthase (iNOS) becomes activated and produces NO,[28] which can diffuse both apically towards the vessel lumen, or basally toward the underlying smooth muscle cells.[29] Once in the smooth muscle cell NO interacts with

cyclic guanosine monophosphate (cGMP) initiating a process that results in the sequestration of calcium, depriving the muscle cell of the ability to contract, and thus allowing the vessel to dilate.[30] However, the lymphatics are very sensitive to NO concentration[31] with several lymphatic-related disease symptoms/causes being alterations in lymphatic pumping function including lymphedema, which has been known to have aberrant NO concentrations.[32] Therefore, the putative therapeutic solution to restoring lymphatic pumping function in these diseases is to restore the signaling levels of NO to overcome whatever disease-induced adulteration of NO signaling has occurred.

2.2.4 Clinical therapies for NO modulation

Because of the important role that NO plays in multiple physiological processes, including neurotransmission,[33] vascular regulation,[34] immune response,[35] and cytotoxicity,[36] there have been many attempts at modulating NO for therapeutic purposes. For example, NO delivered in the form of nitrate is used to control pain from angina, a disease affecting 9 million people in the US with 500,000 new cases every year, and has been found to annually cost the healthcare system around $1.9 billion.[37] NO has also been investigated in several clinical trials for use with other cardiovascular treatments to control blood pressure in adults with prehypertension,[38, 39] which affects 25-50% of adults worldwide,[40] and to improve the function of the heart following heart transplant or left ventricular assist device placement.[41] For pulmonary diseases NO is inhaled in its gaseous form, and is the current standard of care for persistent pulmonary hypertension in newborns, which affects 1.9 per 1000 live births.[42] NO has also been explored for the treatment of various cancers, including lymphoma where a variety of NO

donors have been shown to be chemosensitizers[43-45] as well as exhibit direct cytotoxicity.[45-49]

2.2.5 Molecular carriers of nitric oxide: NO donors

NO donors are molecular carriers of NO. While much research has gone into NO donors for therapeutic potential, only two types of NO donor are used clinically: organic nitrates and diazeniumdiolates (NONOates).[50] Despite the exclusiveness of these two types of NO donors, there exists other promising NO donor candidates, including the endogenous S-nitrosothiols. Endogenous S-nitrosothiols (R-SNO), which include S-nitrosocysteine, S-nitroso-albumin, and S-nitrosoglutathione (GSNO) represent a major class of NO-nucleophile adducts that facilitate NO's transport *in vivo*.[51-53] R-SNO are formed on free thiols either through reactions with nitrosating agents[54] or by transnitrosation (i.e., by transfer of NO from other nitrosothiols),[55, 56] giving R-SNO the ability to be formed under a wide range of (patho)physiological conditions.[57] Therefore, R-SNO represent an attractive and physiological NO chemistry that has been exploited to harness both native NO signalling and transport activity in biological systems.[50]

2.2.6 Lymphatic-targeting drug delivery strategies

Despite the versatility of NO as a potential therapeutic in a broad array of pathologies, several challenges exist with utilizing NO for lymphatic-related therapy. First, NO participates in many interrelated physiological processes that each have different requirements for NO signalling.[29, 58, 59] In some cases depletion or attenuation of NO signalling may produce negative effects such as in vascular regulation,[60] whereas in the case of inflammatory responses overproduction of NO can

lead to loss of lymphatic function.[31] Consequently, a lymphatic-targeted NO-based therapy would need to be tightly controllable, since NO levels vary significantly across physiological processes, pathologies, and locations.[24, 25, 28, 29, 61] Combined with the extremely short half-life[62, 63] of NO requiring it to mediate its action near its synthesis source,[62] targeted NO donation remains highly difficult.

The second challenge to delivering NO, especially in the context of lymphatic-related therapies, is the result of lymphatic delivery barriers.[9, 11] Due to the physiology of the lymphatic system, typical intravenously administered molecules do not result in appreciable delivery to lymphatics, with a considerable portion of administered agent accumulating instead in the lung, kidney, and liver. As a result, direct injection techniques are typically utilized for lymphatic targeted delivery strategies.[10, 64] Predominantly macromolecular size aspects of the connective tissue physiology govern the feasibility of lymphatic and lymph delivery (Figure 2.1) despite the influence of interstitial flow on transporting injected agent into the draining lymphatics. Since non-fenestrated blood capillaries are permeable to molecular species less than 5 nm in hydrodynamic diameter,[65] they are rapidly cleared after injection,[66] reducing their potential for lymphatic exposure. Conversely, since the pore size of the extracellular matrix (ECM) limits the movement of macromolecular species through the interstitium, infused nanoformulations ~100 nm or larger become entrapped[67] and are too poorly suited to lymphatic-targeted drug delivery applications (Figure 2.1). Therefore species roughly 5 nm or larger, but smaller than 100 nm, are largely impermeable to the blood capillaries within healthy tissues[65] and can only be efficiently cleared by lymphatic drainage mechanisms. Lymphatic targeting is therefore optimized by agents or

formulations roughly tens of nanometers in hydrodynamic diameter, including the synthetic formulations ~30 nm Pluronic-stabilized poly(propylene sulfide) NP[67] used in this work.

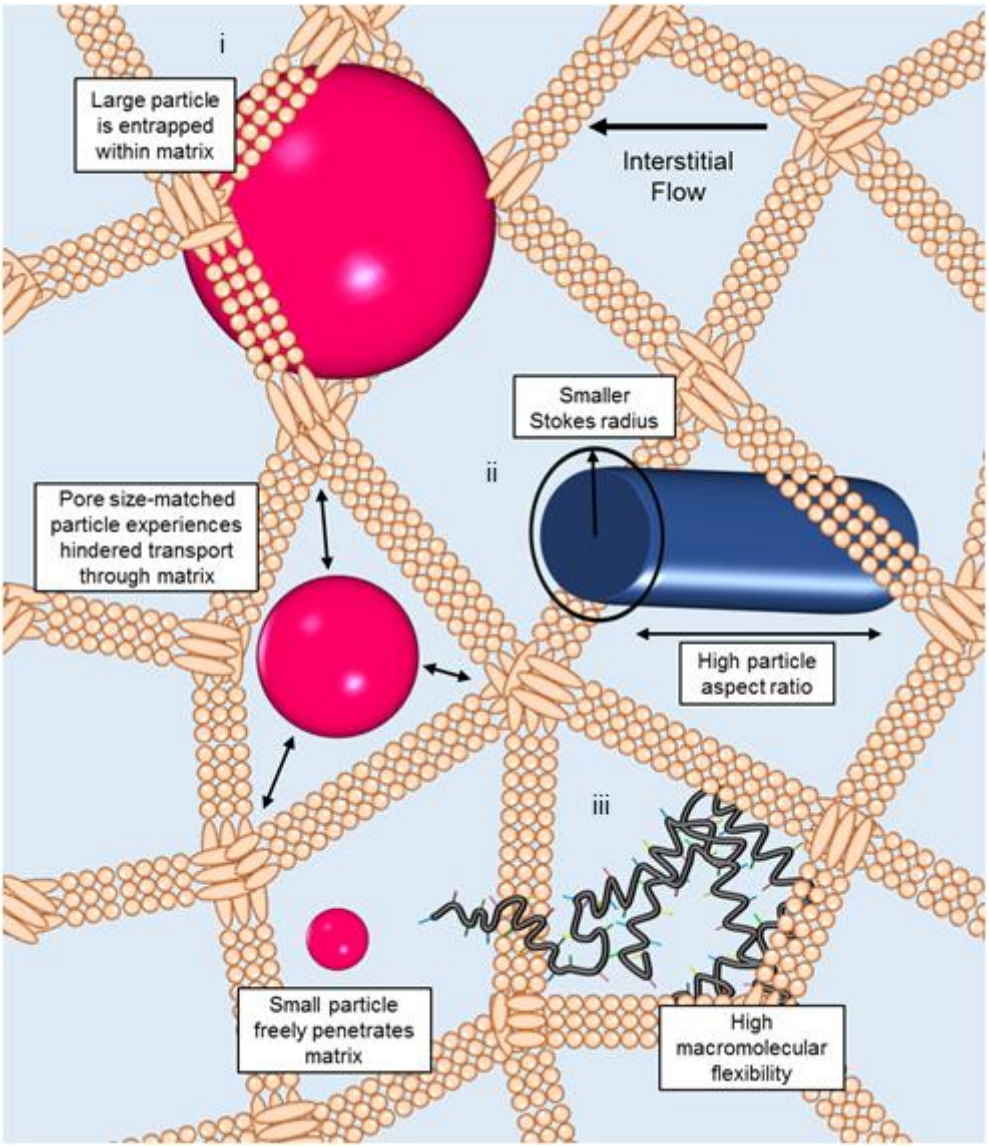

Figure 2.1: Within the interstitium under the influence of slow interstitial fluid flow, macromolecular transport is restricted by the ECM. (i) Large (>70 kDa) but not small molecular species become entrapped by the gel-like ECM.[64] At similar hydrodynamic radii, penetration through the ECM is increased by (ii) high particle aspect ratios, which correspond to a smaller Stokes radius along one carrier dimension,[68] and (iii) flexibility of the macromolecular assembly, such as that exhibited by biopolymers.[11, 67]

In addition to achieving lymph accumulation via transluminal transport, and perhaps most importantly for NO therapy, delivery of agents directly to the lymphatic endothelium is of interest. NO is known to cause dilatory responses in lymphatic vessels, despite the fact that areas of increased NO concentration such as the lymphatic valves[24, 28] have been found, there is no quantitative understanding about how NO signalling levels impact lymphatic pumping function. This has important ramifications for lymphatic targeting since physiological NO levels are required to maintain basal lymphatic functionality,[26] whereas infra[27] and supra-physiological[31] levels of NO, as are seen in many disease states, impede lymphatic contractility and pump function.

2.2.7 Drug delivery vehicles for NO modulation

Given the importance of the lymphatics as a tissue target and the pronounced effect NO has on lymphatic function, modulation of NO within lymphatics offers a promising means of restoring endogenous NO signalling and alleviating lymphatic deficiencies that contribute to many diseases. Drug delivery systems offer a promising solution; they encompass a wide variety of carriers composed primarily of lipids and/or polymers, and serve the purpose of altering the pharmacokinetics and biodistribution of their associated small molecule drug (Figure 2.2, upper left). There has been expansive research into novel formulations of drug delivery vehicles including: synthetic micelles, dendrimers, NP, microspheres, liposomes, etc.[66, 69, 70] While each carrier has its advantages and has found use for specific applications and/or targets, drug delivery vehicles in general all work by increasing the molecular weight of the delivered drug;[71] this results in a reduction of the clearance rate by the reticuloendothelial system and an increase in

circulation time. In order to utilize NO-modulation for lymphatic therapy, formulation of NO donors into a lymphatic specific carrier is required.

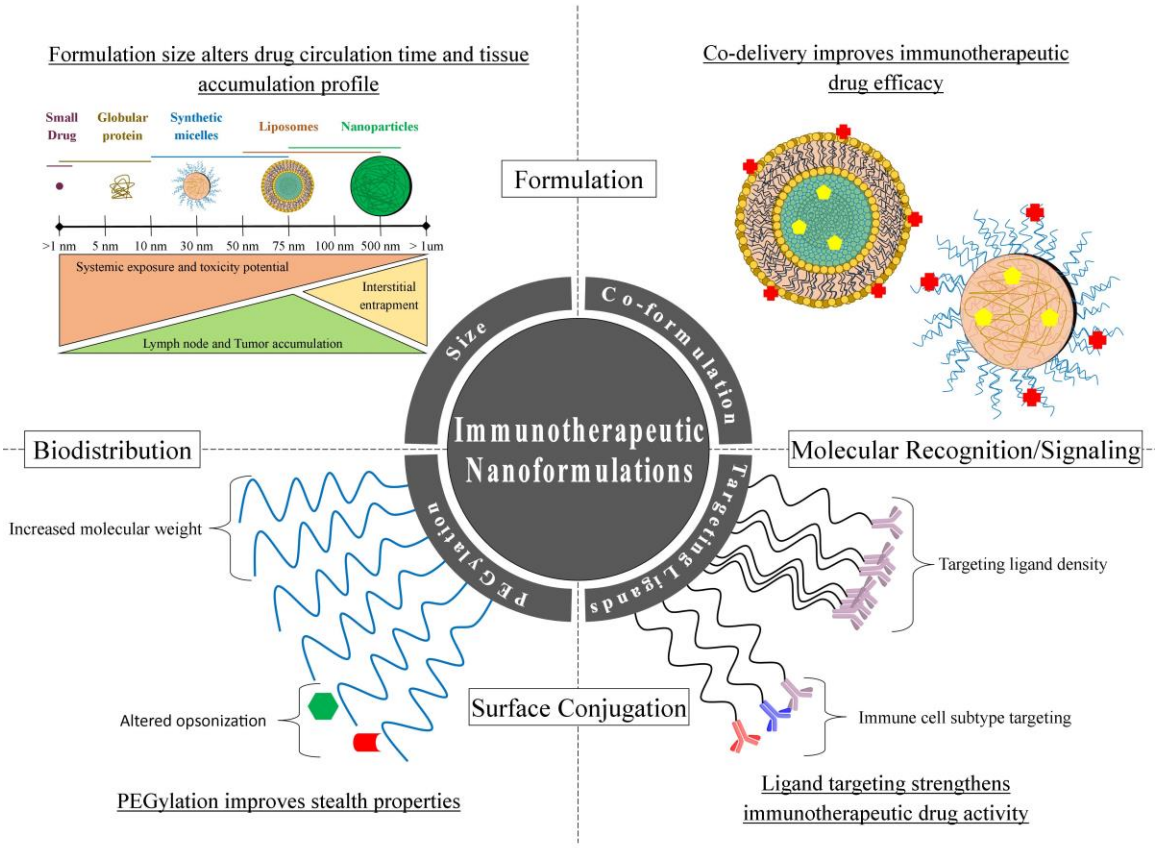

Figure 2.2: Schematic diagram of nanoformulations that improve immunotherapeutic drug efficacy. Top left: nanoformulations that increase the effective hydrodynamic size of drugs improve their circulation times by resisting glomerular filtration, enhance tumor accumulation by the enhanced permeability and retention effect, and may promote lymphatic uptake from the interstitium. Top right: co-delivery via co-formulation improves the synergistic signaling activity of multiple immunotherapeutic agents, for example, antigen and adjuvant in vaccine applications. Bottom left: PEGylation increases the effective hydrodynamic size and stealth properties of nanoformulations to increase drug half-life after infusion. Bottom right: ligand targeting can increase uptake by immune cells in a density-dependent fashion. PEG poly(ethylene glycol).[71]

While there have been several examples of reformulation of NO donors to achieve improved pharmacokinetics and biodistribution including improving circulation time

through polyethylene glycol (PEG) conjugation[72] and NO bioactivity through multi-valency,[73] there have been no attempts to create a NO donor specifically for targeting lymphatics.[74] Several examples exist of larger molecular weight NO donors including a 64-valency R-SNO dendrimer donor[73] and NO-containing NP;[75-79] however, all of these approaches remain insufficient for NO-modulation within the lymphatics because such formulations are non-optimized for lymphatic uptake.[74]

2.3 LN drug delivery strategies

2.3.1 LN physiology and its role in adaptive immune responses

LN are lymphoid tissues comprised primarily of immune cells with a supporting stroma whose primary function is to facilitate contact between lymphocytes in the mounting of adaptive immune reactions. They are thus central targets in immunotherapy applications, such as vaccines[80] or immune suppressive regimens.[81] Most primary adaptive immune responses against peripheral pathogens are initiated in the T cell area of the LN, therefore how the mechanisms involved in the antigen presentation between dendritic cells (DCs) and T cells depend on LN structure are important to LN drug delivery. Antigen presentation to T cells is thought to occur via two distinct mechanisms (Figure 2.3). The first pathway is well characterized and involves the migration of peripheral DCs that acquired peripheral antigen and then trafficked through the afferent lymphatics into the T cell areas of the draining LN (Figure 2.3).[82] The second pathway of antigen presentation is most often the target of drug delivery strategies and functions independently of the cellular-mediated pathway. This second pathway involves the acquisition, presentation, and cross-presentation of soluble antigen that transports passively from the periphery to the LN-resident DCs that then initiate T cell activation

(Figure 2.3).[82] These putative distinct “waves” of antigen presentation – cellular trafficking vs. soluble draining – are thought to induce functionally different T cell responses due to both their differences in timing as well as potency of DC activation.[82] In fact, regarding CD4 T cell responses, peptide:MHC II presentation by LN-resident DCs, especially lymphatic-sinus lining DCs, was shown to rapidly and sufficiently induce many aspects of T cell activation including IL-2 receptor expression and proliferation, indicating that soluble antigen transport to the LN is an important step in T cell activation, despite the requirement for the arrival of more potent antigen presenting peripheral DCs in order to induce a longer lasting and more potent CD4 T cell response.[82, 83] Likewise, for CD8 T cell responses, it has been shown that conduit-lining DCs can directly sample antigen from the conduits, resulting in earlier T cell activation independent of peripheral DCs migrating several days later. Therefore, the mechanism by which soluble transport of peripheral antigen reaches and distributes to the cells within the LNs is of high importance for the generation of adaptive immune responses.

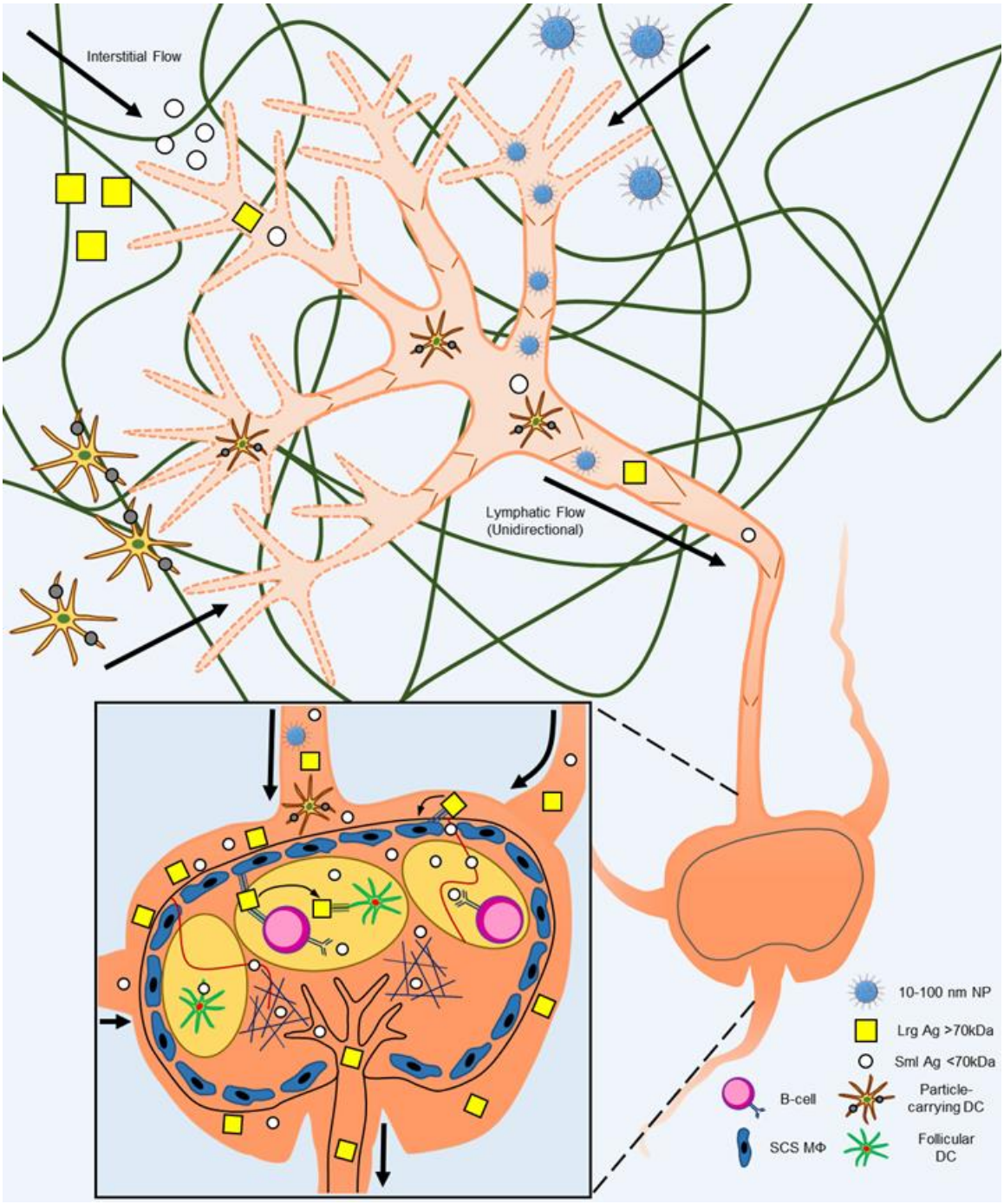

Figure 2.3: Principles of LN targeting including the major transport barriers of the interstitium and the LN subcapsular sinus. Antigen presenting cells such as DC take up large particles (particle-carrying DC) and actively migrate to LN. Synthetic carriers such as NP 10–100 nm in diameter (optimum for penetration of the interstitial extracellular matrix) as well as protein antigens are carried from the interstitium by interstitial and lymphatic flows to draining LN. Lymph-borne solutes are distributed within LN in a size dependent fashion. For example, large protein antigens (Lrg Ag) are taken up by subcapsular macrophages (SCS MF) and

transferred to follicular DC either directly or as mediated by B cells. Small protein antigens (Sml Ag), however, are efficiently taken up by follicular conduits and directly transported to B cell follicles or the T cell cortex. Thick arrows, direction of flow. Thin arrows, direction of antigen transfer to and between LN-resident cells.[11]

For the last two decades the role of the reticular LN network in the distribution of antigen to deep LN cells including DCs and B cells has been explored extensively. Canonical studies demonstrated that soluble molecules within the lymph do not move freely through the cortical parenchyma of the LN, rather, they primarily are found within the reticular network's conduit system (Figure 2.3, insert). The reticular network, which functions as the LN's infrastructure, is a mesh of collagenous fibers that connects the floor of the subcapsular sinus to high endothelial venules (HEVs) through the extracellular matrix of the sinus endothelium and the basement membranes of the HEVs.[84, 85] Within this meshwork, "conduits" of the reticular network are formed. Composed of highly specialized extracellular matrix, these conduits consist of a central core of interstitial matrix molecules, collagen types I and III, which is surrounded by a basement membrane-like structure that is then ensheathed by a layer of fibroblastic reticular cells (FRC). The uniqueness of the conduit comes from its basement membrane, which does not separate two cellular compartments as is the norm, but rather surrounds an acellular lumen through which soluble molecules are transported. Additionally, an extracellular matrix layer containing fibrillin-1 and fibrillin-2 exists between the collagen core and the basement membrane, and has been shown to be important in facilitating DC-mediated contact involved in sampling conduit-resident antigen.[84]

This reticular network has been shown to restrict access of lymph-borne material to the cortical parenchyma which is important in not only preserving the naïve state of the

lymphocyte microenvironments, but also in protecting from a wide variety of immunogenic molecules that would adversely influence an immune response occurring within the cortex, such as microbes and their soluble products during microbial infections.[85] The efficiency of this barrier has been extensively shown to depend on the size of the lymph-borne molecules (Figure 2.3) with high molecular weight (MW) tracers all but virtually excluded from conduit and cortex access by the subcapsular sinus. The fate of these high MW tracers as well as large particulates has been shown to be scavenging by either the lymphatic-sinus processes of sinus-lining DCs or CD169+ subcapsular sinus macrophages (Figure 2.3), both of which resulting in rapid CD4 T cell responses, although CD169+ subcapsular sinus macrophages have been shown to proceed through B cell transfer of antigen opposed to DC presentation.[83, 86-88] Conversely, low MW tracers experience graduated but not absolute exclusion, with molecules under 70 kDa having access to the conduits.[84, 85] However, permeation of these low MW molecules from the conduits to the lymphocytes within the paracortex is mostly restricted, indicating that for immune challenges with limited antigen concentration this might be a significant barrier, but with larger concentrations direct lymphocyte access could be possible on a physiologically significant scale. Interestingly, there exists a limit to the protection of the cortical parenchyma by the reticular barrier as very small molecules such as tritiated uridine (~350 daltons)[89] and acridine orange (302 daltons)[85, 90] have free movement of throughout the cortex. In terms of how this conduit system affects the delivery of antigen to LN-resident DCs and their subsequent presentation to T cells, it has been shown that resident DC are in close contact with the conduits and have access to their contents through extensions of their processes into the

conduit lumen (Figure 2.3).[84] These DCs are immotile while on the conduits, but once they have taken up their antigen they no longer interact with the fibrin structural backbone of the conduit extracellular matrix core, and become more motile and migrate to the T cell paracortex to present antigen.[84, 88]

2.3.2 LN diseases and current treatment

The LN are the primary organs where adaptive immune responses of the body occur, and as such their health is important to maintaining a functioning immune system.[1] The primary disease associated with LN is the presence of cancer, which can occur in LN by one of two mechanisms: it can originate in the LN, in which case its referred to as lymphoma, or it can spread there as a result of metastasis from another primary tumor site.[91, 92] In America, more than 15.5 million people have a history of cancer, and it is estimated that in 2018 there will be around 1.7 million new cancer cases diagnosed.[93] This tremendous number of new and total cancer cases will result in over 600,000 Americans dying in 2018, or more than 1600 deaths per day, making cancer the second most common cause of death in the US behind heart disease.[93] Of all of these deaths, more than 90% will occur due to metastasis, with the tumor-draining LN commonly being the first organ of metastasis for many types of cancer.[92] This function of LN has important clinical promises for diagnostic utility in staging disease as well as mounting anti-cancer immune responses due to the presence of tumor-derived antigen within these sentinel LN. Sentinel LN are therefore critically involved in directing anti-tumor immune response and suppression,[94, 95] and consequently, both chemotherapeutic[96] and immunotherapeutic[10] interventions targeting these LN have been explored. Lymphomas, on the other hand, originate in the LN and result in over

80,000 diagnoses and 20,000 deaths per year.[93] Regardless of the etiology, cancer in the LN presents interesting opportunities for treatment including immunotherapy, which is a type of treatment that uses the body's own immune system to treat the cancer and includes: checkpoint inhibitors, cancer vaccines, and non-specific cancer immunotherapies and adjuvants.[97]

Despite these advanced treatments, there still remain great challenges with improving immunotherapeutic outcomes. Based on the mechanism of adaptive immune response whereby an APC will encounter cancer antigen, either exogenously administered or endogenously encountered from the draining tumor site, and activate cytotoxic T cells with the cognate T cell receptor for the antigen, many cancer vaccines or adjuvants rely on cell mediated trafficking to the LN in order to elicit an immune response.[71] However, recently taking advantage of the second mechanism of antigen delivery to LN has become popular with myriad drug delivery systems designed to improve upon the efficiency of antigen transport. Due to the structure of the lymphatics and the partitioning of solutes within the LN, both of which are favor opposing size scales of molecules, there however, remains a significant technological gap in exploiting passive diffusion of administered therapeutics, which occur on a more rapid time scale than cellular mediated delivery, in order to achieve an immune response.[11]

2.3.3 LN targeting drug delivery strategies

Direct injection of LN has shown promise for immunotherapy,[98] but is too laborious and impractical for most drug delivery scenarios. Since LN are bathed in lymph drained by afferent lymphatics from the periphery in a steady state fashion, drug delivery design principles discussed previously optimizing for lymphatic uptake will be applicable

for LN delivery (Figure 2.2 and 2.3). As with lymphatic targeting, after direct injection in the periphery, interstitial flow follows a one-way path toward the lymphatic capillary and subsequently to the draining LN, resulting in a highly facile yet robust LN targeting. Design wise, the formulation must mainly be small enough so as to not be entrapped by the tissue interstitium, yet large enough not to be cleared into the circulation after injection, corresponding to roughly 10-100 nm in hydrodynamic radius, and ideally 20-40 nm.[66, 67, 99, 100] However, this size dynamic changes within the LN as the structure of the LN controls access of antigen to the cells, as solutes and particulates undergo size-based distribution within the LN.[8, 85, 101] The complex filtering taking place in the LN plays a critical role in the rate, extent, and distribution of agent accumulation that may influence drug efficacy, required dose, associated toxicities, and cellular access. For example, large soluble antigen such as virus-like particles and exosomes are excluded by the subcapsular sinus, which represents a barrier to deep access to the LN parenchyma where cortical T cells reside.[8, 85] While CD169 positive macrophages, which line the subcapsular sinus, are capable of scavenging these large particulate antigens and presenting them to active B cells, this results instead in a putative mechanism for rapid humoral responses.[86-88] Small molecules < 70 kDa penetrate more deeply into LN as the result of enhanced shunting through LN conduits relative to larger molecules.[84] These conduits pass near centralized LN structures where T cells reside,[8, 84] and are lined with follicular DCs that are able to scavenge antigen within the conduits and present it directly to T cells.[84] This mechanism to achieve T cell responses is thought to occur on a much quicker time scale than cellular-mediated delivery of antigen from the periphery.[84]

While the advantages of using the targeted delivery strategy for lymphatic uptake also apply to LN including dose sparing and minimizing the potential for undesirable off-target effects and/or toxicities,[102] these data support the concept that despite nanoformulations of an intermediate nanoscale size being ideal for lymphatic partitioning after injection in the periphery, small molecules have increased potential to travel freely within the LN cortex and elicit T cell responses. This model might be utilized to optimally target LN-resident cells via controlled release strategies of co-formulated drug such as the multi-stage release strategies that have previously been used to improve intratumoral drug penetration,[103] but have never been applied to LN delivery.

2.3.4 Drug delivery vehicles for LN targeting

Several immunotherapeutic schemes targeting LN have been developed (Figure 2.2), with most approaches tested to date exploiting the drainage function of lymphatics as a delivery mechanism after administration in peripheral tissues. This principle has been explored for LN targeting using both synthetic materials, including nanoformulations comprised of Pluronic-stablized poly(propylene sulfide),[67, 104] polymer dendrimers[66, 100] and poly(γ-glutamic acid)-L-phenylalanine ethylester,[99] as well as biologically derived biopolymers, such as hyaluronic acid[105] and albumin.[102] Such approaches have been used to improve LN delivery and bioactivity of co-formulated small molecules,[106] oligonucleotides,[10, 102, 107] as well as proteins and peptides.[80, 102, 108]

Micelles are composed of block copolymers that self-assemble to sizes from several nm to several hundred nm. Micelles offer the notable advantage in drug delivery applications of the ability to encapsulate hydrophobic drugs within their core and deliver

this cargo to tissues and cells.[71] For example, Reddy et al. explored the effect of increasing micelle size range on LN accumulation and retention over time. Micelles were synthesized at sizes of 20, 45, and 100 nm using PEG-stabilized poly(propylene sulfide) NP. 20 nm NP were most efficiently transported through the lymphatics to the LN compared to the 45 and 100 nm NP, and were furthermore retained longer within the LN up to five days post-injection.[67] Additionally, the cellular fate of the LN-retained NP was assessed and found to be exclusively with APCs, with reports of upwards of 50% of APCs being positive for 20 nm NP. This data demonstrated the size-based principles behind lymphatic-targeting of LN, and also hints at the cellular access afforded by such particulate delivery vehicles.[67]

While this drug delivery strategy for LN delivery utilizes a highly used design criteria to optimally target lymphatics and therefore achieve LN accumulation, strategies that seek to overcome the drawbacks of the large particulate delivery vehicle once inside the LN have yet to be explored. In cancer such multi-stage release strategies have previously been for similar purposes, such as to improve intratumoral drug penetration, but these have yet to be applied to LN delivery.[109] Within tumor therapy multi-stage strategies exploit tumor pathologies including using the upregulation of specific enzymes, such as matrix metalloproteinases, which are responsible for much of the tissue remodeling in cancer[110] to achieve target site-restricted degradation of a carrier and release of loaded drug. A particularly innovative approach designed to facilitate increased intratumoral drug penetration is the degradation of tumor-accumulating NP ~100 nm in diameter to a smaller, more diffusive size regime via the proteolytic activity of matrix metalloproteinase within the tumor microenvironment.[103] The advantage of such a

multistage system is the ability to overcome perivascular entrapment by the dense collagenous extracellular matrix within solid tumors that stymies drug bioactivity.[68] Given the transport barrier similarities between the tumor perivasculature and the LN subcapsular sinus and reticular conduits, such a scheme has the significant potential to improve the LN penetration of immunotherapeutic drugs to deep immune cells including T cells.

2.3.5 LN-targeted immunotherapies

Immunotherapy encompasses the use of checkpoint inhibitors, cancer vaccines, and non-specific cancer immunotherapies and adjuvants,[97] alone or in combination therapy. Using multiple agents with synergistic activity has been proposed for a variety of indications. The rationale is that co-treatment with drugs that exert complementary or orthogonal signaling function may amplify the desired response. In other scenarios, multiple agents are required for functionality and necessitate co-delivery to the same cell population(s).[1, 97]

Among the promising cancer immunotherapy solutions, vaccines are promising as they are the most effective form of immune modulation developed to date, and involve the conditioning of adaptive immune response via multiple immunological signals. In its most basic form, vaccination entails exposure of the immune system to attenuated or inactivated pathogen. Antigen, the substance or part of the pathogen to which the immune response is generated against, is taken up, processed, and presented by APCs to antigen-specific lymphocytes that recognize the specific antigen.[111] The local immune microenvironment at the time of antigen presentation dictates the differentiation programs followed by proliferating lymphocytes. Nature has thus evolved APCs to

recognize numerous pathogen-associated molecular patterns such that upon exposure to pathogen these cells become activated, produce stimulatory cytokines, and surface express maturation co-stimulatory molecules.[112] Hence, antigen-specific lymphocytes proliferate as the result of antigen recognition in an immune stimulatory microenvironment, driving the induction of robust adaptive immunity.[111]

In order to mimic the effects of such vaccination strategies using a technology with finer-tuned control of dose for improved safety, engineered material systems have been developed. Formulations that enhance the delivery of both antigen and the immune stimulatory signal, termed an adjuvant, to their same target cells, and to ensure their efficient synergistic interactions, have been explored in an approach called "co-delivery" (Figure 2.2).[113] Anionic polymerization of propylene sulfide can be carried out within micelles composed of Pluronic F127, an amphiliphic block copolymer made from PEG-poly(propylene glycol)-PEG.[114] The resulting 30 nm diameter poly(propylene sulfide) NP have been explored in several applications for their capacity of deliver immunotherapeutic drugs to LN for immunomodulation. In de Titta et al.[107] toll-like receptor (TLR) 9 ligand CpG oligonucleotides were conjugated to these polymer NP. Upon footpad injection, NP-conjugated CpG elicited a more potent maturation response of draining LN-resident dendritic cells relative to free CpG. Furthermore, when co-injected with NP conjugated to the chicken ovalbumin protein (OVA), treatment with CpG-conjugated NP more potently induced antigen-specific effector and memory T cell responses relative to treatment with free CpG. Capitalizing on this T cell activation, vaccinated mice were challenged with OVA expressing murine lymphomas and melanomas and a significant retardation in tumor formation was found in mice vaccinated

with OVA-conjugated NP co-infused with CpG-conjugated NP rather than free CpG. These results emphasize the potential for LN delivery to improve the potency of cancer vaccines.[107]

Taking this concept a step further, in Thomas et al. the use of endogenous tumor antigen was exploited for therapeutic vaccination against cancer. In the previous work tumor antigen was co-delivered with adjutant to induce a potent anti-tumor immune response. However, the tumor-draining LN (TDLN) is known to be bathed in tumor-derived antigen,[115] and therefore the LN-resident cells may already be in a state of activation against endogenous tumor antigen, requiring only then the delivery of adjuvant to elicit a robot anti-tumor immune response. Elaborating upon this integral role of the TDLN in tumor immunity,[116] Thomas et al. explored how the sole delivery of immunotherapeutic adjuvant drugs to the TDLN vs. non-TDLN influenced tumor progression and development of anti-tumor immunity without delivery of exogenous antigen.[10] In this work, tumor lymphatic drainage was biased by implanting murine B16F10 melanomas in the left dorsal skin of mice, thereby focusing lymphatic drainage to the tumor-draining ipsilateral LN and creating non-TDLN on the contralateral side. When fluorescently-labeled, the aforementioned poly(propylene sulfide) NP were found to accumulate appreciably only in LN ipsilateral to the site of intradermal injection. With daily administration in the dermis ipsilateral to the tumor, adjuvant drug-loaded NP resulted in a slowing of tumor growth not observed when administered intravenously or in the skin contralateral to the tumor. The NP-mediated delivery to the LN was crucial to this effect since treatment with free drug with or without NP co-infusion had no influence on tumor growth. These differences in efficacy were attributed to the observed increases

in the maturation and activation status of dendritic and T cells resident within the TDLN. Correspondingly, drug loaded NP delivery to TDLN boosted the adaptive immune response to endogenously produced tumor antigen that also accumulated within TDLN, as indicated by an increased frequency of tumor infiltrating antigen-specific T CD8+ cells. These results illustrate the potential for TDLN-targeted drug delivery for tumor immunotherapy.[10]

CHAPTER 3. S-Nitrosated Polypropylene Sulfide Nanoparticles for Thiol-Dependent Transnitrosation and Toxicity Against Adult Female Filarial Worms[13]

3.1 Introduction

NO mediates its effects through its chemistry in a variety of physiological signaling processes including vasodilation,[117] inhibition of platelet aggregation,[118] and cytotoxicity[36] in a manner analogous to phosphorylation.[52] NO is highly diffusive, but due to its chemical reactivity is purported to have an extremely short half-life on the order of 5–10 s.[63] Controlled delivery and release strategies for NO are thus highly attractive for a range of therapeutic applications,[119-121] but challenging to achieve within deep tissue targets.[29]

To enable NO's physiological effects to be exerted over much farther distances than its reactivity-limited diffusion distance would permit, NO *in situ* can form reversible adducts with endogenous nucleophiles[23] or convert to its more stable oxidized forms, nitrite (NO_2^-) and nitrate,[122] all of which can revert to NO under certain physiological conditions.[122, 123] Endogenous R-SNO, which include S-nitrosocysteine (SNO-CYS), S-nitroso-albumin, and S-nitrosoglutathione, represent a major class of NO adducts that facilitate NO's transport *in vivo*.[51] R-SNO are formed on free thiols either through reactions with nitrosating agents[54, 124] or by transnitrosation (i.e., by transfer of NO from other nitrosothiols)[55, 56] giving R-SNO the ability to be formed under a wide range of (patho)physiological conditions.[57] Therefore, in addition to NO_2^- and nitrate, which have previously been explored for therapeutic delivery as prodrugs,[125] R-SNO

represent an attractive and physiological NO chemistry that has been exploited to harness both native NO signaling and transport activity in biological systems.[50]

Brugia malayi , one of three filarial worms responsible for lymphatic filariasis, are transmitted through a mosquito's saliva, injected into a host's dermis, where they make their way to the lymphatics, grow and multiply, and can eventually cause several chronic diseases including elephantiasis.[126] There are an estimated 120 million people, most of whom reside in the developing world, who harbor these parasites with another 1 billion people identified as at risk for infection.[3] While there are several treatment options available to remove the microfilaria progeny that spread the disease, there are no lymphatic localized therapies that target the adult worms in the lymphatics where they reside. Hence, people currently infected face few treatment options.[3]

NO has been implicated as an effector cytotoxic molecule in the immune response to a variety of pathogenic parasites.[126-128] Previous work has shown that *B. malayi* are susceptible to exogenously delivered NO[129] and demonstrated potential for physiological R-SNO, SNO-CYS,[130] and S-nitrosoglutathione,[131] to mediate damage to several types of parasites. Due to their small size, however, commercially available NO donors and physiological R-SNO have low potential after injection to accumulate within lymphatic vessels[11, 15, 132, 133] where these parasites reside, curbing their utility as antifilarial therapeutic agents. Whereas small molecules < 5 nm in hydrodynamic size are freely blood permeable and are thus rapidly cleared into the systemic circulation,[11] drug targeting to lymphatics is significantly enhanced for nanoscale drug delivery systems ≈30 nm in hydrodynamic size[11] and NO formulation approaches improve both donor circulation times[6] and NO bioactivity.[72] A NO-

encapsulating nanoformulation could therefore facilitate the targeted, controlled, and efficient delivery of NO to eradicate filarial parasites resident within lymphatic tissues.

Herein, we report the synthesis and modification of thiolated NP with NO in order to harness the physiological nitrosothiol chemistry for NO delivery and bioactivity using a synthetic polymer system. These NO-containing NP, SNO-NP, stably encapsulate high levels of NO and facilitate its controlled release. In particular, we demonstrate that the bioactive form of released NO from SNO-NP, either NO_2^- or SNO-CYS, depends on the ratio of free CYS, a common endogenous low molecular weight thiol important in transnitrosation reactions,[57] to SNO-NP. Furthermore, the cytotoxic activity of SNO-NP against *B. malayi* adult female filarial worms, for which there is no existing treatment, is accelerated in the presence of CYS due to the formation of SNO-CYS. Since these synthetic NP have well-documented lymphatic targeting activity after intradermal injection,[10] these results provide a strong rationale for therapeutic use of SNO-NP in eradication of *B. malayi* that reside intralymphatically *in vivo* and for other deep tissue NO delivery applications.

3.2 Materials and Methods

3.2.1 Synthesis and characterization of SNO-NP

NP were synthesized as previously described.[10, 114, 134] Briefly, 500 mg of Pluronic F127 (Sigma-Aldrich, St. Louis, MO, USA, P2443) was added to 10 mL of degassed Milli-Q water, allowed to dissolve for 30 min with stirring, and was again degassed. To this solution, 400 μL of propylene sulfide (Sigma-Aldrich, P53209) was added under argon and stirred for 30 min. Initiator weighing 7.8, 14.4, 28.8, or 43.4 mg (1.9, 3.7, 7.4, and 11 × 10^{-3} M , respectively) was reacted with 322 μL of sodium

methoxide (Sigma-Aldrich, 156256) and then added under argon. 1,8-Diazabicyclo[5.4.0] undec-7-ene (DBU) (Sigma-Aldrich, 139009) was added under argon to the solution 15 min later and the entire reaction stirred for 24 h. The solution was subsequently exposed to air for 2 h and dialyzed for 3 d against 4 × 5 L of Milli-Q water using 100,000 Da molecular weight cut off cellulose membrane dialysis tubing (Spectrum Lab., Rancho Dominguez, CA, USA, 131414). NP size was measured by dynamic light scattering and a small volume was lyophilized to obtain the total NP weight concentration. 1 H NMR (400 MHz, $CDCl_3$) was used to calculate the weight percent of Pluronic F127, poly(propylene sulfide), and initiator in the NP.[134] Ellman's assay (Thermo Scientific, Rockford, IL, USA, 22582) was used to determine the concentration of NP free thiols. Thiolated NP were S-nitrosated by reacting equal volumes of NP with sodium nitrite (Sigma Aldrich, 237213) solution in strong acid. Unreacted free acidified nitrite was capped with addition of ammonium sulfamate (Sigma Aldrich, 228745). SNO-NP were further dialyzed before use in transnitrosation and *B. malayi* experiments.

3.2.2 Determination of SNO and NO_2^- concentration using modified Saville and Griess assays

Acidified nitrite solution was prepared by mixing equal volumes of 2 N HCL with sodium nitrite solution (aqueous). Sulfanilamide (Sigma-Aldrich, S9251) solution was prepared by dissolving 34 mg sulfanilamide in 1 mL of 0.4 N HCL. Mercuric chloride (Sigma-Aldrich, 215465) solution was prepared by dissolving 10 mg of mercuric chloride in 1 mL of water. N-(1-naphthyl)ethylenediamine dihydrochloride (Sigma-Aldrich, 222488) solution (5.4×10^{-3} M) was prepared in 0.4 N HCL. In reactions where excess acidified nitrite was removed, an eightfold molar excess of ammonium sulfamate was added to the solution. The Saville assay,[135] which measures S-nitrosothiol

concentration, was performed by mixing 70 μL of the S-nitrosated thiol solution with 100 μL of Solution A (one part mercuric chloride solution and four parts sulfanilamide solution) or 100 μL of Solution B (one part water and four parts sulfanilamide solution) and then mixing these solutions with 80 μL of 5.4×10^{-3} M N-(1-naphthyl)ethylenediamine dihydrochloride solution. The Griess assay, which measures free NO_2^-, is the same as the Saville, except without the addition of Solution A. For both assays, after a 10-min incubation at room temperature, the absorbance was read at 540 nm and the difference between Solution A and Solution B represents the S-nitrosothiol signal. S-nitrosothiol and free NO_2^- concentrations were calculated from a standard curve of S -nitrosoglutathione.[136]

3.2.3 Degradation and transnitrosation studies

SNO-NP were prepared by the standard S-nitrosation procedure described above. SNO-NP were then dialyzed with 100,000 Da molecular weight cut off cellulose membrane dialysis tubing against 5 L of Milli-Q water overnight. Following dialysis, SNO-NP were brought to pH 7.4 using 10× phosphate buffer saline (PBS) without calcium and magnesium and diluted to $1–2 \times 10^{-3}$ M NO concentration in complete medium. S-nitroso-N-acetyl penicillamine (SNAP) solutions were made in PBS, pH to 7.4, and diluted to $1–2 \times 10^{-3}$ M NO concentration in complete medium. SNO-NP in complete medium were mixed with CYS to 0.1, 1, and 10× the SNO-NP concentration. Solutions were incubated in closed vessels at 37°C and nitrite and SNO concentrations monitored over 100 h. Transnitrosation studies were conducted as described above except SNO-NP were incubated in the presence of varying amounts of CYS for 45, 365, and 1460 min at 37°C, after which 250 μL of the solution was fractionated on a 1 cm × 30 cm

Sepharose CL-6B (GE Healthcare, Pittsburg, PA, USA, 17-0160-01) column. Eluted fractions were analyzed for NO_2^- and SNO using the Griess assay and Saville assay, respectively.

3.2.4 Brugia malayi motility and death studies

Freshly isolated adult female *B. malayi* parasites were obtained from the National Institutes of Health Filarial Research Resource (FR3)[137] at the University of Georgia (Athens, GA, USA). Upon receipt, worms were washed and resuspended in 50 mL of complete medium (endothelial basal medium (Lonza, New York, USA) supplemented with 20% fetal bovine serum (Atlanta Biologicals, Lawrenceville, GA, USA), 1% glutamax, 1% penicillin-streptomycin-amphotericin (Gibco, New York, NY, USA), 25 mg/mL cyclic-AMP and 1 mg/mL hydrocortisone acetate (both from Sigma-Aldrich)). The worms were then maintained at 37°C in a 5% CO 2 incubator for at least 18 h prior to experimentation. Individual worms were subsequently plated in 2.5 mL of complete medium in a 24-well culture plate preincubated at 37°C in a 5% CO 2 for 1 h prior to the addition of worms. All treatment solutions were prepared the day of the experiment, except SNO-NP, which were S-nitrosated and dialyzed the prior evening. All treatment solutions were prepared in 1 × PBS without calcium and magnesium at a pH of 7.4. 500 μL of each treatment was added to the worms in replicates of four. Following the addition of treatments, the worms were incubated and 5 s video segments at 10 min intervals were recorded using a custom imaging hardware assembled and maintained within the incubator. Worm motility was quantified using a Lucas-Kanade optical flow algorithm implemented in LabVIEW (National Instruments, Austin, TX). The velocity vectors obtained between two subsequent frames were summed for an entire worm-

containing well and then averaged over the length of the video segment giving us the motility metric. Worm death was defined when the motility metric (normalized to pretreatment baseline) fell and remained below 10% of its normalized value. The 10% threshold was used after it was determined that below that the algorithm was quantifying noisy pixels due to vibrations in the incubator. Data representative of individual treatment groups run in quadruplets in two to five independently run experiments.

3.2.5 Statistical analysis

Data are expressed as mean ± standard deviation. Statistical analysis was carried out using Prism 6 (GraphPad Software Inc. La Jolla, CA, USA). Death curves were analyzed using a Log-rank (Mantel-Cox) test for significance. Time until death was analyzed using an ordinary unpaired one-way analysis of variance (ANOVA) with Tukey multiple comparison correction. Statistical significance was defined as and represented by $p \leq 0.05$ (*), $p \leq 0.01$ (**), and $p \leq 0.001$ (*** and §§§).

3.3 Results and Discussion

3.3.1 SNO-NP synthesis and characterization

SNO-NP were formed by S-nitrosation of synthetic thiolated NP synthesized by emulsion polymerization[134] (Figure 3.1a). Amphiphilic block copolymer Pluronics, including F127 (PF127) explored here as well as F68,[138] self-assemble in water to form micelles, which are able to make an emulsion with propylene sulfide and, in the presence of a deprotected thiolated initiator, activate living anionic polymerization within the micelle core.

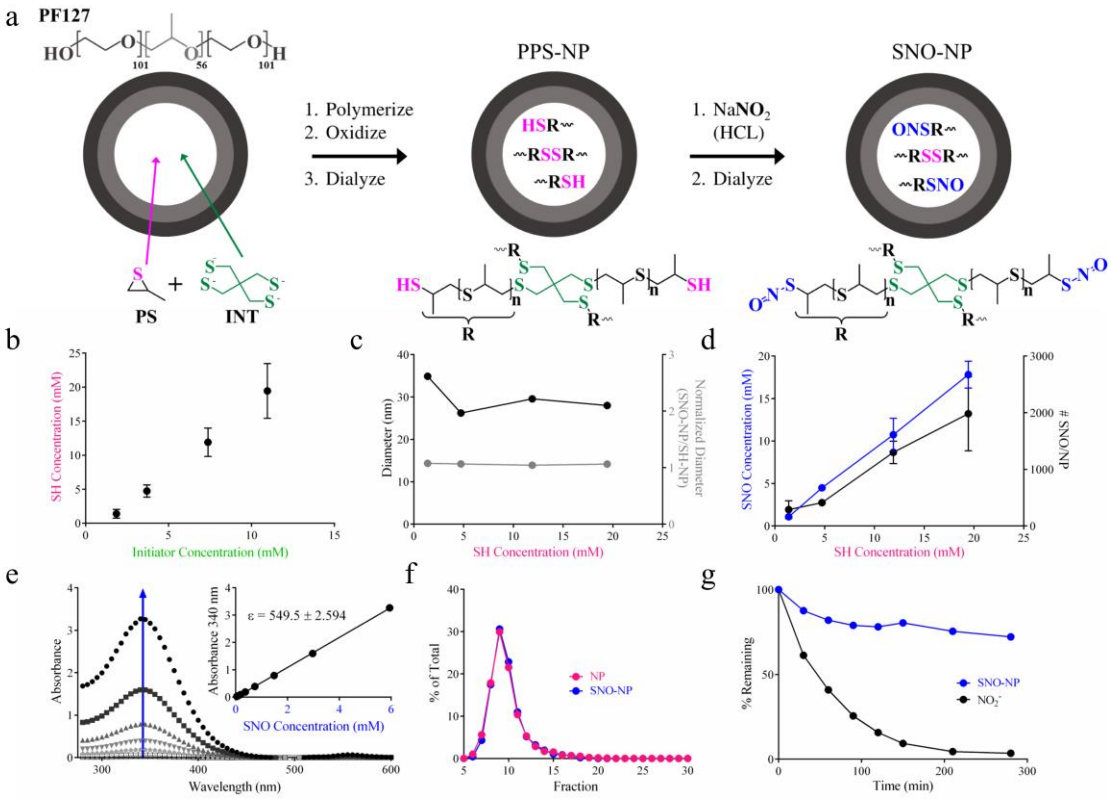

Figure 3.1: Synthetic polymer NP are loaded with NO through the formation of physiological NO adducts, S -nitrosothiols (SNO), with NP SH. a) NP synthesis and S-nitrosation scheme to create S-nitrosothiol (SNO) NP (SNO-NP). b) Particle SH concentration is controlled by initiator concentration during emulsion polymerization synthesis. c) NP diameter remains unchanged by SH concentration and NO loading. d) SNO concentration and number per NP is proportional to NP SH concentration. NP-encapsulated NO is e) in the form of SNO as demonstrated by UV absorbance peaks at 340 and is f) NP bound. e) Arrow indicates increasing SNO-NP concentration. Data shown for a highest SNO-NP concentration of 5.6 × 10^{-3} M with approximate twofold dilutions. Inset demonstrates calculation of molar extinction coefficient that was found to be 540 $M^{-1}cm^{-1}$. g) Whereas nitrite (NO_2^-) remaining after S-nitrosation of SH-NP is rapidly dialyzed away, SNO signal by the Saville assay is retained.[13]

As the concentration of initiator was varied, different degrees of polymerization of poly(propylene sulfide) (PS) were achieved (Figures 3.2 and 3.3a-c). This resulted in an increasing concentration of free thiols (SH) (Figure 3.1b) as well as ratio of SH to disulfide (Figure 3.3d) at the completion of polymerization after solution oxidation with increasing concentration of added initiator with little effect on NP size (Figure 3.1c).

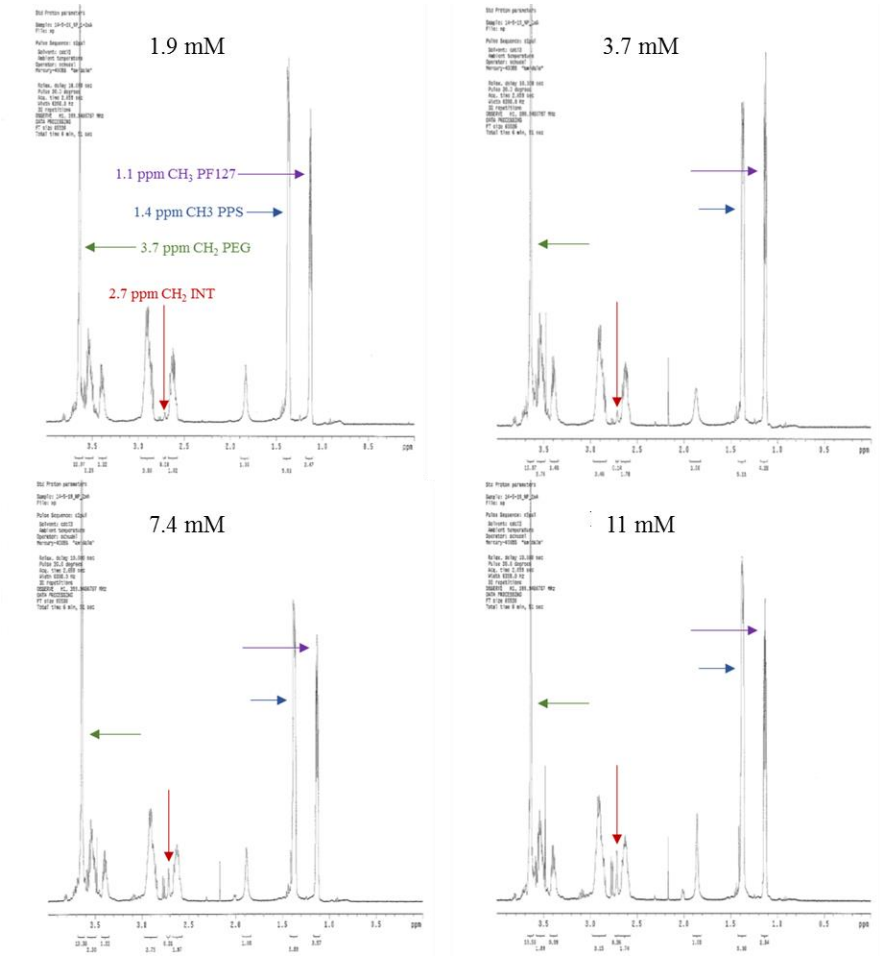

Figure 3.2: ^{1}H NMR data of lyophilized NP solution. The following have been assigned according to van der Vlies et al.[134] as the functional group peaks: 1.1 ppm – CH_3 Pluronic (-CH_2-CH(CH_3)-O-), 1.4 ppm – CH_3 poly(propylene sulfide) (-CH_2-CH(CH_3)-S-), 2.7 ppm – CH_2 initiator (-C-CH_2-S-), and 3.7 ppm – CH_2 PEG (-CH_2-CH_2-O-). The integral of each peak is displayed under the axis. Normalizing each integral to the number of H atoms (3, 3, 2, and 4 respectively) and multiplying by the weight of the functional group allows for the mass percentage of NP solution and degree of polymerization to be determined. Pluronic is taken as the combination of the -CH_2-CH(CH_3)-O- and -CH_2-CH_2-O- fragments.[13]

Dialyzed NP were subsequently S-nitrosated by introduction of acidified nitrite, enabling formation of NO S-nitroso adducts (SNO) with the NP core free thiols. With increasing concentration of NP SH there was a proportional increase in SNO concentration created as measured by a modified Saville assay,[56] indicating efficient S-nitroso adduct formation (Figure 3.1d) that was determined to be >90% for all starting

NP free thiol concentrations. This occurred with no change in NP size (Figure 3.1c) and resulted in up to an estimated 2000 SNO per NP (Figure 3.1d). To confirm SNO adduct formation within NP, SNO-NP were analyzed via UV-vis absorbance. SNO-NP exhibited the characteristic absorbance wavelength of primary thiol S-nitroso adducts at ≈340 nm,[73] that increased with concentration (Figure 3.1e) giving a molar extinction coefficient of 540 $M^{-1}cm^{-1}$ (Figure 3.1e, inset) consistent with previously reported R-SNO.[55] Furthermore, the SNO signal coeluted with that of the thiolated NP during column chromatography (Figure 3.1f), demonstrating the stability of the SNO adduct. Additionally, over the course of dialysis at room temperature against water in a membrane with a 100,000 molecular weight cut-off (MWCO), SNO signal did not decline appreciably while free NO_2^- from the S-nitrosation process was effectively removed as the pH of SNO-NP was brought to physiological levels (Figure 3.1g).

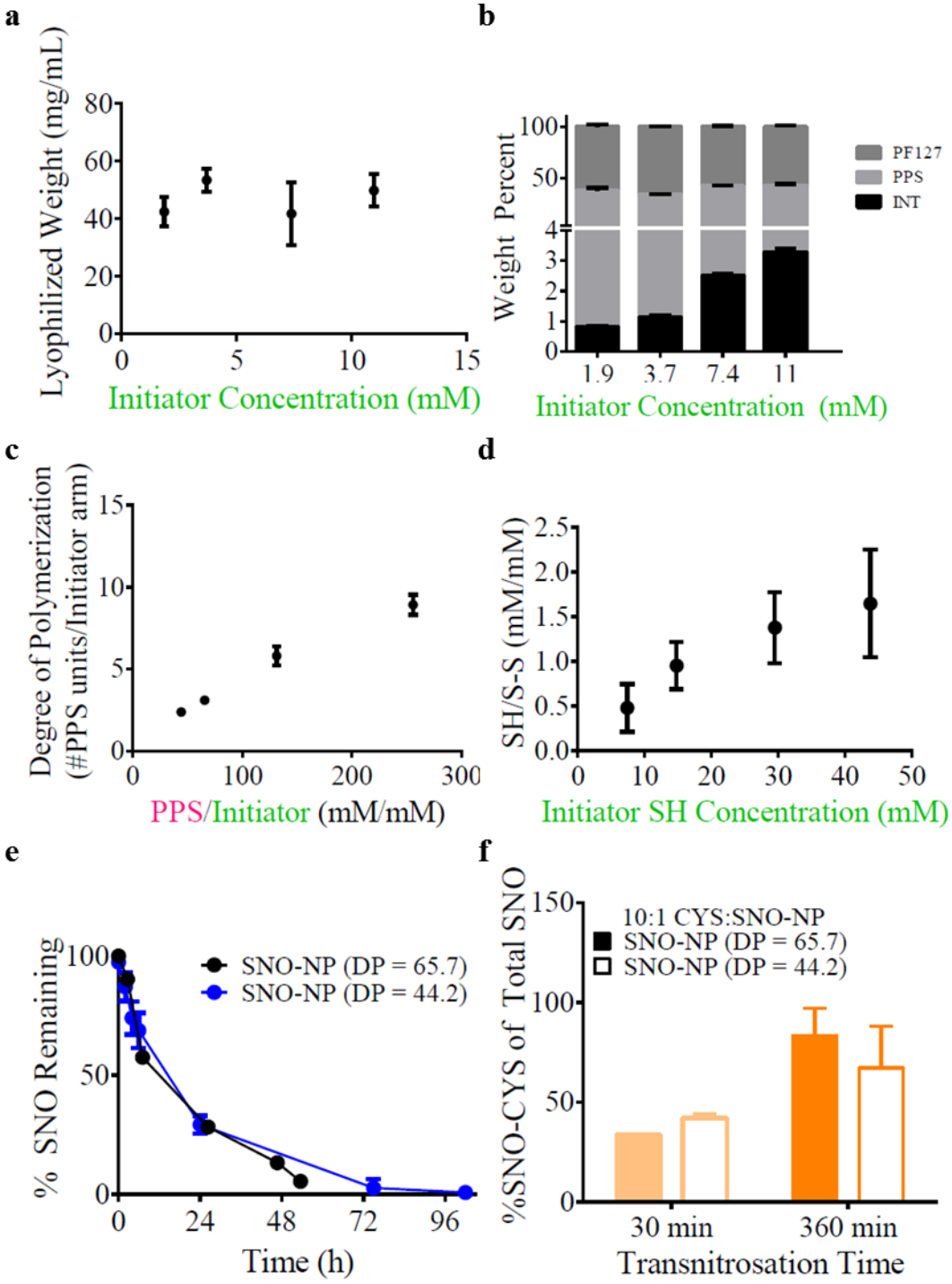

Figure 3.3: Characterization of NP polymerization reaction, S-nitrosothiol decay, and transnitrosation. a) Lyophilization data showing that the total NP polymer weight/mL is unaffected by initiator concentration. 100 µL samples of NP solution synthesized under different initiator concentrations were lyophilized and the weight percent of polymer was determined. b) Increasing initiator concentration during polymerization results in increasing the weight percent of initiator incorporated into

the NP solution. NP were synthesized under different initiator concentrations and lyophilized. The weight percent of each constituent component, Pluronic F127, poly(propylene sulfide), and initiator were determined using ^{1}H NMR (Figure 3.2). c) Degree of polymerization of propylene sulfide increases as molar ratio of propylene sulfide to initiator is increased. NP were synthesized with different initiator concentrations, lyophilized, and analyzed via ^{1}H NMR (Figure 3.2). Using specific peak assignments and normalizing each peak to the number of hydrogen atoms per repeat group, the total number of poly(propylene sulfide) groups and initiator groups were determined. Taking the ratio of poly(propylene sulfide) groups to initiator groups and dividing by the number of arms per initiators (four), the number of poly(propylene sulfide) repeats per initiator and the degree of polymerization were determined. d) The ratio of thiol to calculated disulfide bond concentration increases with increasing initiator thiol concentration. NP were synthesized with different initiator concentrations. Assuming no initiator loss, the ratio between the measured final free thiol concentration and remaining disulfides as determined by the added amount of initiator thiols was determined. e) Degradation of SNO-NP at 37°C is unaffected by degree of polymerization. SNO-NP synthesized with 7.4 and 11 mM initiator, corresponding to degrees of polymerization (DP) of 65.7 and 44.2, respectively, showed similar rates of NO release at 37°C. f) The extent of transnitrosation of SNO-NP to CYS at 37°C is unaffected by degree of polymerization. SNO-NP synthesized with 7.4 and 11 mM initiator, corresponding to degrees of polymerization (DP) of 65.7 and 44.2, respectively, showed similar extents of transnitrosation to CYS over time at 37°C.[13]

3.3.2 SNO-NP S-nitrosothiol decomposition and transnitrosation

We next explored the release of NO from SNO-NP under physiological conditions. In complete serum-containing media at 37°C, decay of SNO signal from 1×10^{-3} M of SNO-NP over 100 h was comparable to that of 1×10^{-3} M of SNAP, a commercially available synthetic small molecule NO donor[123] that is similar in size and structure to some endogenous R-SNO, which has been extensively used to study a wide variety of NO-regulated processes including inflammation,[138] vasodilation,[139] and inhibition of platelet aggregation.[123] The rate of NO release from SNO-NP was not influenced by the degree of PS polymerization (Figure 3.3e). However, at 6 and 24 h post incubation, SNO-NP exhibited faster release (32% and 70%, respectively) of SNO relative to SNAP (7% and 50%) (Figure 3.4a). In distinct contrast to SNAP, SNO-NP

also resulted in the significant accumulation over time of NO_2^- (Figure 3.4a), likely resulting from preferential reaction with oxygen due to its increased concentration within the hydrophobic NP core, in which oxygen is more soluble than aqueous media.[140] SNAP, on the other hand, being a small molecule NO donor that releases NO directly into a less oxygen dense environment[23] that may have potential for interactions with serum species,[141] results in no NO_2^- accumulation.

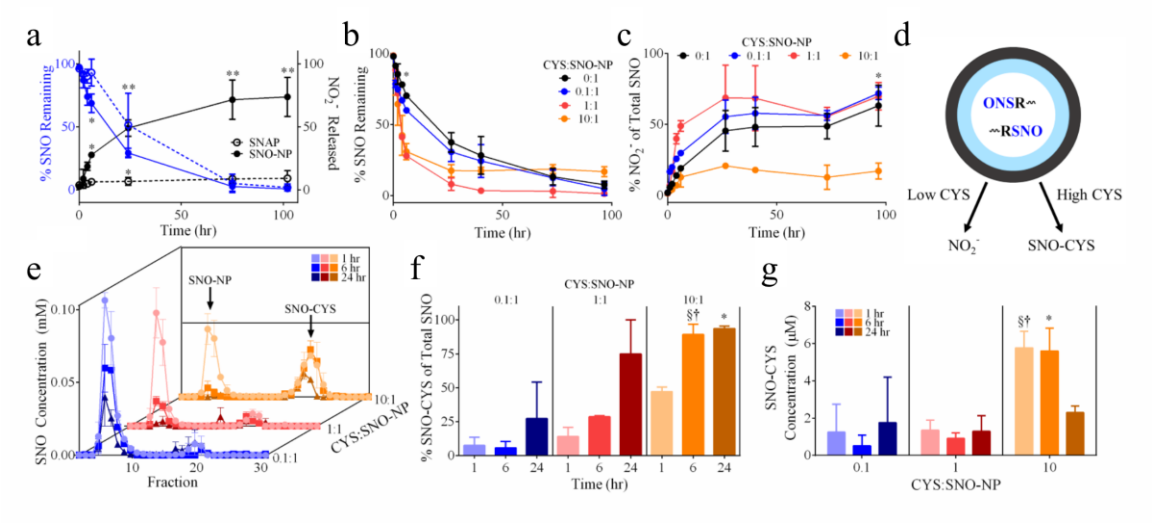

Figure 3.4: SNO-NP mediate transnitrosation under high but not low concentrations of physiological SH CYS in complete medium at 37°C. a) Under conditions of no exogenously added CYS, decay of SNO from SNO-NP is comparable to that of low molecular weight NO donor, S-N-acetyl penicillamine (SNAP) but results in formation of nitrite (NO_2^-). b,c) High (10:1) but not low (0:1, 0.1:1, and 1:10) ratios of CYS to SNO-NP result in long-lived SNO species (b) and minimal SNO-NP release of NO_2^- (c). d) Scheme of free thiol (CYS)-dependent NO release from SNO-NP to form NO_2^- or SNO-CYS via transnitrosation. e) Column chromatography fractionation of NP and CYS at various CYS:SNO-NP ratios reveals increased formation of SNO-CYS with increasing coincubation time and increasing CYS:SNO-NP ratio f,g). a-c) * $p < 0.05$ and ** $p < 0.01$ by two-way ANOVA with matching and post hoc Bonferroni tests. f,g) *, §, † $p < 0.05$ by two-way ANOVA with matching and post hoc Bonferroni tests relative to 0.1:1 at 1460 min, 0.1:1 at 375 min, and 1:1 at 375 min, respectively. In all experiments, a SNO-NP concentration of 1×10^{-3} M SNO was used.[13]

We next evaluated whether SNO-NP could donate NO to physiological thiols

through transnitrosation.[55] In complete medium, the free thiol concentration was found to be $<0.025 \times 10^{-3}$ M as measured by Ellman's assay. To probe how the presence of free thiols may drive transnitrosation, we added CYS and monitored SNO decay from SNO-NP and the formation of NO_2^- over time (Figure 3.4b,c). CYS was mixed with 1×10^{-3} M of SNO-NP at the following ratios of CYS:SNO-NP (i.e., SH from CYS to SNO from SNO-NP): 0:1, 0.1:1, 1:1, and 10:1. CYS to SNO-NP ratios of 1:1 and 10:1 accelerated the decay of SNO signal from SNO-NP relative to low and zero CYS ratios (Figure 3.4b). However, an increase in SNO signal that was not statistically significant was observed at long times after coincubation for the highest ratio tested (10:1, Figure 3.4b), suggesting long lived SNO species under conditions of excess CYS. Furthermore, whereas low CYS to SNO-NP ratios (0.1:1, 1:1) resulted in the appreciable accumulation of NO_2^- in a manner analogous to NO release by SNO-NP with no added CYS, a 10:1 ratio of CYS to SNO-NP did not (Figure 3.4c). These data suggest that under conditions of low vs. high CYS, NO is released from SNO-NP by either of two distinct pathways: to NO_2^- in the case of low or no free thiols or to R-SNO via transnitrosation in the case of high thiol concentration (Figure 3.4d).

To test this hypothesis, the extent of transnitrosation as determined by the formation of SNO-CYS after coincubation of 1×10^{-3} M of SNO-NP with varying ratios of CYS was determined. Since the Saville assay could not discriminate between SNO retained by SNO-NP vs. that from newly created SNO-CYS via transnitrosation, the two SNO species were separated using size exclusion column chromatography after prescribed times of coincubation. This technique was able to detect the ratio of remaining SNO amongst the two species, SNO-NP and SNO-CYS, by comparing the collected

fractions to those previously obtained for the individual species (Figure 3.4e). By virtue of their larger size, NP eluted in early fractions, whereas small CYS eluted in later fractions as verified by Ellman's assay and iodine staining.[10] We found that SNO-CYS constituted a larger percent of remaining SNO at late times for all CYS to SNO-NP ratios tested but only represented a significant portion of the remaining SNO for 10:1 CYS:SNO-NP (Figure 3.4f). In terms of absolute amount, this corresponded with an appreciable increase in SNO-CYS concentration for only the 10:1 CYS to SNO-NP (Figure 3.4g). The extent of transnitrosation by SNO-NP was not appreciably affected by degree of PS polymerization (Figure 3.3f).

3.3.3 SNO-NP biological activity in filarial worm model

To demonstrate SNO-NP function as an antiparasitic agent, we devised a setup in which adult female worms were individually incubated in wells containing complete medium and quantified motility over 96 h. We have previously used a similar experimental configuration to monitor worm motility and health over time as well as evaluate worm responses to antiparasitic agents.[142] Worm motility in response to treatment normalized to pretreatment was then plotted over time. Concentrations of NO treatment groups ranged from 1×10^{-3} to 2×10^{-3} M.

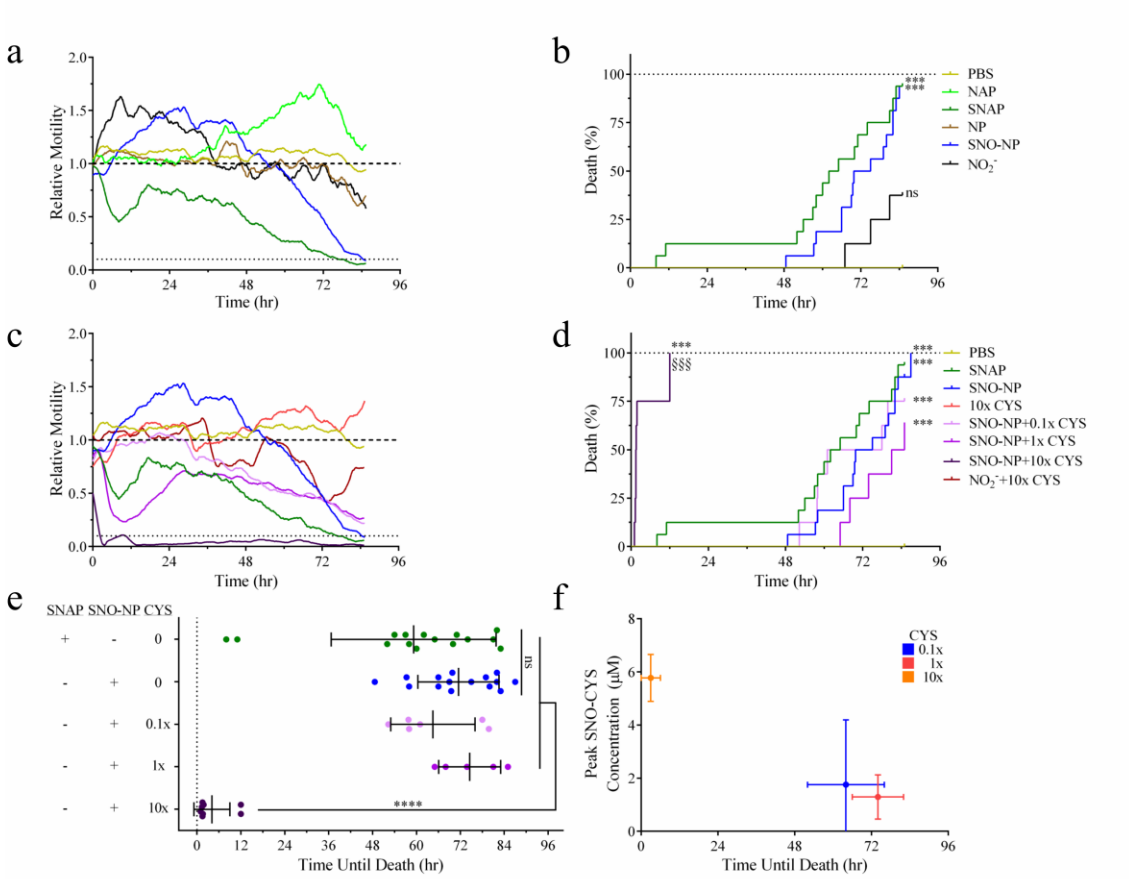

Figure 3.5: SNO-NP-mediated killing of adult female *B. malayi* filarial worms is accelerated with increasing ratios of low molecular weight thiol CYS to SNO-NP. a) Worm motility is reduced by NO donors SNO-NP and b) S-N-acetyl penicillamine (SNAP) and results in worm death at similar times. c) Increasing ratio of CYS to SNO-NP accelerates SNO-NP-mediated reductions in worm motility. d,e) Worm death induced by SNO-NP occurs more quickly at the highest ratios of CYS to SNO-NP relative to SNAP. Data in all panels from at least two independently run experiments. a,c) Data represent the average motility of n ≥ 8 worms. b,d) * and §§§ p < 0.001 by Log-rank test. e) * p < 0.5 by one-way ANOVA with multiparameter comparison correction (Tukey's test). f) Shortest time until worm death induced by SNO-NP corresponds to the ratio of CYS to SNO-NP that results in the highest observed levels of formed SNO-CYS concentrations. In all experiments, SNONP and SNAP concentrations of 1–2 × 10^{-3} M SNO were used.[13]**

We found that the motility of SNAP-treated worms decreased quickly upon coincubation with SNAP, while control N-acetyl penicilamine (NAP)-treated worms showed no reduction (Figure 3.5a). Treatment with SNO-NP but not NP alone also resulted in a reduction of worm motility though the response was much delayed relative

to SNAP (Figure 3.5a). However, the death curve (Figure 3.5b) and the time until death (Figure 3.5e) defined as when motility dropped below 10% of baseline, were similar for both SNAP and SNO-NP-treated worms. We hypothesized that this discrepancy in effect on motility but not time until death may result from SNAP but not SNO-NP penetration into the worms in order to mediate its effects. This idea is supported by findings that the worm's cuticle, the highly cross-linked collagenous structure lining the worm's limiting membrane,[143] is impermeable to large antibody and complement complexes,[144] but not to small molecules such as glucose or amino acids, thus making it impermeable to the SNO-NP.[145] Furthermore, it has been previously hypothesized that endogenous R-SNO, which are similar in molecular weight and hydrodynamic size to SNAP, mediate antiparasitic effects through their uptake by worms as the result of their similarity to natural analogues[130] and by S-nitrosating key proteins[146] such as cysteine proteases.[128, 147] To test this hypothesis, worms were incubated with SNO-NP in the presence of 0:1, 0.1:1, 1:1, and 10:1 CYS:SNO-NP. Treatment with CYS alone did not have a negative effect on worm motility and did not result in any worm death. When worms were incubated with SNO-NP at a 0.1:1 ratio with CYS, a similar effect on worm motility as that of SNO-NP alone (Figure 3.5c) was found. However, when CYS was present at a 1:1 ratio, the reduction in motility closely matched that induced by SNAP (Figure 3.5c). Intriguingly, when CYS was present at the ratio 10:1 with SNO-NP, the reduction in motility induced by treatment was almost immediate (Figure 3.5c) and resulted in a dramatically faster time until death than that of SNAP (Figure 3.5e). Worm treatment with SNO-NP in combination with increasing amounts of CYS up to a ratio of 1:1 resulted in the same death curve as SNAP relative to PBS (Figure 3.5d). However,

treatment with SNO-NP in combination with CYS at the highest ratio tested (10:1) resulted in death curves that were accelerated relative to those induced by treatment with other CYS:SNO-NP ratios and SNAP (Figure 3.5d). This significant difference, as exemplified by the rapid time until death of 10:1 CYS:SNO-NP (Figure 3.5e), may be a result of the higher amount of total SNO-CYS created when CYS is added at a high ratio relative to SNO-NP (Figure 3.5f). Although cysteine is present in the lymph at ≈100 × 10^{-6} M,[148] SNO-NP undergo significant dilution following intradermal administration, accumulating within lymph in draining LN at a ≈30–100-fold lower concentration relative to that administered in the dermis.[10] Hence if the dose used *in vitro* here was administrated intradermally, SNO-NP would still result in CYS:SNO-NP ratios >3–10. Additionally, SNO-CYS (187 Da), which is approximately the same size as SNAP (220 Da), may kill the worms faster either because it is absorbed more quickly than SNAP or because it is better at mediating the effects of the NO it carries. In addition to their higher potential for lymphatic targeting relative to SNAP, these results highlight the potential for SNO-NP to effectively treat parasites through its unique NO-releasing mechanisms.

3.4 Conclusions

In conclusion, we have demonstrated the synthesis and characterization of SNO-NP for the delivery of NO reservoirs NO_2^- and R-SNO. We demonstrate that SNO-NP release SNO through either the formation of NO_2^- or by transnitrosation. Furthermore, we establish antiparasitic activity of SNO-NP corresponding with the extent of R-SNO formation determined by the relative ratio of CYS to SNO-NP (Figure 3.5f). Implementing a synthetic polymer nanoformulation to deliver high levels of per NP NO via the physiological S-nitrosothiol chemistry represents an innovative approach to

achieve therapeutic delivery of NO. Given the unique and previously reported lymphatic targeting activity of these NP, this represents a novel formulation for the delivery of NO in the elimination of adult female filarial worms.

CHAPTER 4. S-nitrosated poly(propylene sulfide) Nanoparticles for Enhanced Nitric Oxide Delivery to Lymphatic Tissues[149]

4.1 Introduction

The lymphatics are involved in a wide variety of diseases either as the primary tissue of interest, such as with lymphedema[2] or lymphatic filariasis,[3] or as an accessory to the pathologies of other diseases, such as with myocardial infarction[4, 5, 150] and cancer.[10] Due to the integral role lymphatics play in tissue fluid regulation,[6] lipid transport,[7] and immune cell functions,[8, 9, 151] an estimated forty million patients worldwide[20, 21] endure the combined effect of all diseases in which the lymphatics are affected. Despite the high prevalence of lymphatic-associated diseases, treatment methods, especially for diseases where the lymphatics are the primary tissue of interest, remain stagnated or in some cases nonexistent. As one example, the current standard for the treatment of lymphatic filariasis, an infection of lymphatic tissues by parasitic worms, is the use of antibiotic cocktails that distribute systemically to eliminate the microfilaria offspring that spread disease but do not result in appreciable drug accumulation within the lymphatics where the adult worms reside.[3] Moreover, standard therapy for lymphedema, one of the morbidities associated with both lymphatic filariasis infections and sentinel LN removal following breast tumor resection, employs only a combination of compression and physical therapy.[22] For diseases where the lymphatics are not the primary target but are critically involved in the disease pathology or may be useful therapeutically, such as immunotherapy[10, 152-154] or LN-directed chemotherapy (e.g., for the treatment of sentinel LN metastases),[155] there exist few

approved treatments that are specifically formulated to enhance delivery to lymphatics, leaving open the possibility of a range of undesired consequences including reduced treatment efficacy and toxicities related to accumulation in off target tissues.[156]

A therapeutic of particular interest for the treatment of lymphatic-related diseases is NO, an extremely promiscuous signaling molecule that takes part in a variety of physiological processes ranging from vasodilation,[58, 117, 118, 157, 158] to neural signaling,[29] to immune cell cytotoxic defenses.[31, 35, 46, 159] Because of the important role that NO plays in multiple physiological processes, there have been many attempts at modulating NO for therapeutic purposes. For example, NO delivered in the form of nitrate is used to control pain from angina, a disease affecting nine million people in the US with 500,000 new cases every year, and has been found to annually cost the healthcare system around $1.9 billion.[37] NO has also been investigated in several clinical trials for use with other cardiovascular treatments to control blood pressure in adults with prehypertension,[39] which affects 25–50% of adults worldwide,[40] and to improve the function of the right of the heart following heart transplant or left ventricular assist device placement.[41] For pulmonary diseases NO is inhaled in its gaseous form, and is the current standard of care for persistent pulmonary hypertension in newborns, which affects 1.9 per 1000 live births.[42] NO has also been explored for the treatment of various cancers, including lymphoma where a variety of NO donors have been shown to be chemosensitizers[43-45] as well as exhibit direct cytotoxicity.[45-49]

Despite the versatility of NO as a potential therapeutic in a broad array of pathologies, several challenges exist with utilizing NO for lymphatic-related therapy. First, NO participates in many interrelated physiological processes that each have

different requirements for NO signaling.[29, 58, 59] In some cases depletion or attenuation of NO signaling may produce negative effects such as in vascular regulation,[60] whereas in the case of inflammatory responses overproduction of NO can lead to loss of lymphatic function.[31] Consequently, a lymphatic-targeted NO-based therapy would need to be tightly controllable, since NO levels vary significantly across physiological processes and pathologies.[24, 29, 61] Combined with the extremely short half-life[62, 63] of NO requiring it to mediate its action near its synthesis source,[62] targeted NO donation remains highly difficult. The second challenge to delivering NO, especially in the context of lymphatic-related therapies, is the result of the structure and location of the lymphatics.[9, 11] To focus delivery to within the locoregional lymphatic drainage basin, direct injection in the upstream peripheral tissue interstitium is most commonly utilized,[160-162] with uptake being most favorable for macromolecular species in the range of approximately 10–100 nm in hydrodynamic diameter.[163, 164] Since the significant majority of existing NO donors are small molecules and would thus exhibit poor selectivity for lymphatic uptake after administration in peripheral tissues,[9, 11, 133, 163, 164] a critical technology gap exists in facilitating NO delivery to lymphatic tissues (Figure 4.1a).

We previously developed[13] a NO encapsulation strategy that utilizes NP comprised of synthetic polymers that have well described profiles of lymphatic uptake[67] and biodistribution into lymphatic tissues.[104] We demonstrated that these S-nitrosated NP, that we refer to as SNO-NP, facilitate the controlled and sustained release of NO, enabling its cytotoxic activity against adult female *Brugia malayi* filarial worms, which are responsible for the lymphatic disease known as lymphedema.[3]

Herein, we report on the preclinical testing of the NO donating activity of these SNO-NP in an *in vivo* lymphatic delivery model. We measured over the course of 72 h the levels of various reactive nitrogen species (RNS) accumulating within systemic tissues, plasma, and LN draining the site of intradermal injection of SNO-NP and benchmarked against a commonly used, commercially available small molecule NO donor used for chemosensitization[Sullivan 2008] and radiosensitization of cancer,[43] S-nitroso D,L-penicillamine (SNAP). We further assessed the impact of NO donation on lymphatic tissues by looking at lymphatic transport of NP and remodeling of the draining LN, including effects on LN-resident cells, as well as resulting inflammation at the site of injection and systemic toxicity. Our results show that donation of NO to LN when mediated by lymphatic-draining SNO-NP is dramatically improved relative to a small molecule NO donor and does not result in a measurable decrease in LN-resident cell viability or extent of NP uptake or increases in local or systemic levels of inflammation.

4.2 Materials and Methods

4.2.1 Materials

All materials were purchased from Sigma-Aldrich unless otherwise noted.

4.2.2 Synthesis and characterization of SNO-NP and SNAP

Thiolated NP were synthesized as previously described.[13] Briefly, a 0.5% solution of pluronic F127 was made in degassed Milli-Q water. To this solution, 400 mL of propylene sulfide was added under argon and stirred for 30 min, after which, initiator weighing 14.4, 28.8, or 43.4 mg (3.7, 7.4, and 11 mM, respectively) and reacted with 322 mL of sodium methoxide added under argon. 1,8-diazabicyclo[5.4.0] undec-7-ene was added under argon to the solution 15 min later and the entire reaction stirred for 24 h.

The NP solution was exposed to air for 2 h following the reaction and dialyzed for 3 days against 4 x 5 L of Milli Q water using a 100,000 Da molecular weight cut off cellulose membrane dialysis tubing (Spectrum Lab., Rancho Dominguez, CA, USA, 131414). The NP were S-nitrosated before each experiment by reacting equal volumes of NP with sodium nitrite solution in strong acid. Unreacted free acidified nitrite was capped with addition of ammonium sulfamate and purified from the SNO-NP solution using 7 kDa Zeba columns (Thermo Fisher). SNAP solution was prepared by dissolving SNAP in 1x PBS solution. S-nitrosothiol (SNO) concentrations in solutions were measured using the method of Saville (described below). For experiments that required fluorescent labeling of NP, NP were reacted with Alexa Fluor 647 C2 Maleimide (Thermo Fisher) followed by excess of N-ethylmaleimide (NEM) until free thiols were no longer detectable by Ellman's assay. The solution was purified of free Alexa Fluor 647 and NEM using a PD-10 column (GE Healthcare, Pittsburg, PA, USA, 17-0851-01). NP size was determined by dynamic light scattering (Malvern Instruments).

4.2.3 IVIS imaging

Fluorescent imaging was performed with an IVIS® Spectrum instrument (Perkin Elmer). Animals were injected intradermally in the forearm with a solution of Alexa Fluor 647-NP or of SNO treatment group either with or without Alexa Fluor 647 labeling. Twenty-four hours later the animals were sacrificed. To assess Alexa Fluor 647-NP drainage to LN, animals were imaged using Ex: 640, Em: 680 and an exposure of 0.1 s. For the SNO-NP colocalization experiment with NO, immediately after the animals were sacrificed, the skin was removed and 5 µL of a 1:1 solution of 4-Amino-5-methylamino-2',7'-fluorofluorescein diacetate (DAF-FM DA) (Cayman

Chemical), which works to identify NO through fluorescence due to the nitrosation of the diamino group resulting in a fluorescent triazole that has a 160-fold increase in fluorescent quantum yield and a fluorescence profile similar to fluorescein (FITC),[165] and 1% mercuric chloride was injected into the brachial LN on the right side. The animals were then immediately imaged for both the Alexa Fluor 647-NP using 647 channel and DAF using the FITC channel (Ex: 500, Em: 540) at an exposure of 0.1 s. Total fluorescent counts and radiant efficiency (p/s sr uW) were evaluated for each experiment and treatment group using elliptical regions of interest in Living Image Software (Perkin Elmer). Fluorescent signal for Alexa Fluor 647-NP LN drainage was normalized to the fluorescent signal measured at the site of injection.

4.2.4 Use of animals

All animal procedures were performed with Institutional Animal Care and Use Committee (IACUC) approval and animals were housed in a central animal facility at Georgia Institute of Technology.

4.2.5 Quantification of NP LN accumulation

To determine the amount of NP accumulated in draining LN, either fluorescence quantification of fluorescently labeled NP[10, 104] or a modified assay measuring PEG using Iodine and barium chloride, which form a barium-iodide complex of the glycol, was performed.[166, 167] For the fluorescent quantification of percent of injection, LN homogenate was taken and read at 655/675 nm, and the concentration of Alexa Fluor 647-NP was determined using a standard curve of Alexa Fluor 647-NP that was allowed to react at 37°C for 24 h. For the iodine PEG assay centrifuged LN homogenate, BaCl solution in 1N HCL, and KI solution supplemented were reacted. The

absorbance was measured at 535 nm, and the concentration of NP was determined using a standard curve of NP diluted in 1x PBS.

4.2.6 Determination of SNO, NO_2^-, and $ONOO^-$ concentration using modified Saville, Griess, and coumarin boronic acid assays

The Saville and Griess assays, which work on the principle of a two-step diazotization reaction between a sulfanilamide-based diazonium ion, formed from nitrite under acidic conditions, coupled with N-(1-naphthyl)ethylenediamine dihydrochloride (NEDD), were performed as previously described.[13] Briefly, sample solution (NO donor, tissue homogenate, or plasma) was mixed with either sulfanilamide solution or mercuric chloride solution prior to mixing these solutions with NEDD or 0.4N HCl. Absorbance was read at 540 nm and the difference between mercuric chloride and sulfanilamide solutions and the difference between sulfanilamide solution with and without NEDD taken as the SNO and NO_2^- signals, respectively. SNO and free NO_2^- concentrations were calculated using a standard curve of S-nitroso-beta-mercaptosuccinic acid. Sample peroxynitrite ($ONOO^-$) was measured using a 1:1 mixture with 100 mM coumarin boronic acid (Cayman Chemical) (10 mg/mL in Dimethylformamide (DMF) diluted in 1x PBS), which works to identify $ONOO^-$ through oxidation by ONOO- to the fluorescent probe coumarin in a stoichiometric fashion, or PBS to determine tissue background and fluorescence measured at 370/455 nm after 15 min of reaction (short time to limit possible measurement of hydrogen peroxide, which occurs at a much slower rate) $ONOO^-$ was calculated using a standard curve of $ONOO^-$ solution (Cayman Chemical) in 0.3N NaOH.

4.2.7 SNO release studies

SNO-NP solutions in 1x PBS were incubated in closed vessels at 37°C and SNO concentrations monitored over 72 h using the Saville assay.

4.2.8 In vivo SNO LN delivery time course studies

C57BL/6J mice were injected intradermally in the forelimbs with 30 µL of treatment solution. The animals were maintained under isoflurane anesthesia for the duration of the injection. At the indicated times post-injection, animals were anesthetized using isoflurane and blood harvested by cardiac puncture using a 27-guage needle and 1 mL syringe prefilled with 15 µL 50 mM ethylenediaminetetraacetic (EDTA). The blood was transferred to a microvette tube containing K4EDTA (microvette) and stored on ice until analysis (<1 h). Animals were then sacrificed by cervical dislocation and tissues, including LN, spleen, kidneys, and liver, were separately harvested, homogenized and weighed in preweighed tubes containing zirconium beads and 450 µL 13 PBS as previously described.[163, 164] Plasma was prepared from whole blood by centrifugation at 2000 g for 10 min, transferring the plasma layer into a microtube and retaining the supernatant. The homogenates (other than those prepared from harvested LN) were diluted lower to 5 wt/wt% in 1x PBS to reduce background for the Saville and Griess assays.[60, 168-170] All homogenate solutions were subsequently centrifuged at 10,000 g for 20 min and supernatants transferred for determination of SNO, NO_2^- , and $ONOO^-$ concentrations using the Saville, Griess, and coumarin boronic acid assays, respectively, described above.

4.2.9 Flow cytometry

Mice were injected with SNO treatment group either with or without Alexa Fluor 647 labeling. Twenty-four hours later the mice were sacrificed and both LN

from the same injection side of the animal were placed in 900 µL PBS on ice in the dark. One hundred microliters of 10 mg/mL Collagenase (Roche) solution in PBS was added to each LN well and incubated for 1 h at 37°C. LN were then gently separated through a 70 mm cell strainer into 50 mL conical tubes using a 1 mL syringe plunger. Ten milliliters PBS was added to push cells through and then the cells were spun down at 300 g for 5 min. The cells were counted and then plated in their entirety into a round bottom 96-well plate. The cells were stained with 100 µL of 2.4G2 solution, followed by Zombie Aqua Live/Dead (Biolegend) solution, and then finally monoclonal anti-mouse mAb (Biolegend) (BV411 CDllc; BV650 B220; BV711 CD3; PE CD169; AF700 CD11b). Data was acquired in a LSRFortessa (BD Biosciences) flow cytometer with compensation using either calibration beads (Thermo Fisher) or single-stained cells. Data analysis was performed using FlowJo software (FlowJo).

4.2.10 Histology

Two percent paraformaldehyde fixed forelimbs were paraffin embedded, sliced to 10 µm thickness, decalcified, and stained with hematoxylin and eosin. The slices were imaged using a Hamamatsu Nanozoomer.

4.2.11 Statistical analysis

Data are expressed as mean6standard error of the mean. Statistical analysis was performed using Prism 6. Statistical significance was defined as $p \leq 0.05$.

4.3 Results

4.3.1 SNO-NP characterization

We previously described an NO-donating NP formulation[13] based on the

formation of SNO within oxidation-sensitive poly(propylene sulfide)-core, pluronic block copolymer corona NP.[94, 108] These NP are sufficiently small (approximately 30 nm in diameter for optimum lymphatic uptake[9, 11, 67, 163, 164] to be taken up into lymphatic vessels and passively transported to the draining LN[10, 67, 104] over the course of several days after injection (Figure 4.1b,c) proportional to the administered NP dose (Figure 4.1d)

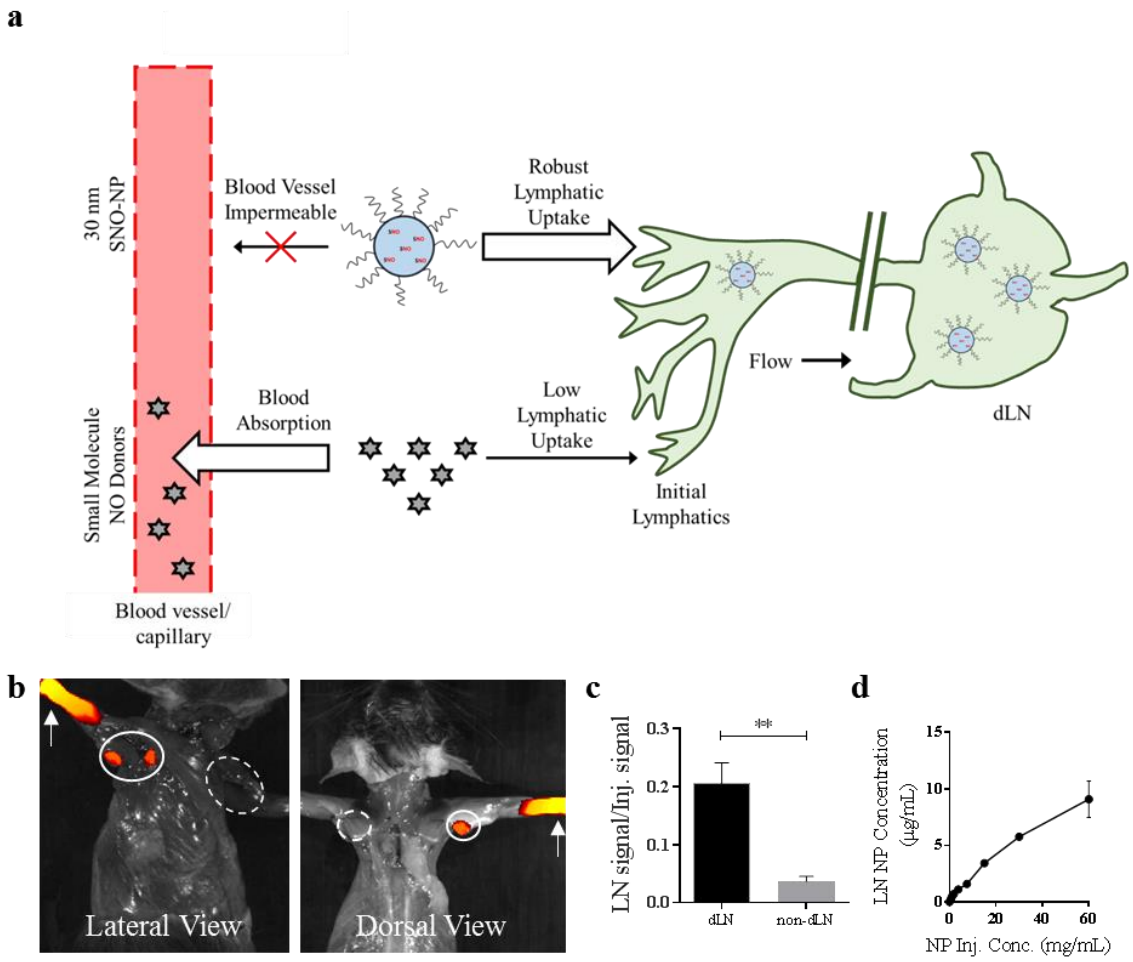

Figure 4.1: NO delivery to lymphatic tissues using lymphatic-draining NPs. a) By virtue of their blood impermeability that prolongs their retention at the site of injection, hydrodynamically large drug delivery vehicles such as 30 nm lymphatic-draining NP have enhanced lymphatic uptake relative to small molecules, which can be leveraged to enhance LN delivery of encapsulated NO. Representative IVIS images (b) and quantification (c) of Alexa Fluor 647-labeled NP transport from

the site of injection (white arrows) in the forearm skin to the draining ipsilateral (closed line) axillary and brachial LN (dLN) but not nondraining contralateral (dashed line) LN (non-dLN) after 24 h. n=6 samples per group. d) NP drain to LN from the site of injection in a manner proportional to the starting concentration of injected NP. **p<0.01.[149]

In this NP formulation, the high concentration of free thiols in the hydrophobic NP core allows for efficient and rapid loading of NO through the formation of SNO (Figure 4.2a). This reaction occurs very quickly and reaches peak efficiency, as determined by the concentration of SNO measured compared to the total NP thiol concentration, between 10 and 20 min of reaction time (Figure 4.2b). SNO formation is also most efficient when the acidified nitrite is between 2 and 4 equivalents of NP free thiol (Figure 4.2c,d), likely due to the process of high concentrations of nitrite converting to a nitrosating species in low pH resulting in several side reactions occurring between the acidified nitrosating species and SNO formed[23, 171] that often cause the SNO decomposition. Formation of SNO-NP does not alter NP hydrodynamic size (Figure 4.2e), which can be synthesized to a range based on the pluronic-to-propylene sulfide monomer ratio used,[114] nor polydispersity (data not shown), indicating that the acidic nitrosating conditions do not affect the Pluronic critical micelle concentration nor promote degradation of the stabilizing core disulfide bonds. To ensure that the loaded NO will maintain its stability in the NP over time and as dilution occurs, as well as the capacity of multiple SNO doses to be utilized in a controlled manner, we tested the degradation of the SNO from SNO-NP at 37°C. SNO-NP were diluted to one of three concentrations: 10, 5, and 1 mM. SNO decay from SNO-NP was steady over the entire 72 h for each tested dilution (Figure 4.2f) and the decay half-life was insensitive to starting SNO concentration (Figure 4.2g), indicating that as the SNO-NP concentration changes *in vivo* the release profile of NO is not significantly altered.

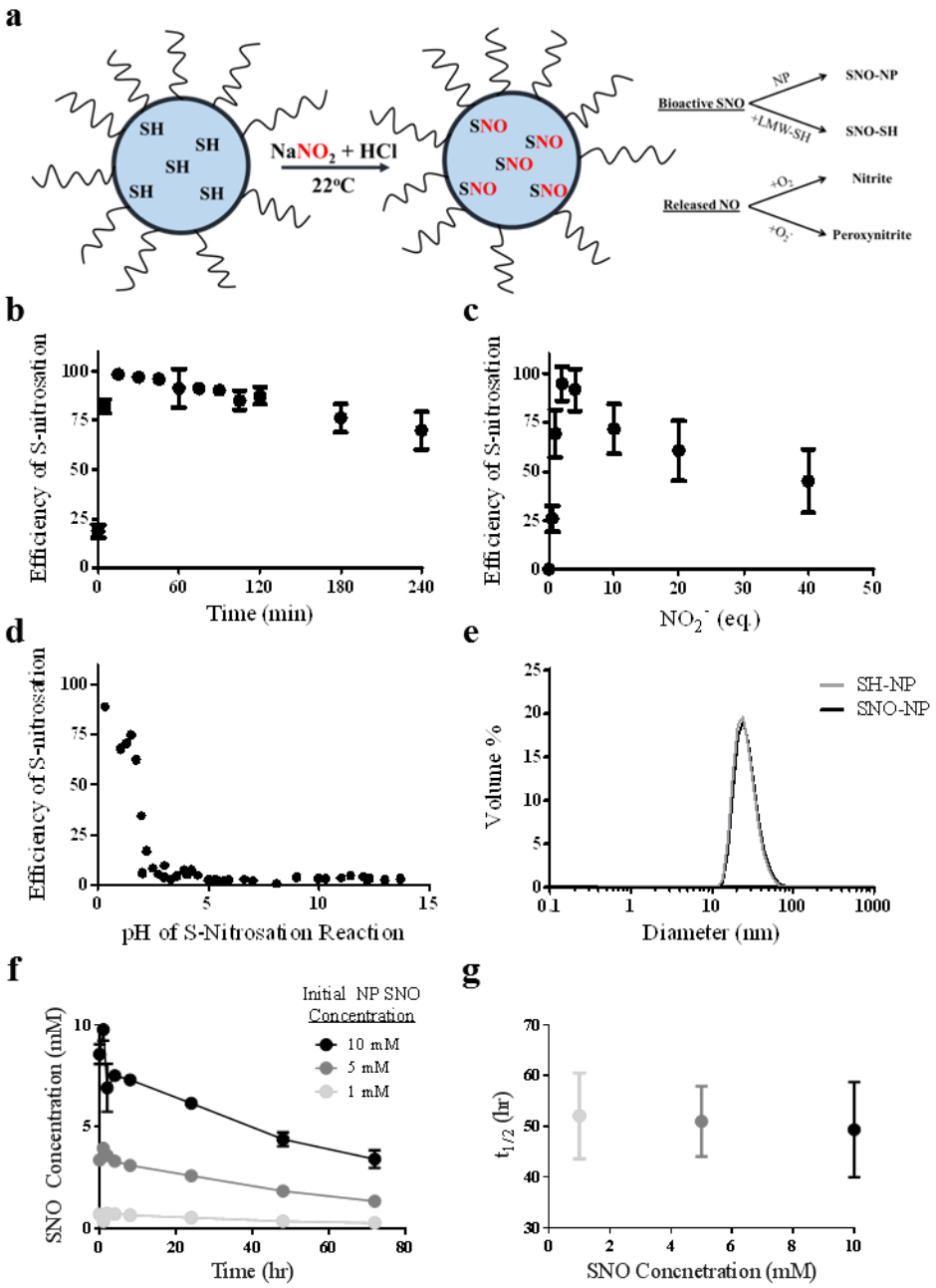

Figure 4.2: Synthesis and characterization of S-nitrosothiol poly(propylene sulfide) NPs (SNO-NP). a) Schematic of micellar structure of pluronicstabilized, poly(propylene sulfide) NP containing free core thiols that become S-nitrosated using an acidified sodium nitrite protocol at room temperature. SNO on the SNO-NP can either be retained on the NP or can be transnitrosated to a low molecular weight thiol (LMW-SH); NO that is released from the SNO-NP will be either oxidized with oxygen to nitrite, or will interact with superoxide and form peroxynitrite. b) Efficiency of S-nitrosation reaction, defined as the amount of S-

nitrosothiol that can be generated per amount of starting free thiol concentration, reaches a maximum around 15 min. c) Efficiency of S-nitrosation reaches a maximum at 2–4 eq. sodium nitrite to free core thiols. d) Low pH is required for the S-nitrosation reaction with sodium nitrite and free core thiols. e) SNO-NP are stable and the same size as unmodified NP, indicating that the Pluronic-stabilized, poly(propylene sulfide) NP structure remains stable under these conditions. f) SNO decay from SNO-NP at different starting SNO concentrations over 3 days. g) The approximately 50 h half-life of the SNO release from SNO-NP is constant at 37°C regardless of starting SNO concentration. n=3 samples per group.[149]

4.3.2 In vivo NO donation

We next implemented a well described intradermal forearm lymphatic delivery model, whose lymphatic network efficiently drains to the ipsilateral axillary and brachial LN (Figures 4.1b and 4.3a),[10] to assess the delivery and retention of NO delivered through SNO-NP or standard small molecule SNAP. Whole animal imaging of NP and NO probe DAF-FM DA (mixed 1:1 with HgCl II), fluorescence 24 h post-injection revealed that only SNO-NP, which accumulated within LN draining the site of intradermal injection (Figure 4.3 a,b), and not SNAP resulted in appreciable LN NO signal (Figure 4.3c,d).

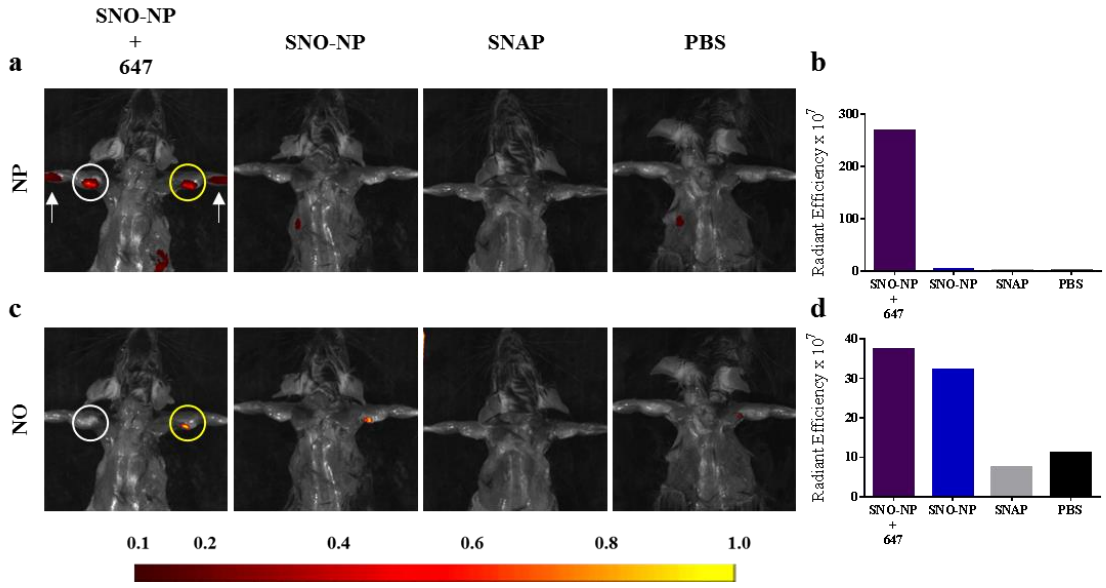

Figure 4.3: Colocalization of NO and SNO-NP fluorescence in LN draining site of injection demonstrates NP-mediated lymphatic transport facilitates NO delivery to LN. Representative IVIS images (a, c) and quantification (b, d) of Alexa Fluor 647 (a, b) and NO probe DAF-FM DA (c, d) fluorescence in draining LN associated with SNO-NP, but not SNAP administration in the forelimb skin. White arrow, intradermal site of treatment group injection; white circle, LN draining the site of intradermal injection; yellow circle, DAF-FM DA injected LN.[149]

Next, using the absorbance-based assays of Saville and Griess to measure RNS within harvested, homogenized tissues through endpoint analysis, we found that following intradermal administration of SNO-NP or SNAP loaded with 20 mM SNO, that SNO was only significantly elevated in the LN over the course of 72 h post-injection relative to control (saline injected) animals when delivered through the SNONP (Figure 4.4a). These results are consistent with our image-based detection of LN-delivered NO (Figure 4.3) and confirm our hypothesis that small molecule NO donors are not sufficiently transported to the LN, requiring, instead, lymphatic-draining NP that can be leveraged to achieve robust SNO accumulation within the LN. Neither nitrite (NO_2^-) nor $ONOO^-$, RNS implicated in NO bioactivity[122] and cytotoxicity,[172, 173] respectively, were detected at levels above background for any assayed time post-injection with either

NO donor (Figure 4.4b,c). As the result of SNO-NP, SNO levels in plasma were elevated 1 h post-injection, but returned to near baseline (saline) by 24 h post-injection (Figure 4.4d). SNAP, on the other hand, resulted in a higher but not statistically significant different plasma SNO concentration relative to saline-control-treated animals over the course of the experiment (Figure 4.4d), most likely owing to a constant clearance from the interstitial site of injection. No changes in plasma NO_2^- and $ONOO^-$ levels compared to saline controls were measured over the time course of experimentation (Figure 4.4e,f). RNS levels in the spleen, kidneys, and liver remained unchanged relative to saline controls over the course of the experiment for both NO donor treatment groups, except in the case of the liver where there was a small increase in $ONOO^-$ measured in animals treated with either NO donor (Figure 4.4h). Within draining lymph node (dLN), however, SNO levels above those in saline-treated animals were found to be elevated 100-fold for SNO-NP- relative to SNAP-treated animals (Figure 4.4g). $ONOO^-$ exposure was also modestly elevated in LN as the result of SNAP treatment (Figure 4.4h). Neither NO_2^- nor $ONOO^-$ concentrations were elevated in plasma, whereas SNO levels increased, with SNO-NP and SNAP treatment differing approximately twofold, but not to statistically significant levels (Figure 4.4i).

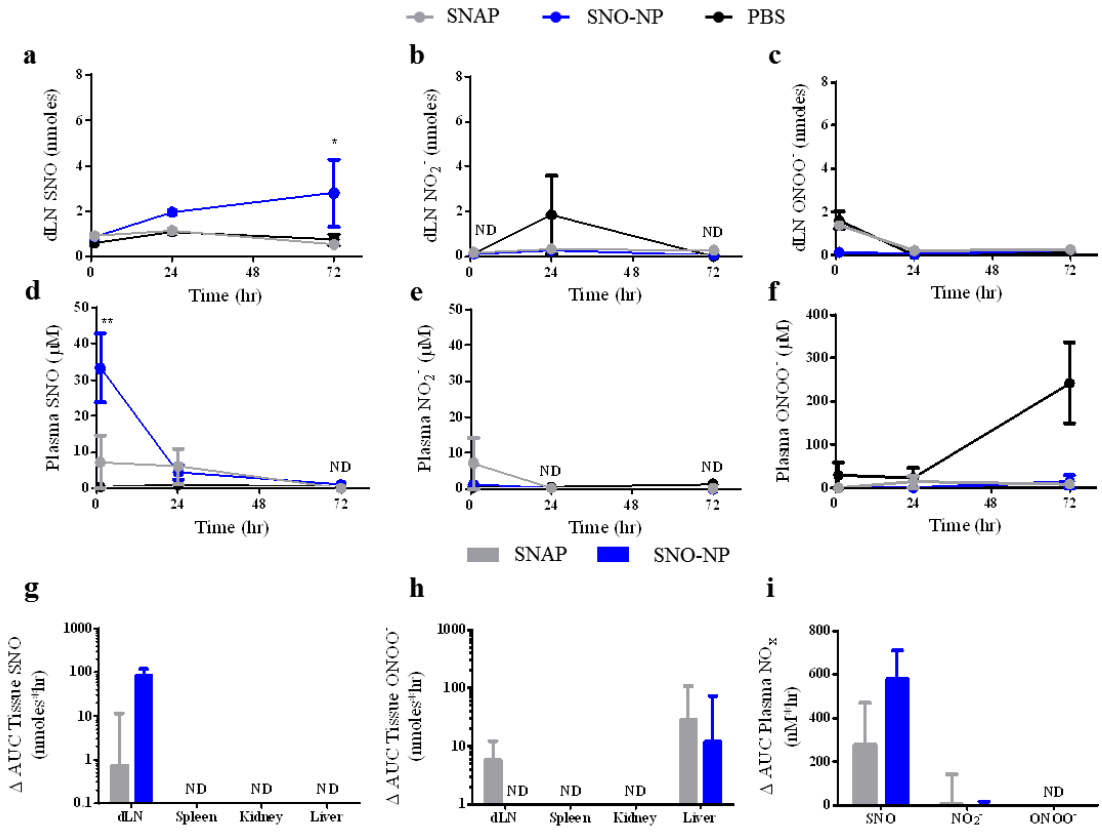

Figure 4.4: SNO-NP improve delivery of SNO to LNs draining the site of intradermal injection compared to small molecule NO donor. a) SNO-NP showed improved delivery and retention over 72 h of SNO to LN compared to SNAP. * indicates statistically greater SNO for SNO-NP compared to SNAP. b) No appreciable accumulation of nitrite within LN for either SNO-NP or SNAP compared to control. SNO-NP and SNAP signals were not detectable (ND) at 1 or 72 h. c) No appreciable accumulation of peroxynitrite within LN for either SNO-NP or SNAP compared to control. d) SNO-NP showed early spike in SNO concentration within plasma, whereas SNAP peaks at 24 h. PBS and SNAP signals were ND at 72 h. ** indicates statistically greater SNO for SNO-NP compared to SNAP. e) No appreciable accumulation of nitrite within plasma for either SNO-NP or SNAP compared to control. SNO-NP and SNAP signals were ND at 24 and 72 h. f) No appreciable accumulation of peroxynitrite within plasma for either SNO-NP or SNAP compared to control. g) SNO-NP showed greater bias of SNO delivery compared to SNAP to LN than to plasma. Levels of SNO accumulation in the spleen, kidney, and liver were ND. h) There was a modest accumulation of peroxynitrite in the LN for SNAP but not SNO-NP, whereas in the liver there was a larger, but not statistically significant, difference in accumulation of peroxynitrite in the liver. The accumulation of peroxynitrite in the spleen and kidney was ND for all groups. i) In the plasma there was a noticeable but not statistically significant difference in the area under the curve (AUC) of SNO signal for SNO-NP vs. SNAP.

g–i) PBS AUC was subtracted from SNO-NP or SNAP AUC. For all graphs the columns/points and error bars represent the mean + SEM (n=3–6 samples per group). *p<0.05, **p<0.01.[149]

The capacity of SNO-NP to control the level of NO delivered to lymphatic tissues was next evaluated in an *in vivo* dosing study. SNO dilutions were created through simple dilution of SNO-NP solution or when SNO-NP were formed from NP of differing thiol levels (Figure 4.5a). We found total dLN SNO (Figure 4.5b) but not NO_2^- (Figure 4.5c) levels generated as a result of SNO-NP treatment 24 h post-injection were proportional to the concentration of total SNO administered, irrespective of how the SNO dilutions were generated. Levels of both SNO and NO_2^- in plasma were either not detectable or not statistically higher than saline controls (data not shown), save the highest tested dose of SNO-NP, 20 mM. Suggesting corresponding biological effects on lymphatic tissues, LN draining the site of injection also increased in size proportionally to administered NO amount (Figure 4.5d); an effect attributed to the bioactive SNO since delivery of increasing concentrations of plain NP did not result in changes to the LN (data not shown).

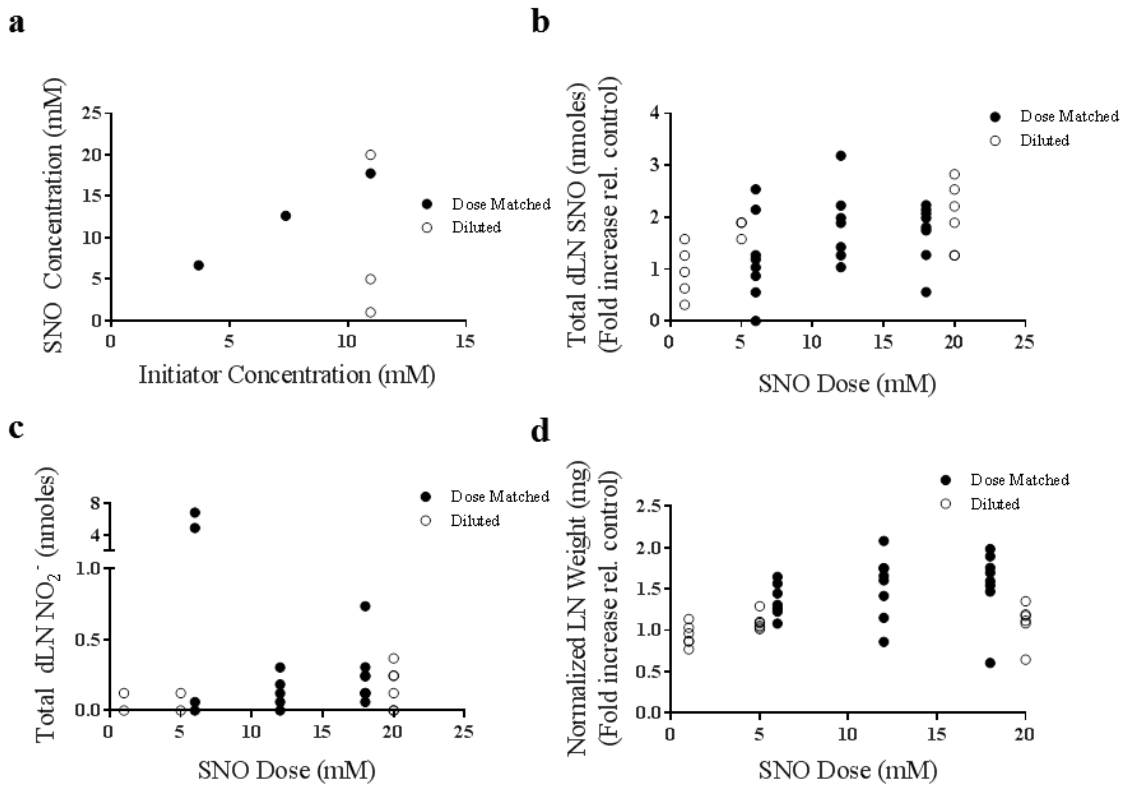

Figure 4.5: SNO-NP can be synthesized to deliver a wide range of SNO doses that accumulate within the dLN in a manner proportional to concentration. a) The SNO concentration of SNO-NP can be modified by either diluting maximally nitrosated SNO-NP with a high starting SNO concentration, or by synthesizing SNO-NP with different initiator concentrations such that the maximal nitrosation results in differing SNO concentrations due to the altered free thiol concentration. b) The total SNO within the dLN at 24 h is proportional to the amount of SNO delivered by SNO-NP either by dilution or by dose-matched NP batches with different initiator concentrations. c) Total nitrite within the dLN at 24 h was relatively insensitive to starting SNO concentration of SNO-NP. d) The weight of dLN 24 h post-injection was increased slightly in proportion to the starting SNO concentration of SNO-NP. For all graphs the columns/points and error bars represent the mean + SEM (n=3–8 samples per group).[149]

4.3.3 SNO-NP effects on dLN-resident cell viability, abundance, and NP uptake

We next sought to begin to elucidate the effect of NO delivery to LN on resident cells. First, the viability of total (Figure 4.6a), CD451 (immune) cell subtypes including lymphocytes (T and B cells, CD3+B220- and B220+CD3-CD11b-, respectively), conventional and plasmacytoid dendritic cells (CDC - CD11c+B220- and PDC -

CD11c+B220+, respectively), and medullary sinus macrophages (MSM): B220-CD3-CD11b+CD11c+CD169+F4/80+; subcapsular sinus macrophages (SSM): B220-CD3-CD11b+CD11c+CD169+F4/80-; medullary cord macrophages (MCM): B220-CD3-CD11b+CD11c+CD169-F4/80+, respectively (Figure 4.6b) resident within dLN 24 h post-injection was found to remain unchanged by SNO-NP treatment relative to control animals, as well as treatment with plain NP and SNAP, as assessed by flow cytometry. Despite no significant changes in viability, the abundance of cells within LN draining the site of injection was dramatically increased by SNO-NP but not SNAP or plain NP treatment; in particular T and B lymphocytes were more abundant, as well as both conventional and plasmacytoid dendritic cells and MCM subtypes, albeit for the later three cell types not to a statistically significant extent (Figure 4.6c). However, the proportionality of LN-resident CD45+ cell subpopulations remained approximately equivalent (data not shown). Notably, while the frequency of total LN-resident cells that took up or were associated with NP 24 h post-injection was somewhat reduced for SNO-NP- relative to NP-treated animals, the total number was negligibly affected by NP-mediated SNO delivery to LN (Figure 4.6d). SNO delivery resulted in NP associating to higher extents with CDC, PDC, and MCM (Figure 4.6e), and at diminished frequencies with LN-resident T and B cells (Figure 4.6f).

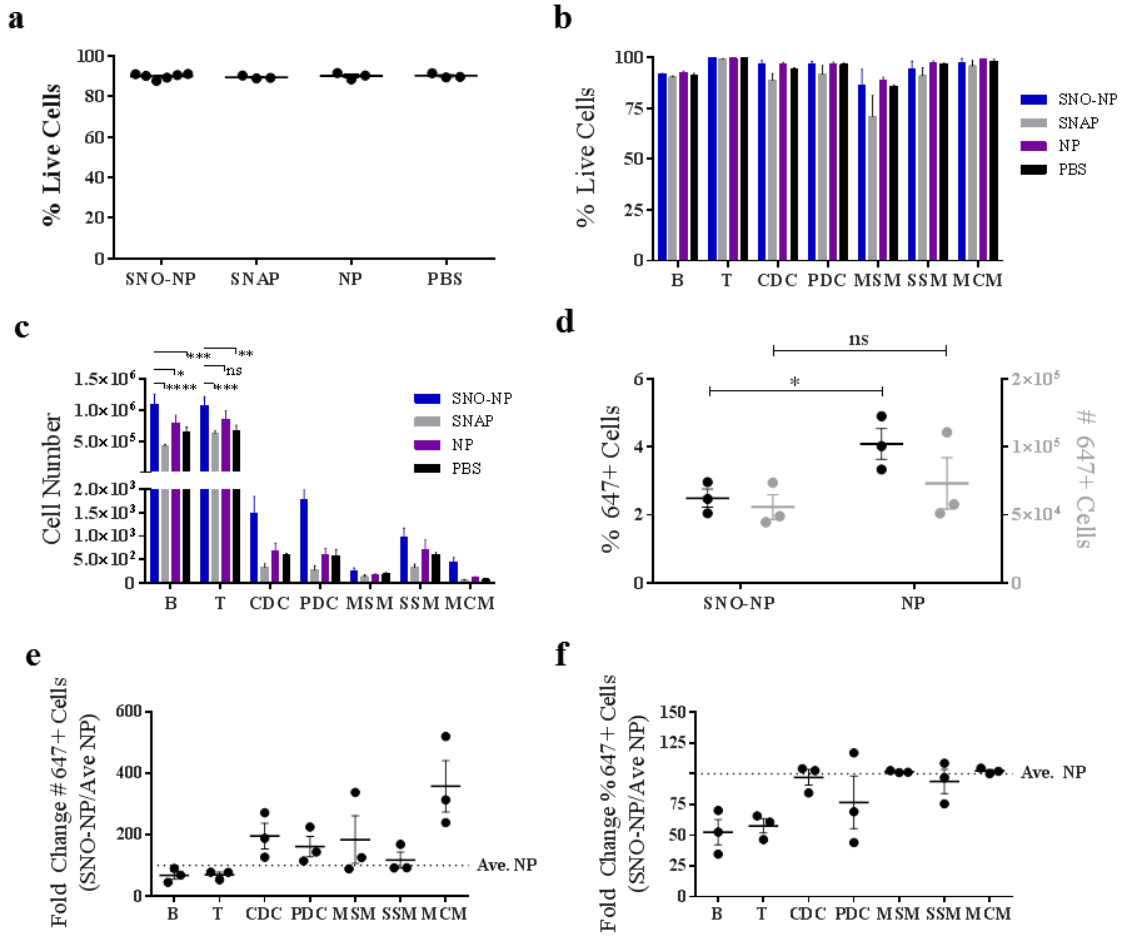

Figure 4.6: SNO delivery by SNO-NP does not negatively affect the viability but increases the number of cells resident within LNs draining the site of intradermal injection, resulting in modestly altered distributions of cellular NP accumulation. a) SNO delivery from SNO-NP did not affect the viability of dLN cells compared to small molecule NO donor SNAP, plain NP, or PBS control. b) SNO delivery from SNO-NP did not alter the viability of any specific cell subtype within the LN compared to other groups. c) SNO delivery from SNO-NP resulted in increased numbers of B and T cells relative to SNAP, plain NP, and PBS control. While SNO delivery from SNO-NP also resulted in increased numbers of other cell types, the results were not statistically significant. d) SNO delivery from SNO-NP resulted in a reduction in both the number and percentage of NP positive cells. e) SNO delivered from SNO-NP resulted in an increased number of NP positive dendritic and macrophage cells while showing a slight reduction in the number of NP positive B and T cells compared to plain NP control. f) SNO delivered from SNO-NP did not affect the percentage of NP positive dendritic and macrophage cells, but did result in a drastic reduction in the percentage of NP positive B and T cells compared to plain NP control. Cells were gated as follows: B cells – B220+CD3-CD11b-; T cells – CD3+B220-; conventional dendritic cells (CDCs) – CD11c+B220-; plasmacytoid

dendritic cells (PDCs) – CD11c+B220+; subcapsular sinus macrophages (SSM) – B220-CD3-CD11b+CD11c+CD169+F4/80-; medullary sinus macrophages (MSM) - B220-CD3-CD11b+CD11c+CD169+F4/80+; and medullary cord macrophages (MCM) - B220-CD3-CD11b+CD11c+CD169-F4/80+. For all graphs the columns/points and error bars represent the mean + SEM (n=3–6 samples per group). *p<0.05; **p<0.01; ***p<0.001; ****p<0.0001; ns, not significant.[149]

4.3.4 Locoregional vs. systemic NO donation-associated inflammation and toxicity

Given NO's pleiotropic and potential cytotoxic effects,[29, 35, 174] local and systemic markers of inflammation associated with NO donor treatment were assessed. Histological analysis of paraffin fixed slices of treated forelimbs revealed no apparent morphological changes in skin quality, thickness, or granularity for either NO donor treatment at 20 mM administered dose compared to saline control (Figure 4.7a). Despite increases in LN size associated with SNO-NP, but not SNAP, treatment, spleens of treated animals remained unchanged in gross size[102, 175] relative to control-treated animals 24 h post-injection (Figure 4.7b). Levels of plasma alanine transaminase (ALT) and aspartate transaminase (AST), markers of liver toxicity,[176] similarly were unchanged at all analyzed times post-injection (Figure 4.7c).

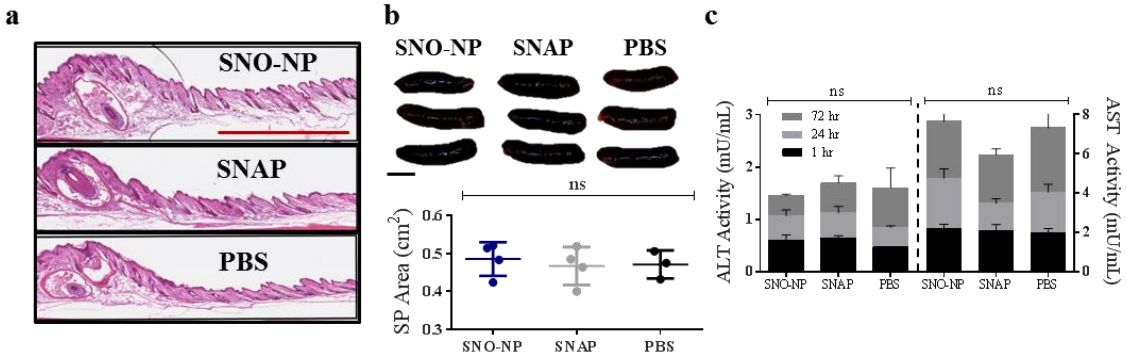

Figure 4.7: Intradermal administration of SNO-NP does not result in local or systemic inflammation. a) Representative images of the inflammation reveal no qualitative difference in skin thickness or cellularity between groups. Red bar, 1 mm. b) Top, representative spleen images from treated mice. Scale bar, 0.5 cm. Bottom, spleen sizes were found to not be statistically significantly different between

groups measured after 24 h treatment. c) There was no statistically significant difference in time-matched alanine transaminase (ALT) or aspartate transaminase (AST) measurements from the plasma over a 72 h time course between groups. n=3–7. ns, not significant.[149]

4.3.5 SNO-NP effects on lymphatic transport

With evidence of SNO-NP enhancing the efficiency of SNO delivery to LN compared to small molecule NO donor SNAP, we sought to determine how changing the dose of SNO delivered would affect the overall lymphatic transport to draining LN, as NO is known to affect lymphatic pumping function.[24, 25] As a metric of lymphatic transport function, total delivered amount of NP to LN was quantitatively assessed by endpoint analysis using an iodine-based absorbance assay on homogenized tissues, which overcomes the significant sensitivity limitations of whole animal imaging. NP accumulation within dLN was sustained, with a steep increase from the time of injection to 1 to 24 h followed by a slower and smaller increase from 24 to 72 h (Figure 4.8a). Furthermore, over the range of SNO concentrations tested (6–20 mM), NP accumulation within LN draining the site of injection was only modestly diminished and in a dose-independent manner 24 h post-injection (Figure 4.8b).

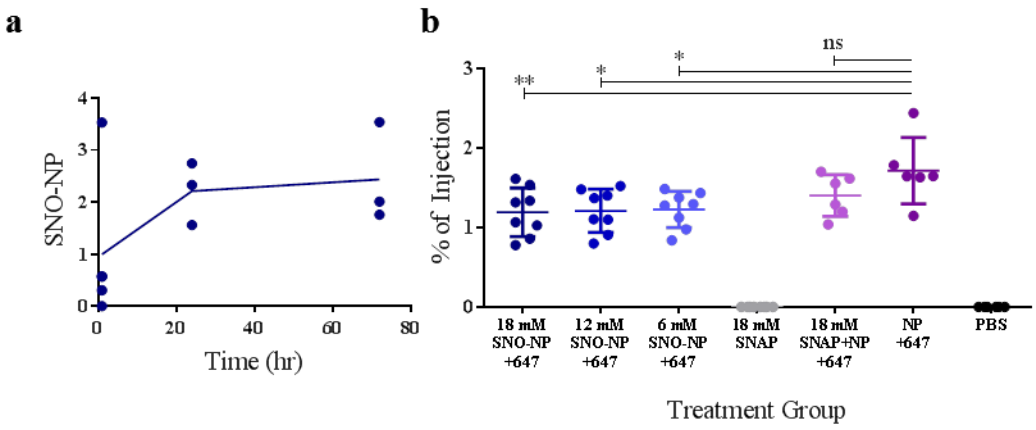

Figure 4.8: SNO-NP efficiently drain to the LN and cause only a modest diminution in total NP LN accumulation. a) SNO-NP drained to and accumulated in the LN over 72 h as measured by iodine PEG stain assay. b) There was no statistically significant difference in the percent of injection of SNO-NP solution when the dose of SNO was altered, however, compared to plain NP the presence of SNO modestly attenuated the overall accumulation of Alexa Fluor 647-labeled NP in LN 24 h postinjection as measured by fluorescence. For all graphs the columns/points and error bars represent the mean + SEM (n=3–8 samples per group). *p<0.05; **p<0.01; ns, not significant.[149]

4.4 Discussion

While there have been several examples of reformulation of NO donors to achieve improved pharmacokinetics and biodistribution, including improving circulation time through polyethylene glycol conjugation[72] and NO bioactivity through multivalency,[73] to our knowledge no attempts have been taken to create a NO donor specifically for targeting lymphatics.[74] Several examples exist of larger molecular weight NO donors including a 64-valency R-SNO dendrimer donor[73] and NO-containing NP;[75-79] however, all of these approaches presumably remain insufficient for NO modulation within the lymphatics because such formulations are non-optimal for lymphatic uptake.[163]

In this work, we explored the *in vivo* NO donating capacity of a SNO-NP delivery vehicle we previously reported that exhibits controlled profiles of NO release in its bioactive form.[13] Rapidly (approximately 10–20 min) nitrosated at close to 100% efficiency at approximately 2–4 molar equivalents of acidified nitrite (Figure 4.2b–d), these SNO-NP leverage a NP formulation, that by virtue of their size (Figure 4.2e) exhibit superior *in vivo* targeting of lymphatic tissues relative to conventional drug formulations (Figure 4.1b–d).[10, 177] We found these SNO-NP, which have a SNO dose-independent half-life of two days, to exhibit sustained levels of accumulation within LN draining the site of intradermal injection (Figure 4.8b). As a result, SNO-NP significantly increase the delivered dose of SNO to LN draining the site of intradermal injection (Figure 4.4a), resulting in an approximately 100-fold increase relative to SNAP in levels of SNO exposure above PBS-treated animals over 72 h post-injection (Figure 4.4g). This was accompanied by only an increase in plasma SNO levels 1, but not 24 or 72 h post-injection (Figure 4.4d), a modest (approximately twofold) and not statistically significant increase in total plasma SNO exposure (Figure 4.4i), and no change in baseline NO_2^- or $ONOO^-$ levels (Figure 4.4(b,c,e,f,h,i). These dose-dependent effects (Figure 4.5), which were consistent whether generated by SNO-NP dilution of changing the extent of nitrosation through NP formulation, demonstrate the selectivity of NO, and predominantly SNO, delivery to lymphatic tissues mediated by SNO-NP is tightly controllable.

We expect much of the SNO measured over the time scales of this study to be SNO remaining on the SNO-NP due to its half-life and high starting concentration. We can also infer that SNAP, which we would expect to be cleared from the skin site of

injection within minutes and to not be able to transport efficiently to the LN due to its size (approximately 220 Da),[11, 163, 164] does not transnitrosate to an appreciable extent to any large molecular weight proteins such as albumin that are capable of better transporting to the LN[102, 178] due to the lack of increased SNO in LN draining SNAP-injected skin tissues (Figure 4.4a). Contrast this with the increased plasma levels of SNO resulting from SNO-NP 1 h post-injection (Figure 4.4d). Because these 30 nm NP do not have efficient access to the blood vasculature[104, 163] they would be retained for prolonged times at the site of injection,[163, 164] and because we have previously reported their propensity to efficiently transnitrosate physiological thiols,[13] we hypothesize that this initial spike is due to rapid transnitrosation of intradermally present small molecule thiols (cysteine, e.g., which can be present in excess of 100 μM [148]). Second, this may explain the only modest and dose independent changes in levels of NP LN accumulation resulting from SNO- vs. plain NP (Figure 4.8a). Because it has been shown that attenuation of lymphatic function (characterized by an increase in diastolic diameter and a reduction in pumping frequency) occurs with application of exogenous NO,[31, 178, 179] it is plausible that NP accumulation within LN would be more dramatically attenuated at times post-injection longer than the 24 h assessed here when more NO has been released from SNO-NP (Figure 4.2f,g). Additionally bolstering these two hypotheses are the fact that NO production in the interstitial space is involved in alterations of the microcirculation[180] resulting in greater blood flow through increased vascular permeability[181] as well as increased arteriolar vessel dilation.[182] These observations, often associated with the tumor vasculature,[182] further explain the 1 hr plasma spike of SNO from SNO-NP as well as the reduction in LN accumulation of

SNO-NP, which likely results from a NO-mediated combination of increased vascular access of the SNO-NP as well as a reduction in lymphatic pumping function.

Despite the highly reactive and potentially cytotoxic nature of NO, we observed histologically no signs of inflammation at the site of SNO-NP injection, as either changes in skin thickness or granularity (Figure 4.7a), which is in line with several studies reporting the lack of inflammatory effects from NO donors.[77, 183-189] Additionally, no increases in $ONOO^-$ were detected in any assayed tissue (Figure 4.4c,f,i), spleen sizes remained unchanged (Figure 4.7b), and plasma alanine transaminase and aspartate transaminase levels remained unchanged relative to saline-treated animals (Figure 4.7c). We did observe, however, increases in LN size (Figure 4.5d) that were potentially explained by flow cytometry analysis revealing dramatic increases in resident immune cell frequencies (Figure 4.6c), an effect potentially arising from the influx of cells circulating in the blood[190] caused by LN-delivered SNO mediated by lymphatic-draining NP. This is supported by measured frequencies of NP association with T and B cells dropping approximately 50% (Figure 4.6f) while total cell counts correspondingly increased approximately 30% (Figure 4.6c). Furthermore, the viability of LN-resident cells was not diminished by SNO-NP treatment (Figure 4.6a,b). Consistent with only modest decreases in total levels of NP accumulation within LN as a result of SNO delivery (Figure 4.8a), the extent of NP uptake by LN-resident cells remained similar (Figure 4.6d). However, SNO-NP did associate at increased levels with dendritic cell and MCM subtypes (Figure 4.6e) corresponding to the measured increases in abundance of these cell subtypes (Figure 4.6c), while the total frequency of NP-associated cells remained similar to plain NP indicating that these cells' barrier/scavenger functions[84,

191, 192] were unperturbed by SNO delivery. On the other hand, T and B cell abundance similarly increased (Figure 4.6c), but total frequencies of NP-associated lymphocytes were nearly inversely reduced (Figure 4.6f), hinting that NO release did not alter access of SNO-NP to these cells and that the reduced frequency was due to a dilution effect. Taken together, these data indicate that delivery of SNO alone or in combination with co-encapsulated drug/agent to LN-resident cells in a manner roughly similar to those described for the plain (non-SNO containing) NP[177] may be efficiently and rapidly achieved also by SNO-NP, while retaining the LN- and cellular biodistribution benefits of NP delivery. Of note, cellular uptake of the SNO-NP should not inhibit the function of subsequently released NO, since transnitrosation within the cell to small molecule thiols, such as cysteine, can occur and intracellular NO-species can be extracellularly released.[193] Therefore, NP-delivered SNO, released as NO either extra- or intracellularly within LN, would presumably be bioactive.

4.5 Conclusion

In summary, we have demonstrated that SNO-NP facilitate the controlled and sustained delivery of SNO to lymphatic tissues in a preclinical *in vivo* mouse model, resulting in a two order of magnitude increase in the accumulation of SNO in the LN over the span of 72 h post-injection above control animals compared a dose-matched small molecule NO donor. Additionally, we found dramatic increases in the abundance of LN-resident lymphocytes, dendritic cells, and MCM despite no apparent LN-resident cell death associated with treatment nor signs of systemic and injection site-localized toxicity after administration. Since NO has shown *in vitro*/*in vivo* promise with lymphatic-related cancer therapy and infectious disease applications but has been unable to progress due to

delivery-related challenges, with further development of this NO delivery technology has the significant potential to advance such NO-based therapeutic approaches through enhancement of lymphatic targeting.

CHAPTER 5. Multi-stage Lymphatic Delivery System Augments Delivery to Lymph Node Paracortex Cells

5.1 Introduction

The targeting of LN, tissues where organized lymphocyte accumulation in the body occurs,[11, 194] has the potential to address a variety of unmet clinical needs including remedying pathologies such as B and T cell malignancies, HIV reservoirs in CD4 T cells, and sentinel LN metastasis[195-198], as well as improving vaccine responses[102] and promoting tolerance.[199] Delivery of drugs to the LN, however, is hampered by several delivery barriers, the primary one of which is achieving lymphatic uptake as LN are accessed by the lymphatics from the periphery following intradermal injection.[17, 67, 104, 200] Due to the structure and location of the lymphatics, molecules within a certain size range are taken up preferentially[11, 133] with molecules in the size range between 5 and 100 nm being shown to favorably drain following intradermal injection.[160-162]

However, this size dynamic changes within the LN as the LN reticular network has been shown to restrict access of lymph-borne material to the cortical parenchyma, which is important in not only preserving the naïve state of the lymphocyte microenvironments, but also in protecting from a wide variety of immunogenic molecules that would adversely influence an immune response occurring within the cortex, such as microbes and their soluble products during microbial infections.[85] The efficiency of this barrier has been extensively shown to depend on the size of the lymph-borne molecules with high MW tracers all but virtually excluded from conduit and cortex

access by the subcapsular sinus.[83, 86-88] Conversely, low MW tracers experience graduated but not absolute exclusion, with molecules under 70 kDa having access to the conduits.[84, 85] However, permeation of these low MW molecules from the conduits to the lymphocytes within the paracortex is mostly restricted, indicating that for immune challenges with limited antigen concentration this might be a significant barrier, but with larger concentrations direct lymphocyte access could be possible and produce physiologically relevant results.

Due to this unique structure of the lymphatics and the partitioning of solutes within the LN reticular network, both of which are favor opposing size scales of molecules, there remains a significant technological gap. To achieve localized delivery to LN, principles of NP-mediated lymphatic targeting are often employed,[81, 104] with previously demonstrated *in vivo* success in tumor immunotherapy models.[10, 104, 107, 201, 202] While the concept of spatiotemporal regulation of delivered cargo is not a new idea for tumor drug delivery,[103, 203, 204] its principles have yet to be broadly applied towards LN targeting.[205] This is most likely due to the limited number of modalities available for facilitating *in vivo* control over the release of cargo.[71] Therefore, systems that have shown utility in tumor drug delivery that rely on enzyme sensitivity or hydrolytic degradation will not be broadly applicable to LN targeting since LN do not normally possess large physiological deviations in soluble enzyme concentrations compared to their draining lymphatics making release of cargo not easily controllable.

In this work, we have created an engineered NP system for enhanced lymphatic uptake and transport to the LN that can release its payload at different rates, thereby tuning the access of LN structures that are targeted, and the amount of cargo that is

released once in the lymphatics. Our approach consists of a two-stage system that combines 30 nm thiolated poly(propylene sulfide) NP[13, 114, 149] with orthogonally-reactive OND linkers that degrade by a retro-Diels-Alder mechanism in a pH- and buffer-insensitive manner at programmable half-lives ranging from hours to days to release small-molecule cargo.[206-208] We showed *in vivo* that the release of cargo within the dLN allowed for improved penetration into the deeper structures of the LN, and utilized our multi-stage NP system to improve immunotherapy for the treatment of cancer by delivering the TLR9 ligand CpG to treat LN lymphomas.

5.2 Materials and Methods

5.2.1 OND linker conjugation design

Oxanorbornadiene linkers undergo relatively rapid Michael addition with thiols to produce adducts that fragment at predetermined rates by a retro-Diels-Alder mechanism. In previous work, we have identified a number of control elements that enable programmability of adduct half-lives by changing functional groups that are present on the OND. These functional group modifications vary in the strength of their effect on adduct stability, producing a range of adduct half-lives that can be tuned to meet the requirements of a given system.[206-208] For example: epoxidation of the electron-rich alkene produces thiol-reactive non-cleavable 5,6-epoxyoxanorbornenes, EONB 3, which is used as a control for OND fragmentation time. The synthesis of all electrophiles 1-5 and 3-Me bearing model dye cargos used in this study is described in the supporting information.

Fluorogenic Dansyl (Dn) Dn-modified OND 1-5 and 3-Me were reacted with free thiols on NP to determine their conjugation efficiency and reaction rate. Conjugation of

Dn-modified OND to NP was monitored by following the increase fluorescence emission (Ex: = 345 nm, Em: = 510 nm) over the course of the reaction.[208, 209] Reactions were performed at OND:thiol mole ratios ranging from 1:3.5 to 1:28, giving the average observed reaction rates for each of the OND variants. As expected, based on our previous work, OND derivatives exhibited somewhat different rates of conjugate addition. Second order rate constants ranging between 5-61 $M^{-1}s^{-1}$ were observed, with 1,4-dialkyl OND 1 and trifluoromethylated 4 providing the slowest and fastest rates of addition, respectively.[206-209] However, the reaction rates of all OND were sufficiently fast such that loading of NP was achieved in under an hour at room temperature, demonstrating that this loading approach should be applicable to a wide variety of biological applications. Following conjugation of the OND to NP, the release rates of model Dn-furan cargo from the OND-Dn-NP conjugates were determined. This was achieved by dialyzing the OND-Dn-NP adducts at 37°C against PBS, and monitoring the fluorescence emission of the dialyzed sample at 510 nm over time. By following the loss of fluorescence from the dialyzed adduct solution, the fragmentation rates of OND-Dn-NP adducts were determined. The rapidly fragmenting OND 1 presented a challenge since the dialysis rate of free cargo was on a similar time scale as the fragmentation of adducts of this derivative. In order to accurately capture the fragmentation rate of adducts of 1, a solution of OND-1-NP was incubated at 37°C and small samples were periodically drawn and separated using size exclusion chromatography. The OND-1-NP fractions were collected and their fluorescence emission measured at 510 nm.

The OND variants exhibited the predicted wide range of half-lives from 23 min for 1, up to a nearly permanent linkage for 5. It is worth noting that in this NP-based delivery

system, we did not observe the expected decrease in adduct half-life for the N-methylsulfonamide derivative 3-Me relative to the parent secondary sulfonamide 3, as we have reported previously for small molecule and protein adducts.[208, 209] As a result, we explored derivative 2 to achieve release rates between those attainable with linkers 1 and 3. We rationalized that adducts of 5-alkyl-1,4-H,H 2 would behave in an analogous fashion to 1,4-unsubstituted OND dicarboxylates.[208] Conjugate addition between NP and small molecule thiol proceeded readily for this derivative (k_{obs} = 21.1 ± 5.0 $M^{-1}s^{-1}$). In contrast to 1-alkyl OND, which provide predominantly the 3-exo-syn Michael adducts, we observed two groups of products separable by chromatography on silica gel after reaction of 2 with beta-mercaptoethanol.

5.2.2 Synthesis and characterization of OND derivatives

A detailed description of materials, synthetic procedures and characterization data for new compounds is described elsewhere.[207, 208] In general, OND electrophiles are prepared by Diels-Alder reaction of substituted furans (1 eq.) and a slight excess (1.3 eq.) of the appropriate electron-deficient acetylene in minimal solvent at 60°C. Dansyl-modified ONDs 1, 3, 4, and 3-Me were synthesized according to methods described previously and have been characterized elsewhere.[208, 209] With the exception of 5-Dn, all Dn-modified ONDs were prepared by Diels-Alder reactions between electron deficient acetylenes and N-dansyl(methylfurfuryl)amine derivatives. In the case of 5-Dn, epoxidation of a t-butyl-carbamate protected OND to form the epoxyoxanorbornene EONB preceded installation of the Dn group to avoid oxidation of the fluorophore. For rhodamine (Rhod)-, FITC-, and coumarin (Coum)-modified electrophiles, conjugation of xanthene and coumarin dyes was performed after the

formation of OND-electrophiles using amide coupling and copper-catalyzed azide-alkyne "click" chemistry, respectively. See supporting information for synthetic schemes and details.

5.2.3 Synthesis of OND-NP

Nanoparticles were synthesized as previously described.[13, 134, 149] Briefly, 500 mg of Pluronic F127 (Sigma-Aldrich, St. Louis, MO, USA, P2443) was added to 10 mL of degassed Milli-Q water, allowed to dissolve for 30 min with stirring, and was again degassed. To this solution, 400 μL of propylene sulfide (Sigma-Aldrich, P53209) was added under Argon and stirred for 30 min. Initiator weighing 28.8 mg (7.4 mM) was reacted with 322 μL of sodium methoxide (Sigma-Aldrich, 156256) and then added under Ar. 1,8-Diazabicyclo[5.4.0]undec-7-ene (DBU) (Sigma-Aldrich, 139009) was added under Ar to the solution 15 min later and the entire reaction stirred for 24 h. After 24 h the solution was exposed to air for 2 h and subsequently dialyzed for three days against 4x5 L of Milli-Q water using a 100,000 Da molecular weight cut off cellulose membrane dialysis tubing (Spectrum Lab., Rancho Dominguez, CA, USA, 131414). NP size was measured by dynamic light scattering. Ellman's assay (Thermo Scientific, Rockford, IL, USA, 22582) was used to determine the concentration of NP free thiols. NP were turned into OND-NP conjugates by reacting OND with excess NP in buffer at pH 7.4 for 1 h. For OND-Dn variants, fluorescence was only present after conjugation and no further purification was required. For OND variants bearing Rhod, FITC, and Coum cargos, due to the non-fluorogenic nature of these OND derivatives and incomplete conjugation, purification was performed via PD-10 column chromatography (GE Healthcare, Pittsburg, PA, USA, 17-0851-01) followed by concentration with 10,000 Da spin filters

(Millipore, Bedford, MA, USA, 42407) to achieve pure OND-NP adducts at the original NP concentration.

5.2.4 Synthesis and preparation of OND-CpG-NP

CpG-B-NH_2-3' 1826 (5′-TCCATGACGTTCCTGACGTT-3'-$(CH_2)_3$-NH_2) was purchased from Eurofins Genomics on the 1 μmol scale. SPO_3-CpG-B 1826 (5′-TCCATGACGTTCCTGACGTT-3'-SPO_3) (PTO-CpG) was purchased from Microsynth on the 1 μmol scale. The 5' was chosen for modification with phosphothioate, while the 3' was chosen for modification with amine because the CpG can tolerate greater modification to the 3' end and still maintain immunostimulatory potency.[210] OND-3-CpG (OND-CpG) was installed on the CpG 3' using EDC/NHS; the OND-CpG was purified using precipitation with glycogen. PDS-NP were synthesized as previously reported.[134] PDS-NP were thiol-activated by adding Dithiothreitol (DTT) to 100 mM for 30 min. The solution was then cleaned of DTT on a PD-10 G25 column followed by collection of the NP fractions and then concentrated to 80-100 mg/mL with a 4 mL 10 kDa Amincon Spin filter at 4000 x g for 30 min and 15 min. The concentrated NP solution was then run on three 5 mL 7 kDa Zeba spin columns at 1000 x g for 2 min in 1x -/- PBS. OND-CpG was added to the NP solution at a concentration of 1 ug/15 μL NP (80 mg/mL) and reacted for 12 h. Following reaction the solution was run on a Sepharose CL6B column 1x30 cm. The fractions were assayed for NP using Iodine[167] and Gel Red for CpG.[10] The OND-CpG-NP conjugate fractions were pooled and concentrated with a 10 kDa Amicon Spin filter at 4000 x g for 30 min. Final concentration of CpG was determined using Gel Red and Iodine standard curves for CpG and NP, respectively; the average concentration of CpG was between 0.4-0.8 ug CpG/30μL NP (40 mg/mL). For

PTO-CpG-NP, PTO-CpG was added to PDS-NP at a concentration of 1 ug/15 µL NP (40 mg/mL) and reacted 12 h. The solution was separated using column chromatography.

5.2.5 Characterization of OND-Dn-NP conjugation and fragmentation rates

Oxanorbornadiene conjugation rates to NP were determined using OND-Dn variants due to their fluorogenic nature. The Dn fluorescence is quenched by the OND electrophile presumably by a photoinduced electron transfer mechanism, and a robust fluorescence is observed following conjugate addition.[208, 209] OND were added at 25, 50, 100, and 200 µM to NP with a thiol concentration of 700 µM (550 µM thiol was used in reactions with 2), yielding a mole range of OND to thiol ratios of 1:3.5 to 1:28 in pH 7.4 phosphate buffered saline. Fluorescence was tracked over the course of conjugation until a plateau was reached. The observed rate constant was determined by fitting to the linear form of the integrated second order rate equation. Fragmentation studies were conducted using dialysis membrane cups of 20,000 MWCO that retain the OND-Dn-NP adduct, but allow for the removal of fragmented OND dye cargo. OND-dansyl variants were reacted in buffer at pH 7.4 with excess NP for 1 h and then transferred to 20,000 MWCO dialysis membrane cups at 37°C. Samples of 4x2 µL were extracted to minimize reduction of dialysate volume throughout the experiment and read for fluorescence at 510 nm using a BioTek Synergy H4 Multi-Mode Microplate Reader. Size-exclusion chromatography on a PD-10 column was employed for 1 because the adduct half-life for this linker is only 23 min and is similar to the rate of dialysis of free dansyl-furan. Samples were prepared using the staggered start method every 10 min for 2 h and incubated at 37°C.

5.2.6 In vitro collagen hydrogel penetration

Collagen hydrogels at 7.5 mg/mL at physiological pH were prepared as reported elsewhere.[103, 211] Briefly, 144 μL of 8.63 mg/mL bovine collagen was mixed with 3.7 μL of 1N NaOH and 19.2 μL of 0.17M EDTA. The collagen solution was drawn into 100 μm capillary tubes (World Precision Instruments, Inc., Sarasota, FL, USA, 1B100-3) and then gelled for 24 h at 37°C. Fluorescein-labeled NP were conjugated to two OND derivatives with different dye cargo (and coumarin), purified and concentrated as described above, and then added to the collagen gel using a 31-gauge syringe. Fluorescence images were taken over the course of 12 h at 37°C using a Zeiss Axio Observer XLmulti S1 to measure the penetration of OND cargo relative to NP. Fluorescein-labeled NP were measured on the GFP channel, 3-Rhod was measured on the RHOD channel, and 1 Coum was measured on the DAPI channel. 16-bit grey scale intensity profiles were drawn from the loaded OND-NP solution through the length of the gel.

5.2.7 In vivo experiments

All animal studies were approved by and adhered to guidelines set forth by the Georgia Institute of Technology IACUC.

5.2.8 Accumulation and multi-off rate studies

In order to determine which OND linker would be most useful *in vivo* we conducted area under the curve studies over 72 h. Using our mouse forearm injection model 30 μL of OND-Dn-NP solution was injected under isofluorane anesthesia intradermally into both forearms of 6-week-old female C57BL6/J mice. The mice were allowed to recover for 24 h before being sacrificed and having axillary and brachial LN

excised and homogenized in 400 μL of DMSO to improve the weak fluorescence signal of dansyl furan in aqueous buffer. Using a standard curve generated in PBS we were able to calculate the percent injection at each time point for each OND linker within the LN homogenate. Using the measured half-lives we were able to calculate the percent of cargo that would be free at 24 h for each OND linker.

In order to demonstrate the full advantage that different OND variants can provide, different mole ratios of OND derivatives 1, 3, and 4 were conjugated to the same NP solution such that the overall release rate of Dn-furan cargo would represent superposed simultaneous release profiles. For this study, OND 1, 3, and 4 were chosen for their greatly differing half-lives. These OND variants were mixed at mole ratios of 8:1:1, 1:8:1, 1:1:8, and 1:1:1 of OND 1:3:4, and their conjugation was monitored by measuring fluorescence emission at 510 nm. The conjugation fluorescence (data not shown), demonstrated that the percent of total OND conjugated from each OND variant is directly proportional to its starting percentage, since the thiol from SH-NP are in excess. The fragmentation half-life for 1 is on the same time scale as that of the conjugation reaction, leaving approximately 50% of its conjugates intact by the time addition was completed, thereby limiting the final conjugated percentage of 1. Following conjugation, the OND-Dn-NP adduct solutions were incubated at 37°C and over the course of 28 h samples were drawn and separated on a size-exclusion column. The OND-Dn-NP fraction eluting first was collected in bulk and its fluorescence emission at 510 nm was measured. Only OND-Dn-NP-conjugated cargo elutes with the NP fraction, enabling the calculation of the percent of cargo still linked to the NP carrier, and the amount that has been released. Model release curves were created using the known

fragmentation rates of adducts of 1, 3, and 4 and the conjugation efficiency to predict the release profile for each of the OND variant ratios.

As predicted by the model, incorporation of 1, which has a half-life of only 23 min, led to an initial burst release of cargo and was observed for all ratios, but was most prevalent for the 8:1:1 mole ratio. When 4 was predominantly incorporated, there was a much slower overall release of cargo, since its half-life is 44 h, as observed for the 1:1:8 mole ratio. The incorporation of 3, which has a half-life of 8.77 h at 37°C, lead to a steadier release observed over the time course of this experiment, particularly for the 1:8:1 mole ratio. When all three OND variants were in an equimolar ratio (1:1:1), the release profile exhibited a steady release rate closely resembling that predicted by the model. The described results demonstrate the versatility and tunability of our OND-NP system for releasing cargo on a defined time scale. These results suggest that the rate of cargo release can be precisely tuned to target specific tissues along the NP delivery vehicle biodistribution route. Such a strategy could be powerful in improving LN delivery of small molecule cargo, where NP are used to facilitate lymphatic uptake and transport to the LN, while OND is used to specifically release cargo once lymphatic uptake has occurred, allowing the released cargo to diffuse deeply within the LN.

5.2.9 IVIS imaging

Fluorescent imaging was performed with an IVIS® Spectrum instrument (Perkin Elmer).[149] Animals were injected intradermally in the forearm with a solution of Alexa Fluor 647-NP or of OND 3-Rhod group either with or without Alexa Fluor 647 labeling. Twenty-four h later the animals were sacrificed. To assess Alexa Fluor 647-NP drainage to LN, animals were imaged using Ex: 640, Em: 720 and an exposure of 0.1 s.

To assess 3-Rhod drainage to the LN, animals were imaged using a modified Rhodamine Red-X channel (Ex: 540, Em: 580) at an exposure of 0.1s. Total fluorescent counts and radiant efficiency (p/s·sr·μW) were evaluated for each experiment and treatment group using elliptical regions of interest in Living Image Software (Perkin Elmer).

5.2.10 Confocal microscopy of LN penetration

Alexa Fluor 647-labeled NP were conjugated to 3-Rhod, purified and concentrated, and then 30 μL was injected intradermally in the forearms of three 6-week-old female C57BL6/J mice. After 24 h the mice were sacrificed and the axillary and brachial LN excised, cleaned under stereoscopic observation, and plated on a glass-bottom 96-well plate for confocal imaging (Zeiss NLO 710). Using a 10x objective lens, 16-bit fluorescence imaging was taken for Alexa Fluor 647 and rhodamine. Z-stacks approximately 6.4 μm in depth were taken through the depth of the LN (approx. 160 μm). In order to acquire the entire LN convex hull tiling was performed and the resulting images were stitched together.

5.2.11 Measurement of NP vs. OND cargo distribution within LN images

Lymph node images were taken on confocal as previously described. Z-stack images were converted to maximum intensity projections and then separated by fluorescence channel. Using a custom image J macro an outline was drawn around the LN boundary with the free from tool in the single channel images. The image was then thresholded to zero pixel value outside of the LN boundary and the custom script returned the coordinates of the outline and the thresholded fluorescence pixels within the LN boundary. Those coordinates were then transferred into a custom MatLab script that calculated and returned the binned minimum distance between the drawn LN boundary

and the thresholded fluorescent pixels. The collected data was gathered for 24 LN samples and the difference between the NP and 3-Rhod signals was calculated and normalized to determine the bias of fluorescence towards each species along distance from the LN border.

5.2.12 In vivo immunotherapeutic tumor treatment

Tumor treatment experiments were conducted by implanting 250K EL4 lymphoma cells i.d. LN tumors were allowed to form over four days and then the mice were treated every day i.d. in the upstream forearm lymphatic drainage basin for five days with 0.75 μg of CpG in either OND, PTO, or free form. LN sizes were recorded at endpoint and assessed grossly with photographs. LN were frozen and sliced and stained with hematoxylin and eosin (HE) stain and assessed for tumor burden by histology. Primary tumor sizes were recorded and the tumor volume was modeled as an ellipsoid.

5.2.13 In vivo functional CpG experiments

30 μL of CpG in either OND, PTO, or free form (0.4-0.8 ug CpG) are injected i.d. into each forearm of a C57BL6 mouse under isoflurane anesthesia. After 24 h the mouse is sacrificed and the LN excised (axillary and brachial are pooled) and placed in 900 μL +/+ 1x PBS on ice. The cells are extracted from the LN as previously reported.[149] Briefly, 100 μL of 10 mg/mL Collagenase D is added and the LN are incubated for 1 h at 37°C. The LN are then mechanically broken up on a 70 μm cell strainer and the 100 μL of cells are plated at a concentration of 10M/1mL. The cells are first blocked with 2.4G2, followed by Live/Dead staining, all staining (Live/Dead – BUV496, B220 – BV650, CD40 – FITC, CD45 – PerCP, CD86 – PE, MHCII – APC, CD11b – AF700, CD11c – APCeFluor 780), and then fixing in 2% PFA. Samples were run on a BD Fortessa. Cells

were gated according to the following markers: BC – CD45+ B220+ CD11c-; CDC – CD45+ B220- CD11c+; PDC – CD45+ B220+ CD11c+; Macrophage – CD45+ B220- CD11c- CD11b+; TC – CD45+ B220- CD11c- CD11b-. Maturation was gated according to the following markers: MHCII vs. CD40 or CD86. The plots were divided into six divisions: MHCII HI-CD40+, MHCII HI – CD40-, MHCII MID - CD40+, MHCII MID CD40-, MHCII LOW CD40+, and MHCII LOW CD40-. The same divisions were created for CD86. Reported markers were for MHCII MID CD40+/CD86+.

5.2.14 Statistical analysis

Statistical analysis: Data is expressed as mean ± standard error of the mean. Statistical analysis was performed using Prism 6. Statistical significance was defined as $p \leq 0.05$.

5.3 Results and Discussions

5.3.1 Time-based intra-lymphatic release of cargo is achieved by OND-NP

These NP possessed high concentrations of free thiols within the hydrophobic core or can be derivatized with modifications to the Pluronic F127 PEG groups allowing for the presence of free thiols on the PEG corona. OND linkers undergo relatively rapid Michael addition with NP thiols to produce adducts that fragment at predetermined rates by a retro-Diels-Alder mechanism (Figure 5.1a). These NP with either core thiols (SH-NP) or Pluronic thiols (PDS-NP) were 30 nm (Figure 5.1b,c) and showed fast conjugation with the OND linkers (Figure 5.2d), with very precise control over the fragmentation rate (Figure 5.1b) and release of cargo from the NP delivery vehicle (Figure 5.1e). In previous work, we have identified a number of control elements that enable programmability of adduct half-lives by changing functional groups that are

present on the OND. These functional group modifications (Figure 5.2a) vary in the strength of their effect on adduct stability, producing a range of adduct half-lives that can be tuned to meet the requirements of a given system (Figure 5.2b).[208, 209] The wide variety of half-lives, especially for adducts of 2, 3, and 4, which have half-lives of 2.77, 8.77, and 44.2 h, respectively, provided an array of useful fragmentation times that could be harnessed for tuning cargo release for different *in vivo* applications.

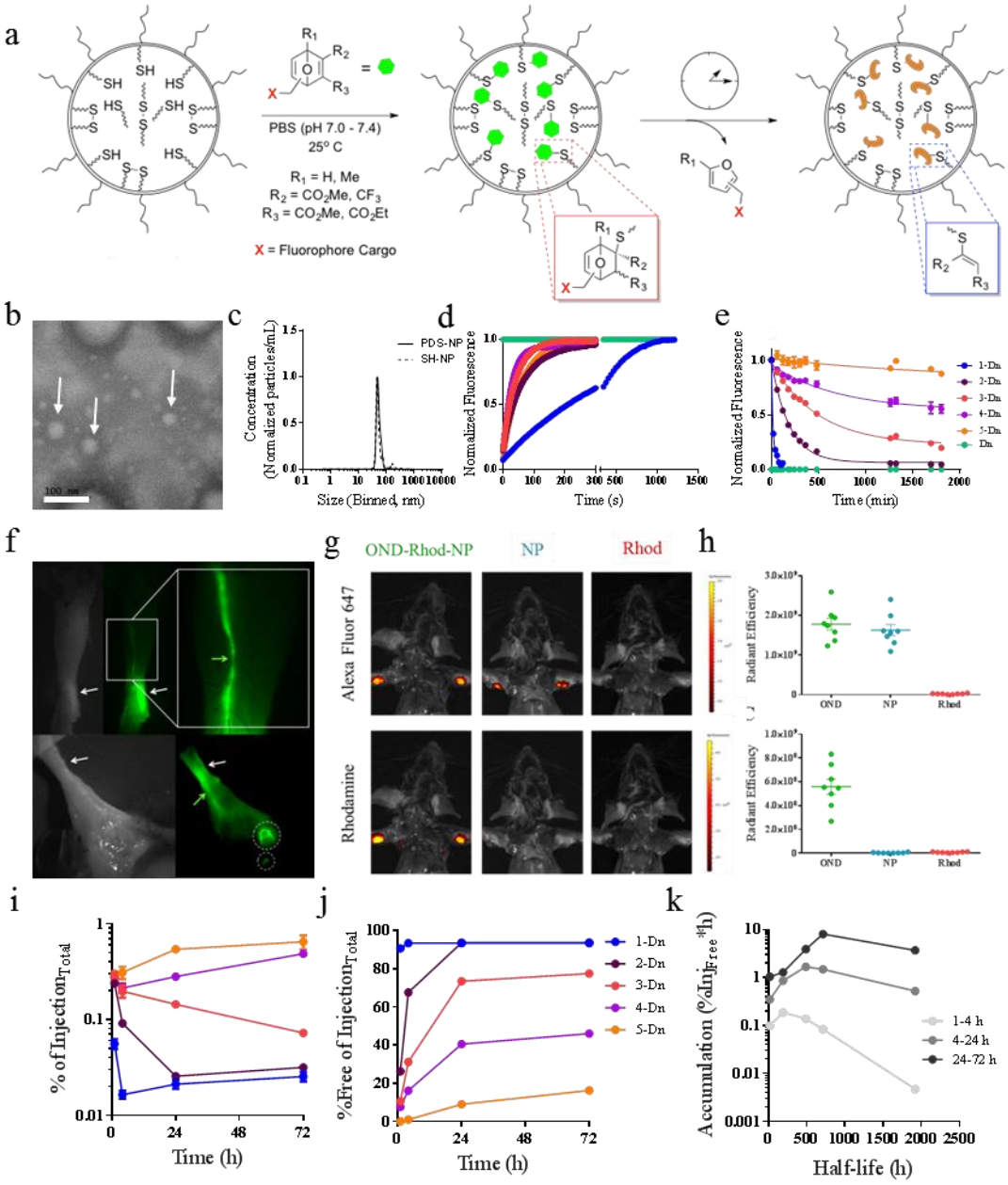

Figure 5.1: Small molecule delivery to lymphatic tissues is enhanced using 30 nm lymphatic-draining NP. a) Poly(propylene sulfide) nanoparticles contain a large concentration of free thiols (SH) in their micelle core that can react through Michael-type addition with OND reagents, forming an OND-SH-NP-adduct. b) Representative TEM image of NP. Arrows indicate 30 nm NP. White bar indicates 100 nm. c) Nanosight of PDS-NP and SH-NP showing 30 nm size. d) Conjugation rate of small molecule ONDs to SH-NP. e) Release curves of OND linkers 1-5 at 37°C demonstrating that release of cargo from NP can be tuned by using different OND linkers. n>3 samples per group. f) Representative near infrared image showing NP transporting within mouse forearm lymphatic vessel (green arrow) to

draining LN (white circles). White arrow, site of intradermal injection. g) Representative IVIS image showing that 3-Rhod only transports to the dLN when conjugated through OND linkage to NP. h) Quantification of IVIS image demonstrating the presence of 3-Rhod signal and 647 signal from NP when conjugated by OND compared to the lack of 3-Rhod fluorescence when administered in free form. n=8 samples per group. i) Percent of injection accumulated in LN of total over time for different OND linker. j) Percent of free cargo divided by total percent of injection over time for different OND linkers. k) Area under the curve (AUC) of released OND cargo for different time periods: 1-4, 4-24, and 24-72 h compared to half-life of OND linker. Peak LN accumulation AUC occurs with increasing linker half-life for later accumulation time periods. n=3 samples per group.

These NP have been previously shown in numerous studies to deliver immunomodulatory drugs as they drain efficiently through the lymphatics (Figure 5.1f) transporting small molecule drug to the dLN in high concentrations.[10, 104, 107] Using whole animal IVIS imaging following lymphatic uptake in our well described intradermal forearm lymphatic transport model, where the lymphatic network efficiently drains the intradermal injection to the ipsilateral axillary and brachial draining-LN (dLN)[10, 149], we found that 24 h post-injection small molecule dye was only measurable in the dLN delivered by OND conjugation to NP (OND-NP). We next assessed the effect of OND half-life on LN accumulation over a 72 h time course using end-point studies in our forearm lymphatic model, and observed that LN accumulation of tethered cargo depended on linker fragmentation half-life (Figure 5.1i), and optimization of this half-life allows for tuning of the percentage of free vs. bound cargo (Figure 5.1j) at various time points of the LN accumulation (Figure 5.1k). We ultimately settled on OND-3 to be our model linker given its moderate LN accumulation (Figure 5.1i) and its >85% released cargo at 24 h (Figure 5.1j) producing the highest area under the curve (AUC) of any linker between therapeutically relevant drainage times of 4-24 h (Figure 5.1k).

a

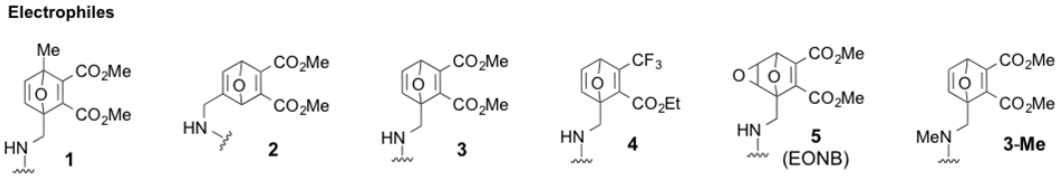

b

Electrophile	$k_{conjugate\ addition}$ ($M^{-1}s^{-1}$)[a]	$k_{retro\text{-}Diels\text{-}Alder}$ ($\times10^{-4}\ min^{-1}$)[b]	$t_{1/2}$ (hr)[c]
1-Dn	5.0 ± 0.3	304 ± 26	0.38 ± 0.03
2-Dn	21.1 ± 5.0	41.7 ± 3.4 (3.5 ± 0.5)[d]	2.77 ± 0.23 (33.5 ± 5.1)[d]
3-Dn	32.8 ± 4.4	13.2 ± 0.6	8.77 ± 0.43
4-Dn	61.3 ± 8.0	2.6 ± 0.2	44.2 ± 3.4
5-Dn	12.6 ± 5.7	0.7 ± 0.1	166 ± 37
3-Me-Dn	22.2 ± 5.5	7.1 ± 0.2	16.4 ± 0.6

Figure 5.2: Based on the functional groups on the OND, retro-Diels-Alder fragmentation occurs at varying rates resulting in the release of furan-modified cargo and leaving a thiomaleate. Epoxidation of ONDs yields epoxyoxanorbornene (EONB) Michael acceptors that form adducts that are incapable of retro-Diels-Alder fragmentation. Dyes with a range of emission wavelengths were selected as model cargos in this study. a) OND and EONB electrophiles and model fluorophore cargos presented in this study. By changing the substituent groups around the OND ring, different rates of retro-Diels Alder fragmentation were achieved. b) Table of rate constants and fragmentation half-lives for different Dn-OND conjugates. OND derivatives exhibited somewhat different rates of conjugate addition. Second order rate constants ranging between 5-61 M-1s-1 were observed, with 1,4-dialkyl OND 1 and trifluoromethylated 4 providing the slowest and fastest rates of addition, respectively.

5.3.2 OND-mediated release of cargo from OND-NP spatially biases cargo penetration both in vitro and in vivo

To assess whether released cargo offered any advantages of penetrating the highly collagenous LN matrix, we turned to a previously published *in vitro* model looking at the diffusion of released OND cargo vs. the NP delivery vehicle in a collagen hydrogel.[103, 211] Fluorophore variants of OND 1 and 3 were synthesized and conjugated to

Fluorescein-labeled NP. The OND-NP adduct was added to a model collagen hydrogel (at a concentration of collagen similar to that of a LN).[194] The diffusion of OND-NP and its released cargo into the collagen hydrogel was tracked with fluorescence microscopy over 12 h at 37°C using three fluorescence channels, one for the NP and one for each OND variant (Figure 5.3a, left). After 12 h of incubation, the penetration of the different cargos was vastly different from each other and from the NP delivery vehicle (Figure 5.3a, right). The short fragmentation half-life of 1 resulted in the farthest and fastest penetration compared to the slower release of cargo from adducts of 3 and the minimal penetration of the NP delivery vehicle.

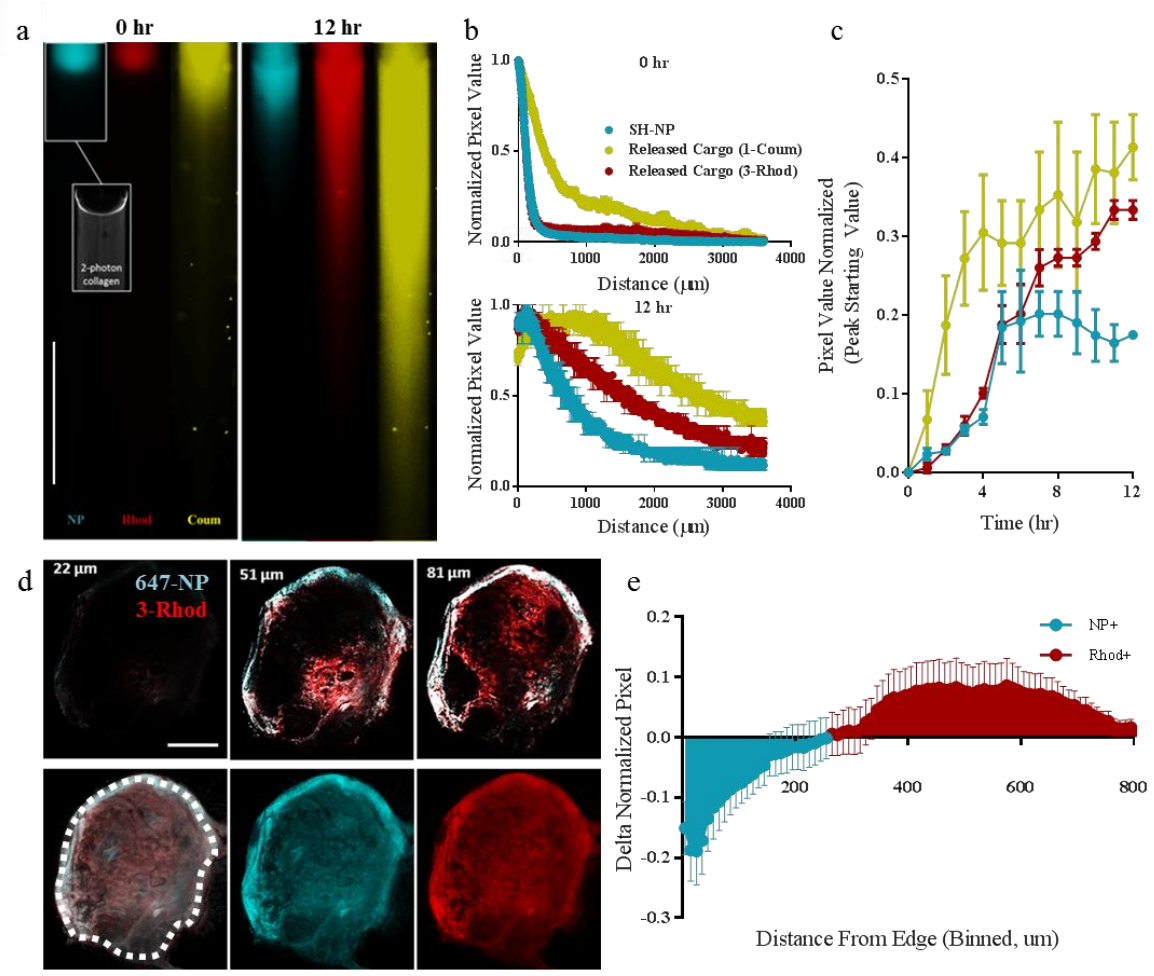

Figure 5.3: *In vitro* and *in vivo* diffusion of released OND cargo. a) Left, Fluorescence images of FITC-labeled SH-NP, 1-Coum, and 3-Rhod at start of imaging in collagen hydrogel at 37°C. Insert, 2-photon image of collagen hydrogel. a) Right, Fluorescence images of FITC-labeled SH-NP, 1-Coum, and 3-Rhod at end of 12 h of imaging in collagen hydrogel at 37°C. White line, 1000 μm. b) Normalized intensity profile across field of view of 0 and 12 h time point for collagen diffusion experiment at 37°C. c) Normalized pixel value to 0 h time point for half-way point in field of view over course of 12 h diffusion experiment at 37°C. Data is from representative experiment with n = 2. Collagen hydrogel was formed at a concentration of 7.5 mg/mL. n=3 samples per group. d) Top, presence of NP and 3-Rhod fluorescence at different Z stack depths of the LN. d) Bottom, Maximum intensity projection of LN. Left) 2-channel overlaid NP and OND cargo fluorescence. Middle) NP channel. Right) 3-Rhod channel. e) Difference in normalized pixel count for each single channel (NP vs. 3-Rhod) vs. distance from the outline (dashed white line). Negative shaded area indicates NP bias, vs. positive red shaded area indicating Rhod bias. n=24 samples per group.

By analyzing the penetration at different time points over the course of the experiment a more quantitative understanding of the impact of release time on cargo penetration was achieved. At the initial time point the penetration of each component was similar (Figure 5.3b, 0 h), with a small amount of cargo from 1 already beginning to penetrate the collagen matrix. Cargo released from 1 rapidly penetrated the collagen hydrogel by 4 h, while the slower cleaving 3 cargo more closely resembled the NP delivery vehicle at this time point (data not shown). By 12 h, 3 cargo had started to penetrate similarly to the earlier released cargo from 1, while the NP delivery vehicle still had minimal diffusion (Figure 5.3b, 12 h). When considering the arrival of dye at a deep point within the collagen hydrogel as would be the case for the LN subcapsular sinus, it can be seen that cargo from 1 arrived quickly, while cargo from the slower releasing 3 arrived more slowly along with the NP delivery vehicle (Figure 5.3c, 0-5 h). However, at later time points, the NP delivery vehicle concentration at a deep point in the collagen matrix plateaued, indicating retarded migration of this species (Figure 5.3c, blue curve, 5-12 h). In contrast, the 1 cargo concentration continued to increase in this time frame, indicating a greater mobility and enhanced penetration of the released cargo species (Figure 5.3c, yellow curve, 5-12 h). These results indicate that differential release of cargo based on time can have a dramatic effect on the ability of cargo to penetrate restricted tissue spaces. Within LN, these results portend that released cargo has a better ability to penetrate deeply into the LN compared to the large NP delivery vehicle.[85]

To demonstrate the benefit of timed-release of cargo within the LN to achieve penetration and accumulation, we performed proof-of-concept *in vivo* studies assessing the spatial distribution and depth of where the released fluorescent cargo penetrated to

within the LN compared to the NP delivery vehicle. Small molecule dye rhodamine was conjugated to 647-labeled NP through OND 3 and injected intradermally in the mouse forearm as before. After 24 h, the axillary and brachial LN were excised, cleaned, and imaged using fluorescent and two-photon confocal microscopy. Z-stacks were taken up to a depth of 160 μm into the LN. We first observed that 3 released rhodamine were present at deeper slices of the LN than NP (Figure 5.3d), which was present mostly in the superficial slices (Figure 5.3d, 51 μm vs. 81 μm). To gain spatial and not just depth information about the released cargo compared to the NP delivery vehicle we further analyzed the LN Z-stacks by creating maximum intensity projections and then processing the images using custom ImageJ and MatLab scripts to obtain the distance between each fluorescent pixel within the LN and the LN boundary (Figure 5.4a-c). By looking at the relative spatial distribution of the single channel fluorescent pixels within the LN from either 3-Rhod released cargo or 647-NP (Figure 5.3d, lower right, blue and red) we found that the shallower distances from the LN boundary (Figure 5.3d, lower left, white dashed outline) were more biased for NP fluorescence (Figure 5.3e, blue) compared to the central, deeper areas of the LN which were biased more for the released 3-Rhod cargo (Figure 5.3e, red).

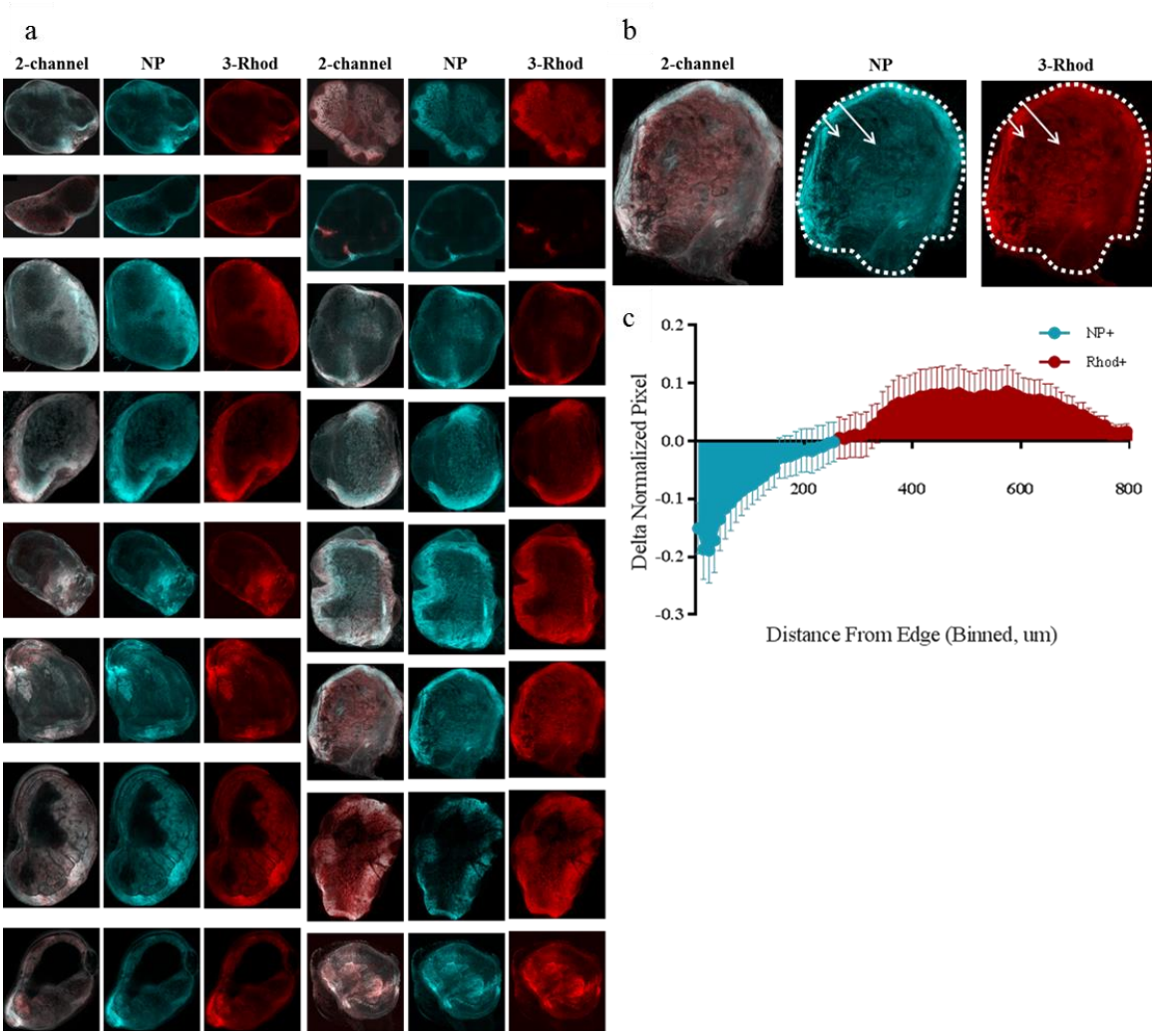

Figure 5.4: LN fluorescence spatial distribution. a) LN confocal images are converted to maximum intensity projections of all Z stacks. Images are separated from 2-channel overlaid into NP and 3-Rhod fluorescence images. b) Outline is drawn around single channel LN images. The custom ImageJ and Matlab program will measure the minimum distance (solid arrow) between each fluorescent pixel and the outline (dashed line). c) Composite graph of the difference in normalized pixel value for NP and Rhod from all LN in (A) vs. the distance from the capsule.

5.3.3 OND-NP bias dLN-resident cellular biodistribution

While the advantages of using a targeted delivery strategy for lymphatic uptake to improve LN accumulation include dose sparing and minimizing the potential for undesirable off-target effects and/or toxicities,[102] studies looking at the distribution of molecules within the LN support the concept that despite nanoformulations of an

intermediate nanoscale size being ideal for lymphatic uptake after injection in the periphery, small molecules have increased potential to travel deeply within the LN conduits and possibly within the cortex (Figure 5.5a).[84, 85] A controlled release strategy of co-formulated drug such as the multi-stage release strategies that have previously been used to improve intratumoral drug penetration,[103] might be utilized to differentially target LN-resident cells by exploiting LN physiology with larger drug delivery vehicles being primarily restricted by the subcapsular sinus, while the released small molecule cargo is free to penetrate the LN conduits that run deep into the cortex allowing access to the great percent of restricted lymphocytes (Figure 5.5b).

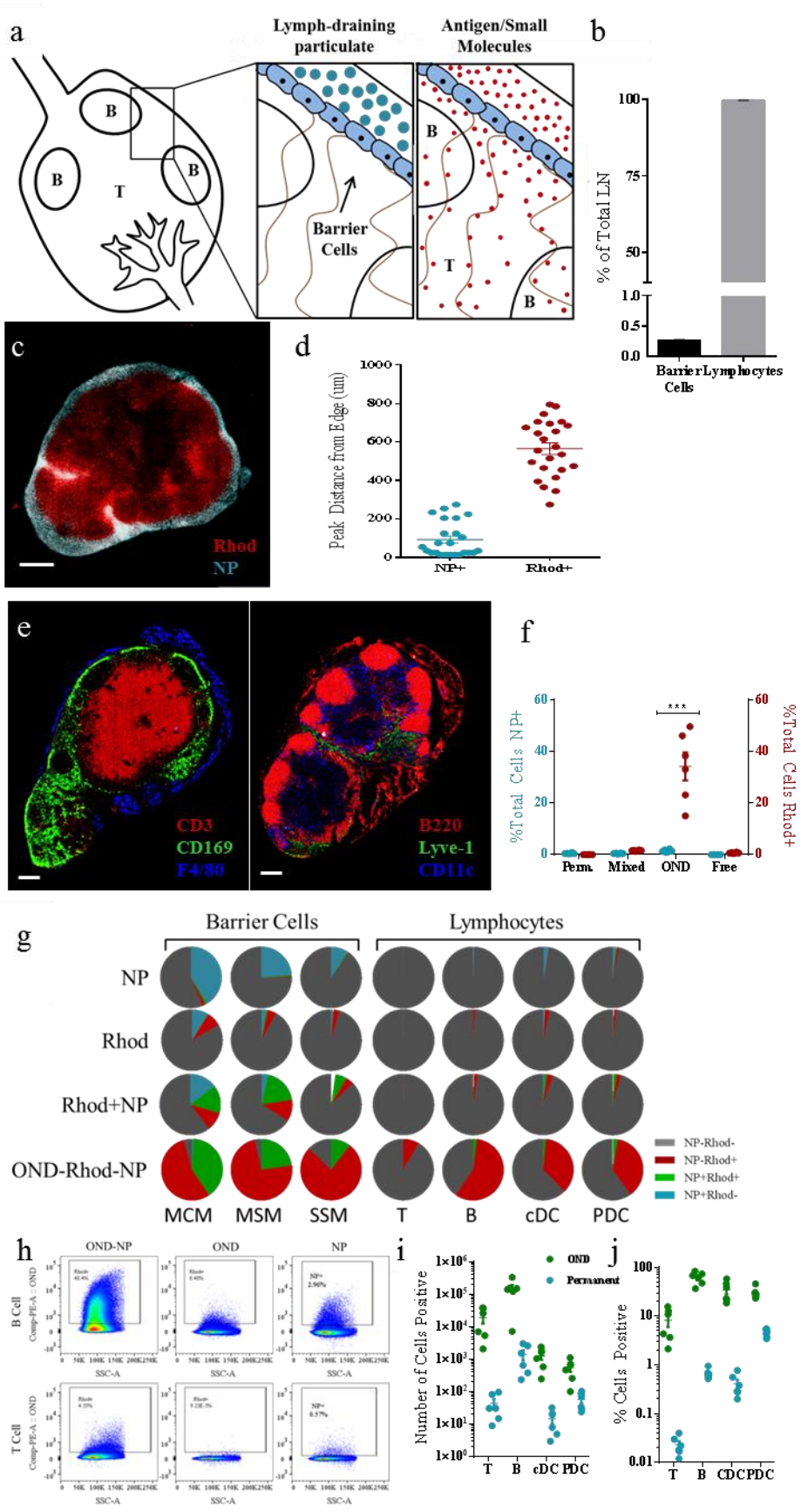
a
Lymph-draining particulate
Antigen/Small Molecules
B
T
Barrier Cells
b
% of Total LN
100
75
50
1.0
0.5
0.0
Barrier Cells
Lymphocytes
c
Rhod
NP
d
Peak Distance from Edge (um)
1000
800
600
400
200
0
NP+
Rhod+
e
CD3
CD169
F4/80
B220
Lyve-1
CD11c
f
%Total Cells NP+
%Total Cells Rhod+
60
40
20
0
***
Perm.
Mixed
OND
Free
g
Barrier Cells
Lymphocytes
NP
Rhod
Rhod+NP
OND-Rhod-NP
MCM
MSM
SSM
T
B
cDC
PDC
NP-Rhod-
NP-Rhod+
NP+Rhod+
NP+Rhod-
h
OND-NP
OND
NP
B Cell
T Cell
SSC-A
i
Number of Cells Positive
OND
Permanent
T
B
cDC
PDC
j
% Cells Positive
T
B
CDC
PDC

Figure 5.5: Cellular distribution of OND cargo within LN. a) Spatial distribution of soluble species within LN shows that large particulates (blue) are restricted by the subcapsular sinus (blue cells) from access to the LN cortex, while smaller antigen and molecules (red) efficiently enter the LN conduits and travel deep within the LN. b) Distribution of cells within the LN showing that the majority of cells, lymphocytes, are currently un-targetable by large particulate delivery vehicles which are restricted by the small number of LN barrier cells. c) Representative image of OND cargo (red) penetrating the central area of the LN greater than the SH-NP (blue), which remained shunted towards the LN capsule. White line, 500 μm. d) Peak distance for the penetration of SH-NP or OND cargo into the LN from the LN boundary. The large distance to which OND cargo is present from the LN boundary mirrors the representative image in (c). n=24 samples per group. e) Representative images staining the LN for CD3 and B220 (red, lymphocyte) vs. CD169, F4/80, lyve-1, and CD11c (green and blue, barrier cells) showing that the lymphocytes are located more centrally in the LN than the barrier cells. f) Breakdown of all LN cells for OND and SH-NP positivity showing that release of OND cargo, which penetrated deeper into the LN (d), afforded access to a much greater percent of the LN cells compared to free cargo or SH-NP. n=6 samples per group. ***p<0.005. g) Distribution of cells positive for OND cargo or SH-NP within the LN. Barrier cells show greater percent of NP+ for SH-NP delivery vehicle while Lymphocytes show greater percent for 3-Rhod when delivered by OND-NP. n=6 samples per group. g) Representative flow cytometry for T and B cells showing dramatic increase in OND signal for OND-NP delivery compared to free Rhod delivery, while NP signal remained relatively low. i) Number of cells positive for OND compared to NP show that release of cargo dramatically increases the total number of cells positive for cargo. n=6 samples per group. j) Percent of cells positive for OND cargo compared to NP show that release of cargo dramatically increases the percent of cells positive for cargo. n=6 samples for all groups. Cells were gated as follows: B cells -B220+CD3-CD11b-; T cells – CD3+B220-; conventional dendritic cells (CDCs) – CD11c+B220-; plasmacytoid dendritic cells (PDCs) – CD11c+B220+; subcapsular sinus macrophages (SSM) – B220-CD3-CD11b+CD11c+CD169+F4/80-; medullary sinus macrophages (MSM) - B220-CD3-CD11b+CD11c+CD169+F4/80+; and medullary cord macrophages (MCM) - B220-CD3-CD11b+CD11c+CD169-F4/80+. For all graphs the columns/points and error bars represent the mean + SEM.

With our data demonstrating that release of cargo afforded some spatial and accumulation differences over permanently bound NP cargo (Figure 5.5c) we assessed the OND cargo and NP peak central fluorescence distance and found that OND cargo was much more centralized within the LN than NP (Figure 5.5d). When we compared these results to immunohistochemistry (IHC) stained slices of naïve LN looking for lymphocytes (CD3 and B220), APCs (CD11c), and barrier cells (CD169, F4/80, LYVE-

1) (Figure 5.5e), we found that lymphocytes and APCs were concentrated in the deep central portions of the LN, whereas the barrier cells remained closer to the LN boundary (Figure 5.5e) demonstrating that the spatial distribution of cells of the adaptive immune system overlapped with the central distribution of released OND cargo hinting at greater access to these cells through cargo release.

We next performed flow cytometry on LN-resident cells to see which cell types were targeted. Using both 647-NP and 3-Rhod as our model small molecule cargo we first assessed the total cellular uptake. Permanently bound cargo (647-NP), 3-Rhod mixed with 647-NP, and free 3-Rhod alone showed very little percent (<1%) of cells positive for cargo (Figure 5.5f). Contrastingly, rhodamine delivered on OND-NP, showed a dramatically increased cellular accumulation, reaching an average of nearly 40% of all dLN-resident cells (Figure 5.5f). Based on our analysis of the IHC slices of naïve LN we next assessed what cell types were responsible for this uptake and if release of cargo was affording differential access of cargo to different cell types. We found that immunotherapeutic cellular targets (T cells, B cells, and DCs) were strongly and primarily Rhod+NP- when delivered by OND-NP, while these cell types were also Rhod+NP- for the free and mixed groups, but at a much lower level (Figure 5.5g, Lymphocytes). Furthermore, we found that the barrier cells (CD169+ SSM, MCM, and MSM) were nearly 100% Rhod+ either as Rhod+NP- or Rhod+NP+ (Figure 5.5g, Barrier Cells). Interestingly, these barrier cells also were Rhod+ for the free, mixed, and permanent groups, but the results were not as strong as for the OND-NP (Figure 5.5g).

We next wanted to delve deeper into our immunotherapeutic targets T, B, and DCs. Using flow cytometry we found that the rhodamine signal massively increased for

both T and B cells (Figure 5.5h, upper), while the NP signal for both of these groups remained relatively subdued (Figure 5.5h, lower) reconfirming the studies showing restricted access to lymphocytes by large particulates.[84, 85] We further quantified this change by looking at both the number of positive cells and percent positive by comparing OND-NP to NP formulation, which is the current state-of-the-art for LN delivery. We first found that the number of T, B, and DCs positive for cargo dramatically increased when the cargo was released via OND-NP with T cells going from hundreds to tens of thousands, B cells going from several thousand to the hundreds of thousands, and DCs going from hundreds to thousands (Figure 5.5i). Interestingly, cargo-positive macrophage numbers remained relatively unchanged by cargo release indicating that NP might already be delivered to this cell type with maximum efficiency (Figure 5.5i). When quantified as a percent positive we recorded nearly 10% of T cells, 60% of B cells, 50% of DCs, and 100% of macrophages being positive for cargo when released by OND-NP (Figure 5.5j), indicating that this system could have dramatic improvements on immunotherapeutic LN delivery.

5.3.4 OND-CpG-NP immunotherapeutic tumor experiments

With all of the data we had supporting the fact that OND-NP-mediated release of small molecule cargo afforded: 1) better accumulation of small molecule cargo within LN; 2) enhanced LN penetration; and 3) increased number and type of cells that are positive for cargo. We next sought to apply our OND-NP system to immunotherapy for cancer. The LN draining the local tumor interstitium has been shown to be an important immunotherapeutic target for tumors since it is bathed in tumor-derived antigen[115] and delivery of adjuvants has previously been shown to be effective in inducing pro-tumor

cytotoxic responses. Therefore, to test our OND-NP system we incorporated the TLR ligand 9 CpG oligonucleotide onto our 30 nm NP using an OND linker (Figure 5.6a), and tested the conjugation and release of OND-CpG from the PDS-NP over 72 h (Figure 5.6b) and found that the release was unchanged with a half-life around 8 h (Figure 5.6c).

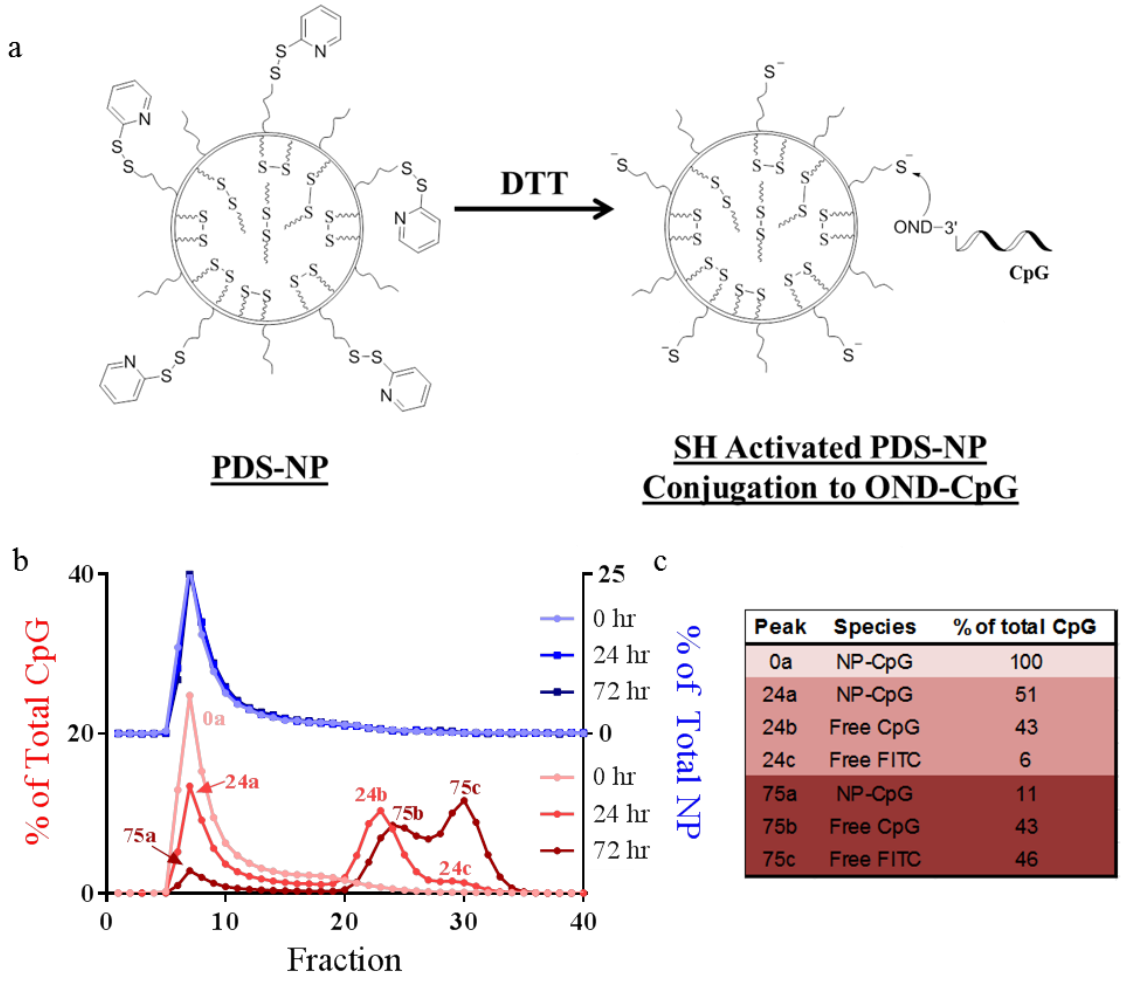

Figure 5.6: Conjugation and release characterization of OND-CpG-NP. a) PDS-NP are thiol-activated and reacted with CpG-OND to create OND-CpG-NP. b) OND-CpG-NP solution was placed in a 37°C water bath and aliquots were withdrawn at 0, 24, and 72 h and run on a CL6B column in order to determine the percent of CpG that coeluted with NP. CpG was measured using GelRed staining and NP were measured using Iodine staining. c) Table of % of CpG for each species in (b).

We next evaluated the efficacy of OND-CpG-NP delivery to the TDLN in treating both primary and LN-metastatic tumors. To this end, we implanted EL4 T cell lymphoma cells in the left shoulder dorsal skin of C57BL/6 mice; after primary tumor establishment and allowing for LN tumors to be formed, four days post implantation we intradermally injected 0.75μg of OND-CpG-NP, NP-disulfide linked CpG (PTO), free CpG, or PBS daily in the limb ipsilateral (i.l.) to the tumor for five days (Figure 5.7a). After 12 days OND-CpG-NP treatment of the i.l. limb resulted in reduced LN size compared to all other groups (Figure 5.7b,c). Furthermore, OND-CpG-NP treated LN were similar in size to that of non TDLN PBS mice (Figure 5.7b,c) indicating a potent anti-tumor immunity. To further support this claim, we also observed an abscopal effect on the primary tumor with OND-CpG-NP treatment of the TDLN resulting in slowing of tumor growth relative to control (Figure 5.7d), with the other CpG groups not resulting in any appreciable therapeutic effect.

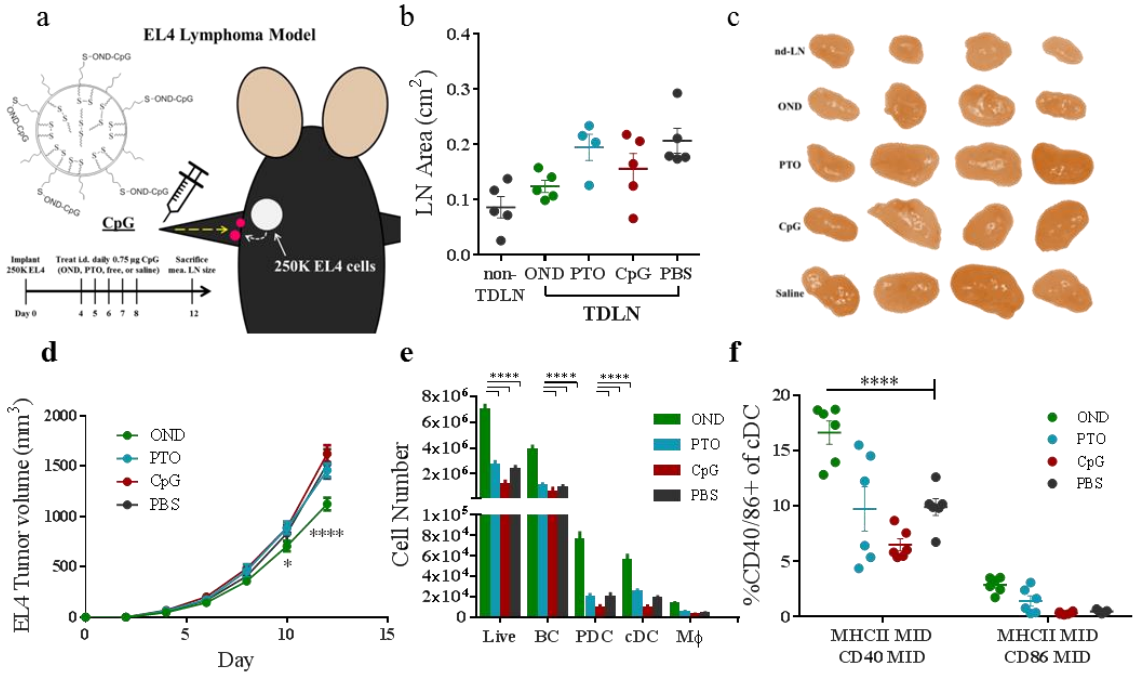

Figure 5.7: *In vivo* CpG delivered from OND-NP dramatically reduces EL4 LN tumor size. a) EL4 dorsal skin tumor implantation diagram. 250K EL4 are implanted in the left dorsal skin of the mouse (white circle). The EL4 tumor cells will drain (dashed white arrow) to the TDLN (pink circles) The CpG solutions are injected intradermally in the mouse forearm, which drains (yellow dashed arrow) to the same TDLNs as the tumor. b) EL4 LN tumor size was reduced with CpG-OND-NP compared to other treatment groups to levels not statistically different than non-TDLN. n=5 per group. c) Representative pictures of LN shows that OND-CpG-NP treated LN are similar to non TDLN. d) OND-CpG-NP slows the growth of the primary tumor while other CpG groups do not. n=4-6 samples per group. n=5 per group. e) The number of total LN cells and cells of each subtype was substantially increased in the LN with CpG-OND-NP treatment. n=6 per group. f) The maturation of cDCs was statistically significantly increased for MHCII MID CD40 MID in CpG-OND-NP treated LN compared to all other groups. For MHCII MID CD86 MID cells, CpG-OND-NP also increased the percentage of CD11c+, but not to a statistically significant amount. n=6 per group. For all graphs the columns/points and error bars represent the mean + SEM.

We next performed *in vivo* tests to help elucidate the dramatic tumor reduction effect caused by delivery of CpG through OND-NP. We injected OND-CpG-NP, PTO-CpG-NP, or free CpG into the forearms of mice and 24 h later analyzed the dLN by flow cytometry for the proliferation and maturation of the APCs. We found that when

administered via OND-NP the CpG caused a large increase in the total proliferation of LN-resident cells, nearly tripling the number of dLN-resident cells from between 1-2M to over 6M for OND-CpG-NP (Figure 5.7e). Furthermore, this increase in cell numbers within the LN-resident cells occurred strongly for all TLR9-positive cell types including B cells, plasmacytoid DCs (PDC), and conventional DCs (cDC) (Figure 5.7e). Delving further within the CD11c+ cDC population, which is primarily responsible for tumor antigen presentation from the conduits to T cells, we found that these cells were of a more mature phenotype as indicated by CD40 and CD86 expression with OND-CpG-NP showing greater expression compared to no change between saline and any other CpG group (Figure 5.7f). Since EL4 lymphoma cells do not express TLR9,[212, 213] these results combined with the tumor data point to a potent systemic immunotherapeutic response.

5.4 Conclusion

In summary, we described a versatile lymphatic-targeting NP system that is able to precisely tune the release profile of conjugated cargo, allowing the cargo to utilize its naturally enhanced diffusivity compared to the larger NP delivery vehicle. We showed that release of cargo from OND-NP increased collagen penetration and dramatically altered the spatial distribution within the LN achieving deeper penetration and access to the more centralized LN structures. This cargo spatial bias aligned with IHC staining showing that the NP restricted from centralized LN access would never be able to access the vast majority of LN-resident immune cells and that OND-NP released cargo could spatial target these cells. When we assessed if this spatial bias resulted in changes to

cellular accumulation and access we found hundreds of fold improvement in the ability to target deep LN-resident cells.

Utilizing our enhanced adaptive immune cell access, we were able to conjugate the TLR9 ligand CpG to our OND-NP and demonstrated a substantial immunotherapeutic response against an EL4 lymphoma model shown by a dramatic reduction in LN tumor size compared to other CpG delivery strategies, and a slowing of the primary tumor growth. This therapeutic response most likely occurred through the proliferation and maturation lymphocytes within the treated LN, demonstrating a potent systemic anti-tumor immune response.

CHAPTER 6. Concluding Remarks and Future Directions

6.1 Conclusions

Current drug delivery for the lymphatics and LNs seeks to overcome several barriers that result in inefficient targeting of the tissue's anatomical location. First, the propensity of small molecule therapeutics to go to the blood following intradermal administration is overcome by formulation into larger drug delivery vehicles, which have blunted blood permeability and therefore result in greater lymphatic uptake efficiency. The second barrier is less appreciated and involves the barrier of the LN structure itself and the resulting regulation of molecular freedom within the LN. Because the LN, especially in the context of cancer – vis-a-vis the TDLN – has recently become a tissue target of interest, many drug delivery strategies solely focus on achieving LN accumulation without analysis of the more important aspect of cellular accumulation. Studies concerning the mechanisms of adaptive immune responses have shed light on these aspects, showing the size-based fate of lymph-borne soluble antigen and their access or lack thereof to the different cell types and compartments of the LN.

Given the research into the microanatomical biodistribution of molecules based on size within the LN, we have designed biomaterials to harness endogenous LN regulating structures to achieve greater delivery of immunotherapeutic payload to the LN-resident cells. In the first aim we explored an endogenous mechanism to achieve release of payload, specifically NO, which has many functions on lymphatics and lymphocytes that have putative therapeutic potential. Our SNO-NP delivery vehicle not

only increased the amount of NO delivered to the LN via standard drug delivery principles, but also hinted at increased cellular access due to the proliferative response of the lymphocytes. In the second aim, we used an engineered linker to release our cargo in a time-based fashion similar to multi-stage delivery systems that have previously been used for tumor targeting, but have never been applied to LNs. We demonstrated that this release afforded increased penetration and cellular access of the cargo, whereas the larger NP delivery vehicle remained blunted from LN penetration. We applied this novel delivery system to the adjuvant, CpG, and showed improved APC maturation as well as immunotherapeutic response against LN and primary lymphoma tumor.

6.2 Contributions to the Field

The overall impact of this work was to address multiple aspects of delivery to LN by recognizing that LN drug delivery should not only concern itself with the tissue target, but importantly with the cellular targets within that tissue. The structure of the lymphatic tissues controls access to the cells involved in the adaptive immune response, and the spatial, temporal, and cellular constraints cannot be accurately addressed by the broad metric of "accumulation" within the target tissue that is achieved by current drug delivery formulation. The main contribution of this work is the fact that we have created the first multi-stage drug delivery systems to overcome both the lymphatic uptake and LN structural delivery barriers to achieve enhanced delivery to cells within the LN.

6.2.1 SNO-NP for enhanced NO delivery to lymphatics/LN

Chapters 3 and 4 of this work detailed the design of a drug delivery vehicle for the transport of NO to deep tissues such as the lymphatics and LN. Our design had several unique advantages over current NO donors in that: 1) the unique size of the SNO-NP

significantly enhanced lymphatic targeting activity; 2) we used an endogenous NO conjugation and release chemistry that was physiologically compatible and degradable, and biologically active; and 3) the system resulted in biological potency with transnitrosation to lymph-borne thiols and cytotoxicty against lymph-resident parasites.

This work, to the best of our knowledge, was the first SNO-delivery NP system designed for both the targeting of LNs and LN-resident cells. This work will help the field by demonstrating that NO can be efficiently delivered to the lymphatics and LN cells. Additionally, this work demonstrates the ability to achieve controlled delivery of NO, a highly reactive molecule, and proposes a novel therapeutic for the treatment of lymphatic-related diseases including lymphatic-resident filarial worms, to which there is currently no targeted cure available.

6.2.2 Multi-stage OND linker for enhanced LN cellular access

Chapter 5 of this work explored the use of an engineered, as opposed to an endogenous (in the case of SNO-NP), release mechanism for achieving enhanced cellular delivery of cargo to LN-resident cells. Our system is one-of-a-kind and improved upon the existing drug delivery systems for LN by: 1) employing a time-sensitive release linker that is insensitive to pH, salt, and enzyme presence to achieve remarkably precise release kinetics of conjugated cargo; 2) combining the lymphatic uptake efficiency of a large NP drug delivery vehicle with the improved diffusivity and LN-structure access of small lymph-borne small molecules to achieve unparalleled LN-resident cellular access; and 3) establishing the importance of cellular access for the generation of adaptive immune responses against cancer.

This work, to the best of our knowledge, is the first "multi-stage" drug delivery system for LN targeting. While there have been a few examples of multi-stage systems for improving the penetration of solid tumors following carrier extravasation into the tumor, there have been no systems exploiting the LN reticular structure by which small antigens are able to access deeper LN cortical cells. Furthermore, this work for the first time proposes that enhancing access to LN-resident cells can improve adaptive immune responses against cancer and should be necessary criteria for any LN drug delivery systems.

6.3 Future Directions

The future directions of my work should seek to further the innovations made in this thesis on lymphatic and LN targeting. No longer relying on the metric of tissue accumulation, future work should always seek to understand the cellular impact of drug delivery to thesis tissues, be it the lymphatic endothelial cells (LECs) or lymphocytes of the lymphatics and LN. Regarding the lymphatics I would like to see the SNO-NP system being used to probe the transport properties of the lymphatics under the influence of differential concentrations of NO. Additionally leveraging the lymphatic targeting of the SNO-NP, I would like to see a future project exploring the *in vivo* cytotoxicity of lymphatic-resident filarial worms to SNO-NP and a characterization of the immune response the results from this treatment. Both of these future projects will have major implications for lymphatic-related diseases that affect millions worldwide. Within the LN I would like to see future projects aimed at expanding the types of molecules delivered via OND-NP. These molecules could be therapeutic in the cases of chemotherapy where delivery of a high concentration of small molecule drug is used to kill LN-resident tumor

cells or they could be used for basic science where molecules such as lymphocyte homing chemokines or selectin inhibitors are delivered in order to probe basic questions about adaptive immune generation between APCs and T cells. Projects such as these would have implications in furthering our understanding of LN physiology as well as adaptive immune mechanisms and will contribute to improving functional outcomes such as vaccine responses and anti-tumor immunity.

6.3.1 SNO-NP for use in understanding the role that NO plays in lymphatic function

Future work using this system should aim to characterize the extra- and intra-lymphatic NO levels required to impair lymphatic transport activity with the long-term goal being to establish a robust, biocompatible NP technology for the tuning of NO levels and lymphatic function *in vivo*. Currently, there are no reliable ways of precisely delivering NO intraluminaly to the lymphatics in order to assess its effect on pumping function. In previous work NO is applied externally to the tissue and then an unknown concentration over an unknown time scale reacts with lymphatic smooth muscle cells altering lymphatic pumping. The SNO-NP platform could be used to precisely deliver a known concentration of NO to the lymphatics with known release kinetics in order to understand exactly how the concentration of NO generated by the lymphatic endothelial cells affects lymphatic function. This work outlines the use of both the mouse forearm lymphatic model as well as the rat tail lymphatic model for assessment using different techniques on the treatment of lymphatics with NO. The importance of this work could extend to lymph edema, which is characterized by aberrant lymphatic pumping, as well as to inflammatory diseases of the lymphatics including obesity and parasitic infection.

6.3.2 SNO-NP as a lymphatic/LN therapeutic

Future work for SNO-NP as a lymphatic/LN therapeutic should seek to exploit NO's therapeutic potential in producing cytotoxicity against lymphatic parasites, reducing lymphocyte proliferation, serving as a chemotherapy sensitizer for lymphoma, or producing chemotherapeutic-resistance to DCs. All of these diseases are uniquely addressable by the SNO-NP system as no other method of NO delivery can target both the lymphatics and LN with precise NO delivery. The work detailed in this thesis should lay the foundation for assessing these therapeutic challenges by using a Jird or immunocompromised mouse model to assess *in vivo* cytotoxicy against lymphatic filarial worms, using the mouse forearm model in Chapter 4 to assess effects of NO on LN-resident T cells and DCs, and using the mouse tumor model in Chapter 5 to assess the effects of NO on chemotherapy resistance of DCs in tumor treatment.

6.3.3 OND-NP for enhanced therapeutic and basic science exploration of the adaptive immune response

Future work for the OND-NP system should aim at exploring the delivery of other treatments to the LN including small molecule chemotherapies as well as using this system to probe basic science questions by delivering integrin inhibitors to alter T cell immunological synapse recognition with APCs. We have done preliminary studies using the topoisomerase-1 inhibitor, irinotecan, which we were able to efficiently conjugate to the NP using OND chemistry.[214] We assessed the potency of this drug *in vitro* against endogenous splenocytes and exogenous EL4 lymphoma cells, and further assessed the *in vivo* effect on LN-resident cells in the dLN to OND-irinotecan. This work could expand upon the tumor immunology work in Chapter 5 by doing a combination therapy to potentiate the adjuvant effects of CpG delivered through OND by producing more antigen in the LN by killing LN tumor cells.

Alternatively, the use of the OND-NP platform for the use in LN basic science has many promising opportunities. In order to elicit potent cytotoxic T cell responses APC activation of T cells is required. The major histocompatibilty complex (MHC) on the APC interacts with the T cell receptor (TCR) on the T cell in what is called the immunological synapse.[111] The MHC has been found to be surround by intracellular adhesion molecules (ICAM) while the TCR is surrounded by leukocyte functional antigen (LFA-1). The interaction between ICAM and LFA-1 is thought to stabilize the weak MHC and TCR interaction and allow for improved signalling. By delivering an inhibitor of this synapse, aspects of the adaptive immune response *in vivo* and *in situ* in the LN could be probed.[215] OND-NP are uniquely suited to deliver this small molecule inhibitor through either direct access to the T cells or by targeting conduit lining DCs that will then interact with T cells.

REFERENCES

1. Senti, G. and T.M. Kündig, *Intralymphatic immunotherapy.* The World Allergy Organization Journal, 2015. **8**(1): p. 9.

2. Dixon, J.B. and M.J. Weiler, *Bridging the divide between pathogenesis and detection in lymphedema.* Seminars in cell & developmental biology, 2015. **38**: p. 75-82.

3. Bockarie, M.J., M.J. Taylor, and J.O. Gyapong, *Current practices in the management of lymphatic filariasis.* Expert Rev Anti Infect Ther, 2009. **7**(5): p. 595-605.

4. Szlavy, L., et al., *Cardiac lymph and lymphatics in normal and infarcted myocardium.* American Heart Journal, 1980. **100**(3): p. 323-331.

5. Szlavy, L., et al., *Early disappearance of lymphatics draining ischemic myocardium in the dog.* Angiology, 1987. **38**(1 Pt 2): p. 73-84.

6. Swartz, M.A., *The physiology of the lymphatic system.* Adv Drug Deliv Rev, 2001. **50**(1-2): p. 3-20.

7. Dixon, J.B., *Lymphatic Lipid Transport: Sewer or Subway?* Trends in endocrinology and metabolism: TEM, 2010. **21**(8): p. 480-487.

8. Roozendaal, R., et al., *Conduits Mediate Transport of Low Molecular Weight Antigen to Lymph Node Follicles.* Immunity, 2009. **30**(2): p. 264-76.

9. Thomas, S.N., N.A. Rohner, and E.E. Edwards, *Implications of Lymphatic Transport to Lymph Nodes in Immunity and Immunotherapy.* Annu Rev Biomed Eng, 2016. **18**: p. 207-33.

10. Thomas, S.N., et al., *Targeting the tumor-draining lymph node with adjuvanted nanoparticles reshapes the anti-tumor immune response.* Biomaterials, 2014. **35**(2): p. 814-24.

11. Thomas, S.N. and A. Schudel, *Overcoming transport barriers for interstitial-, lymphatic-, and lymph node-targeted drug delivery.* Curr Opin Chem Eng, 2015. **7**: p. 65-74.

12. Fox, B.A., et al., *Defining the critical hurdles in cancer immunotherapy.* Journal of Translational Medicine, 2011. **9**: p. 214-214.

13. Schudel, A., et al., *S-Nitrosated Polypropylene Sulfide Nanoparticles for Thiol-Dependent Transnitrosation and Toxicity Against Adult Female Filarial Worms.* Adv Healthc Mater, 2015. **4**(10): p. 1484-90, 1423.

14. Schmid-Schonbein, G.W., *Mechanisms causing initial lymphatics to expand and compress to promote lymph flow.* Arch Histol Cytol, 1990. **53 Suppl**: p. 107-14.

15. Porter, C.J., *Drug delivery to the lymphatic system.* Critical reviews in therapeutic drug carrier systems, 1997. **14**(4): p. 333-394.

16. Porter, C.J.H. and S.A. Charman, *Lymphatic transport of proteins after subcutaneous administration.* Journal of Pharmaceutical Sciences, 2000. **89**(3): p. 297-310.

17. Swartz, M.A., J.A. Hubbell, and S.T. Reddy, *Lymphatic drainage function and its immunological implications: From dendritic cell homing to vaccine design.* Seminars in Immunology, 2008. **20**(2): p. 147-156.

18. Cui, Y., *The role of lymphatic vessels in the heart.* Pathophysiology, 2010. **17**(4): p. 307-314.

19. Taylor, M.J., A. Hoerauf, and M. Bockarie, *Lymphatic filariasis and onchocerciasis.* Lancet, 2010. **376**(9747): p. 1175-85.

20. Organization, W.H., *Lymphatic filariasis: Fact Sheet No 102.* World Health Organization Media Center. Available at: http://www. who. int/mediacentre/factsheets/fs102/en/. Accessed May, 2012. **1**: p. 2012.

21. Organization, W.H., *Global cancer rates could increase by 50% to 15 million by 2020. Available at: http://www.who.int/mediacentre/news/releases/2003/pr27/en/. Accessed September 1,*

2017. 2003.

22. Didem, K., et al., *The comparison of two different physiotherapy methods in treatment of lymphedema after breast surgery.* Breast Cancer Res Treat, 2005. **93**(1): p. 49-54.

23. Hughes, M.N., *Chapter One - Chemistry of Nitric Oxide and Related Species*, in *Methods in Enzymology*, R.K. Poole, Editor. 2008, Academic Press. p. 3-19.

24. Bohlen, H.G., O.Y. Gasheva, and D.C. Zawieja, *Nitric oxide formation by lymphatic bulb and valves is a major regulatory component of lymphatic pumping.* Am J Physiol Heart Circ Physiol, 2011. **301**(5): p. H1897-906.

25. Bohlen, H.G., et al., *Phasic contractions of rat mesenteric lymphatics increase basal and phasic nitric oxide generation in vivo.* Am J Physiol Heart Circ Physiol, 2009. **297**(4): p. H1319-28.

26. Hagendoorn, J., et al., *Endothelial Nitric Oxide Synthase Regulates Microlymphatic Flow via Collecting Lymphatics.* Circulation Research, 2004. **95**(2): p. 204-209.

27. Shirasawa, Y., F. Ikomi, and T. Ohhashi, *Physiological roles of endogenous nitric oxide in lymphatic pump activity of rat mesentery in vivo.* Am J Physiol Gastrointest Liver Physiol, 2000. **278**(4): p. G551-6.

28. Wilson, J.T., et al., *Confocal Image-Based Computational Modeling of Nitric Oxide Transport in a Rat Mesenteric Lymphatic Vessel.* Journal of Biomechanical Engineering, 2013. **135**(5): p. 0510051-0510058.

29. Kerwin, J.F., Jr., J.R. Lancaster, Jr., and P.L. Feldman, *Nitric oxide: a new paradigm for second messengers.* J Med Chem, 1995. **38**(22): p. 4343-62.

30. Feldman, P.G., O.; Stuehr, D., *The surprising life of NITRIC OXIDE.* Chemical & Engineering News Archive, 1993. **71**(51): p. 26-38.

31. Liao, S., et al., *Impaired lymphatic contraction associated with immunosuppression.* Proceedings of the National Academy of Sciences of the United States of America, 2011. **108**(46): p. 18784-18789.

32. Lahdenranta, J., et al., *Endothelial Nitric Oxide Synthase Mediates Lymphangiogenesis and Lymphatic Metastasis.* Cancer Research, 2009. **69**(7): p. 2801-2808.

33. Rand, M.J., *Nitrergic transmission: nitric oxide as a mediator of non-adrenergic, non-cholinergic neuro-effector transmission.* Clin Exp Pharmacol Physiol, 1992. **19**(3): p. 147-69.

34. Ignarro, L.J., et al., *Mechanism of vascular smooth muscle relaxation by organic nitrates, nitrites, nitroprusside and nitric oxide: evidence for the involvement of S-nitrosothiols as active intermediates.* J Pharmacol Exp Ther, 1981. **218**(3): p. 739-49.

35. Laskin, J.D., D.E. Heck, and D.L. Laskin, *Multifunctional role of nitric oxide in inflammation.* Trends in Endocrinology & Metabolism, 1994. **5**(9): p. 377-382.

36. Wink, D.A. and J.B. Mitchell, *Chemical biology of nitric oxide: insights into regulatory, cytotoxic, and cytoprotective mechanisms of nitric oxide.* Free Radical Biology and Medicine, 1998. **25**(4): p. 434-456.

37. Boden, W.E., et al., *Nitrates as an integral part of optimal medical therapy and cardiac rehabilitation for stable angina: review of current concepts and therapeutics.* Clin Cardiol, 2012. **35**(5): p. 263-71.

38. Biswas, O.S., V.R. Gonzalez, and E.R. Schwarz, *Effects of an oral nitric oxide supplement on functional capacity and blood pressure in adults with prehypertension.* J Cardiovasc Pharmacol Ther, 2015. **20**(1): p. 52-8.

39. Schwartz, E., *Study of the effects of an oral nitric oxide supplementon blood pressure in prehypertensive adults. 2013. Available at: https://clinicaltrials.gov/ct2/show/NCT01937754.* 2013.

40. Egan, B.M. and S. Stevens-Fabry, *Prehypertension--prevalence, health risks, and management strategies.* Nat Rev Cardiol, 2015. **12**(5): p. 289-300.

41. Hill, C., *Inhaled nitric oxide and inhaled prostacyclin after cardiac surgery for heart transplant or LVAD placement. Identifier:*

NCT01717209. 2012. Available at: https://clinicaltrials.gov/ct2/show/results/NCT01717209.

42. Walsh-Sukys, M.C., et al., *Persistent Pulmonary Hypertension of the Newborn in the Era Before Nitric Oxide: Practice Variation and Outcomes.* Pediatrics, 2000. **105**(1): p. 14-20.

43. Huerta, S., S. Chilka, and B. Bonavida, *Nitric oxide donors: novel cancer therapeutics (review).* Int J Oncol, 2008. **33**(5): p. 909-27.

44. Kim, J., et al., *Combination of nitric oxide and drug delivery systems: tools for overcoming drug resistance in chemotherapy.* J Control Release, 2017. **263**: p. 223-230.

45. Huang, J., et al., *Nitric Oxide Sensitizes Tumor Cells to Dendritic Cell–Mediated Apoptosis, Uptake, and Cross-Presentation.* Cancer Research, 2005. **65**(18): p. 8461-8470.

46. Tsumori, M., et al., *Cytotoxic effect of nitric oxide on human hematological malignant cells.* Acta Biochim Pol, 2002. **49**(1): p. 139-44.

47. Umansky, V., et al., *Activated endothelial cells induce apoptosis in lymphoma cells.* Int J Oncol, 1997. **10**(3): p. 465-71.

48. Ushmorov, A., et al., *Nitric-oxide-induced apoptosis in human leukemic lines requires mitochondrial lipid degradation and cytochrome C release.* Blood, 1999. **93**(7): p. 2342-52.

49. Secchiero, P., et al., *Activation of the nitric oxide synthase pathway represents a key component of tumor necrosis factor-related apoptosis-inducing ligand-mediated cytotoxicity on hematologic malignancies.* Blood, 2001. **98**(7): p. 2220-8.

50. Miller, M.R. and I.L. Megson, *Recent developments in nitric oxide donor drugs.* British Journal of Pharmacology, 2007. **151**(3): p. 305-321.

51. Orie, N.N., et al., *S-nitroso-albumin carries a thiol-labile pool of nitric oxide, which causes venodilation in the rat.* Am J Physiol Heart Circ Physiol, 2005. **289**(2): p. H916-23.

52. Martinez-Ruiz, A. and S. Lamas, *S-nitrosylation: a potential new paradigm in signal transduction.* Cardiovasc Res, 2004. **62**(1): p. 43-52.

53. Al-Sa'doni, H. and A. Ferro, *S-Nitrosothiols: a class of nitric oxide-donor drugs.* Clin Sci (Lond), 2000. **98**(5): p. 507-20.

54. Goldstein, S. and G. Czapski, *Mechanism of the Nitrosation of Thiols and Amines by Oxygenated •NO Solutions: the Nature of the Nitrosating Intermediates.* Journal of the American Chemical Society, 1996. **118**(14): p. 3419-3425.

55. Meyer, D.J., et al., *Kinetics and equilibria of S-nitrosothiol—thiol exchange between glutathione, cysteine, penicillamines and serum albumin.* FEBS Letters, 1994. **345**(2): p. 177-180.

56. Arnelle, D.R. and J.S. Stamler, *NO+, NO, and NO- donation by S-nitrosothiols: implications for regulation of physiological functions by S-nitrosylation and acceleration of disulfide formation.* Arch Biochem Biophys, 1995. **318**(2): p. 279-85.

57. Zhang, Y. and N. Hogg, *S-Nitrosothiols: cellular formation and transport.* Free Radic Biol Med, 2005. **38**(7): p. 831-8.

58. Stamler, J.S., et al., *Nitric oxide circulates in mammalian plasma primarily as an S-nitroso adduct of serum albumin.* Proc Natl Acad Sci U S A, 1992. **89**(16): p. 7674-7.

59. Miranda KM, E.M., Jourd'heuil D, Grisham MB, Fukuto JM, Feelisch M, Wink DA., *Chapter 3 - The Chemical Biology of Nitric Oxide A2.* Academic Press, 2000(Ignarro, Louis J. Nitric Oxide.): p. 41-55.

60. Sehba, F.A., et al., *Acute decrease in cerebral nitric oxide levels after subarachnoid hemorrhage.* J Cereb Blood Flow Metab, 2000. **20**(3): p. 604-11.

61. Kostourou, V., et al., *The role of tumour-derived iNOS in tumour progression and angiogenesis.* Br J Cancer, 2011. **104**(1): p. 83-90.

62. Lancaster, J.R., Jr. and B. Gaston, *NO and nitrosothiols: spatial confinement and free diffusion.* Am J Physiol Lung Cell Mol Physiol, 2004. **287**(3): p. L465-6.

63. Ignarro, L.J., *Biosynthesis and metabolism of endothelium-derived nitric oxide.* Annu Rev Pharmacol Toxicol, 1990. **30**: p. 535-60.

64. Reddy, S.T., et al., *A sensitive in vivo model for quantifying interstitial convective transport of injected macromolecules and nanoparticles.* J Appl Physiol (1985), 2006. **101**(4): p. 1162-9.

65. Sarin, H., *Physiologic upper limits of pore size of different blood capillary types and another perspective on the dual pore theory of microvascular permeability.* J Angiogenes Res, 2010. **2**: p. 14.

66. Kaminskas, L.M., et al., *PEGylation of polylysine dendrimers improves absorption and lymphatic targeting following SC administration in rats.* Journal of Controlled Release, 2009. **140**(2): p. 108-116.

67. Reddy, S.T., et al., *In vivo targeting of dendritic cells in lymph nodes with poly(propylene sulfide) nanoparticles.* Journal of Controlled Release, 2006. **112**(1): p. 26-34.

68. Chauhan, V.P., et al., *Delivery of molecular and nanoscale medicine to tumors: transport barriers and strategies.* Annu Rev Chem Biomol Eng, 2011. **2**: p. 281-98.

69. Allen, T.M. and P.R. Cullis, *Drug delivery systems: entering the mainstream.* Science, 2004. **303**(5665): p. 1818-22.

70. Kaur, C.D., M. Nahar, and N.K. Jain, *Lymphatic targeting of zidovudine using surface-engineered liposomes.* J Drug Target, 2008. **16**(10): p. 798-805.

71. Schudel, A., M.C. Bellavia, and S.N. Thomas, *Nanosystems for Immunotherapeutic Drug Delivery*, in *Biomaterials in Regenerative Medicine and the Immune System*. 2015, Springer. p. 157-170.

72. Katsumi, H., et al., *Development of polyethylene glycol-conjugated poly-S-nitrosated serum albumin, a novel S-Nitrosothiol for prolonged delivery of nitric oxide in the blood circulation in vivo.* J Pharmacol Exp Ther, 2005. **314**(3): p. 1117-24.

73. Stasko, N.A., T.H. Fischer, and M.H. Schoenfisch, *S-Nitrosothiol-Modified Dendrimers as Nitric Oxide Delivery Vehicles.* Biomacromolecules, 2008. **9**(3): p. 834-841.

74. Saraiva J, S.S.M.-O., Simone Aparecida Cicillini, Josimar de Oliveira Eloy, and Juliana Maldonado Marchetti., *Nanocarriers for Nitric Oxide Delivery.* Journal of Drug Delivery, 2011. **2011**.

75. Jo, Y.S., et al., *Micelles for Delivery of Nitric Oxide.* Journal of the American Chemical Society, 2009. **131**(40): p. 14413-14418.

76. Seabra, A.B., M. Rai, and N. Durán, *Nano carriers for nitric oxide delivery and its potential applications in plant physiological process: A mini review.* Journal of Plant Biochemistry and Biotechnology, 2014. **23**(1): p. 1-10.

77. Kutner, A.J. and A.J. Friedman, *Use of nitric oxide nanoparticulate platform for the treatment of skin and soft tissue infections.* Wiley Interdiscip Rev Nanomed Nanobiotechnol, 2013. **5**(5): p. 502-14.

78. Weller, R.B., *Nitric oxide-containing nanoparticles as an antimicrobial agent and enhancer of wound healing.* J Invest Dermatol, 2009. **129**(10): p. 2335-7.

79. Shin, J.H., S.K. Metzger, and M.H. Schoenfisch, *Synthesis of nitric oxide-releasing silica nanoparticles.* J Am Chem Soc, 2007. **129**(15): p. 4612-9.

80. Nembrini, C., et al., *Nanoparticle conjugation of antigen enhances cytotoxic T-cell responses in pulmonary vaccination.* Proceedings of the National Academy of Sciences, 2011. **108**(44): p. E989–E997.

81. Dane, K.Y., et al., *Nano-sized drug-loaded micelles deliver payload to lymph node immune cells and prolong allograft survival.* Journal of Controlled Release, 2011. **156**(2): p. 154-160.

82. Itano, A.A., et al., *Distinct Dendritic Cell Populations Sequentially Present Antigen to CD4 T Cells and Stimulate Different Aspects of Cell-Mediated Immunity.* Immunity, 2003. **19**(1): p. 47-57.

83. Gerner, Michael Y., P. Torabi-Parizi, and Ronald N. Germain, *Strategically Localized Dendritic Cells Promote Rapid T Cell Responses to Lymph-Borne Particulate Antigens.* Immunity, 2015. **42**(1): p. 172-185.

84. Sixt, M., et al., *The Conduit System Transports Soluble Antigens from the Afferent Lymph to Resident Dendritic Cells in the T Cell Area of the Lymph Node.* Immunity, 2005. **22**(1): p. 19-29.

85. Gretz, J.E., et al., *Lymph-borne chemokines and other low molecular weight molecules reach high endothelial venules via specialized conduits while a functional barrier limits access to the lymphocyte microenvironments in lymph node cortex.* J Exp Med, 2000. **192**(10): p. 1425-40.

86. Junt, T., et al., *Subcapsular sinus macrophages in lymph nodes clear lymph-borne viruses and present them to antiviral B cells.* Nature, 2007. **450**(7166): p. 110-114.

87. Carrasco, Y.R. and F.D. Batista, *B cells acquire particulate antigen in a macrophage-rich area at the boundary between the follicle and the subcapsular sinus of the lymph node.* Immunity, 2007. **27**(1): p. 160-71.

88. Phan, T.G., et al., *Subcapsular encounter and complement-dependent transport of immune complexes by lymph node B cells.* Nat Immunol, 2007. **8**(9): p. 992-1000.

89. Sainte-Marie G., P.F.S., *[Distribution of a diffusible tracer in the subcapsular sinus and the cortex of lymph nodes in the rat]*. Rev Can Biol Exp, 1982. **41**(3): p. 201-8.

90. Harding, S.E., D.B. Sattelle, and V.A. Bloomfield, *Laser light scattering in biochemistry*. 1992: Royal Society of Chemistry.

91. team, T.A.C.S.m.a.e.c., *Lymph Nodes and Cancer.* 2015.

92. Chandrasekaran, S. and M.R. King, *Microenvironment of Tumor-Draining Lymph Nodes: Opportunities for Liposome-Based Targeted Therapy.* International Journal of Molecular Sciences, 2014. **15**(11): p. 20209-20239.

93. Society, T.A.C., *Cancer Facts and Figures 2018. Available at: https://www.cancer.org/content/dam/cancer-org/research/cancer-facts-and-statistics/annual-cancer-facts-and-figures/2018/cancer-facts-and-figures-2018.pdf. Accessed on March 16, 2018.* 2018.

94. Thomas, S.N., et al., *Impaired humoral immunity and tolerance in K14-VEGFR-3-Ig mice that lack dermal lymphatic drainage.* J Immunol, 2012. **189**(5): p. 2181-90.

95. Lund, A.W., et al., *VEGF-C promotes immune tolerance in B16 melanomas and cross-presentation of tumor antigen by lymph node lymphatics.* Cell Rep, 2012. **1**(3): p. 191-9.

96. Liu, R., et al., *Prevention of nodal metastases in breast cancer following the lymphatic migration of paclitaxel-loaded expansile nanoparticles.* Biomaterials, 2013. **34**(7): p. 1810-9.

97. Farkona, S., E.P. Diamandis, and I.M. Blasutig, *Cancer immunotherapy: the beginning of the end of cancer?* BMC Medicine, 2016. **14**(1): p. 73.

98. Jewell, C.M., S.C. Bustamante López, and D.J. Irvine, *In situ engineering of the lymph node microenvironment via intranodal injection of adjuvant-releasing polymer particles.* Proceedings of the National Academy of Sciences, 2011. **108**(38): p. 15745-15750.

99. Shima, F., et al., *Size effect of amphiphilic poly(gamma-glutamic acid) nanoparticles on cellular uptake and maturation of dendritic cells in vivo.* Acta Biomater, 2013. **9**(11): p. 8894-901.

100. Ryan, G.M., et al., *PEGylated polylysine dendrimers increase lymphatic exposure to doxorubicin when compared to PEGylated liposomal and solution formulations of doxorubicin.* J Control Release, 2013. **172**(1): p. 128-36.

101. Hons, M. and M. Sixt, *The lymph node filter revealed.* Nat Immunol, 2015. **16**(4): p. 338-40.

102. Liu, H., et al., *Structure-based Programming of Lymph Node Targeting in Molecular Vaccines.* Nature, 2014. **507**(7493): p. 519-522.

103. Wong, C., et al., *Multistage nanoparticle delivery system for deep penetration into tumor tissue.* Proceedings of the National Academy of Sciences, 2011. **108**(6): p. 2426-2431.

104. Kourtis, I.C., et al., *Peripherally administered nanoparticles target monocytic myeloid cells, secondary lymphoid organs and tumors in mice.* PLoS One, 2013. **8**(4): p. e61646.

105. Bagby, T.R., et al., *Impact of Molecular Weight on Lymphatic Drainage of a Biopolymer-Based Imaging Agent.* Pharmaceutics, 2012. **4**(2): p. 276-295.

106. Bal, S.M., et al., *Co-encapsulation of antigen and Toll-like receptor ligand in cationic liposomes affects the quality of the immune response in mice after intradermal vaccination.* Vaccine, 2011. **29**(5): p. 1045-1052.

107. de Titta, A., et al., *Nanoparticle conjugation of CpG enhances adjuvancy for cellular immunity and memory recall at low dose.* Proceedings of the National Academy of Sciences, 2013. **110**(49): p. 19902-19907.

108. Thomas, S.N., et al., *Engineering complement activation on polypropylene sulfide vaccine nanoparticles.* Biomaterials, 2011. **32**(8): p. 2194-203.

109. Schmaljohann, D., *Thermo- and pH-responsive polymers in drug delivery.* Advanced Drug Delivery Reviews, 2006. **58**(15): p. 1655-1670.

110. Kessenbrock, K., V. Plaks, and Z. Werb, *Matrix Metalloproteinases: Regulators of the Tumor Microenvironment.* Cell, 2010. **141**(1): p. 52-67.

111. Murphy, K. and C. Weaver, *Janeway's immunobiology*. 2016: Garland Science.

112. Takeda, K. and S. Akira, *TLR signaling pathways.* Semin Immunol, 2004. **16**(1): p. 3-9.

113. Laing, P., et al., *The 'Co-Delivery' Approach to Liposomal Vaccines: Application to the Development of influenza-A and hepatitis-B Vaccine Candidates.* Journal of Liposome Research, 2006. **16**(3): p. 229-235.

114. Rehor, A., J.A. Hubbell, and N. Tirelli, *Oxidation-Sensitive Polymeric Nanoparticles.* Langmuir, 2005. **21**(1): p. 411-417.

115. Marzo, A.L., et al., *Tumor Antigens are Constitutively Presented in the Draining Lymph Nodes.* The Journal of Immunology, 1999. **162**(10): p. 5838-5845.

116. Swartz, M.A. and A.W. Lund, *Lymphatic and interstitial flow in the tumour microenvironment: linking mechanobiology with immunity.* Nat Rev Cancer, 2012. **12**(3): p. 210-9.

117. Ignarro, L.J., et al., *Endothelium-derived relaxing factor produced and released from artery and vein is nitric oxide.* Proc Natl Acad Sci U S A, 1987. **84**(24): p. 9265-9.

118. Yao, S.K., et al., *Endogenous nitric oxide protects against platelet aggregation and cyclic flow variations in stenosed and endothelium-injured arteries.* Circulation, 1992. **86**(4): p. 1302-9.

119. Cayatte, A.J., et al., *Chronic inhibition of nitric oxide production accelerates neointima formation and impairs endothelial function in hypercholesterolemic rabbits.* Arterioscler Thromb, 1994. **14**(5): p. 753-9.

120. Mueller, A.R., et al., *The effects of administration of nitric oxide inhibitors during small bowel preservation and reperfusion.* Transplantation, 1994. **58**(12): p. 1309-16.

121. Zhang, F. and C. Iadecola, *Reduction of focal cerebral ischemic damage by delayed treatment with nitric oxide donors.* J Cereb Blood Flow Metab, 1994. **14**(4): p. 574-80.

122. Lundberg, J.O., E. Weitzberg, and M.T. Gladwin, *The nitrate-nitrite-nitric oxide pathway in physiology and therapeutics.* Nat Rev Drug Discov, 2008. **7**(2): p. 156-67.

123. Askew, S.C., et al., *Chemical mechanisms underlying the vasodilator and platelet anti-aggregating properties of S-nitroso-N-acetyl-DL-penicillamine and S-nitrosoglutathione.* Bioorg Med Chem, 1995. **3**(1): p. 1-9.

124. Keshive, M., et al., *Kinetics of S-nitrosation of thiols in nitric oxide solutions.* Chem Res Toxicol, 1996. **9**(6): p. 988-93.

125. Mulsch, A., et al., *Specificity of different organic nitrates to elicit NO formation in rabbit vascular tissues and organs in vivo.* Br J Pharmacol, 1995. **116**(6): p. 2743-9.

126. Brunet, L.R., *Nitric oxide in parasitic infections.* Int Immunopharmacol, 2001. **1**(8): p. 1457-67.

127. Rajan, T.V., et al., *Role of nitric oxide in host defense against an extracellular, metazoan parasite, Brugia malayi.* Infect Immun, 1996. **64**(8): p. 3351-3.

128. Ascenzi, P., A. Bocedi, and L. Gradoni, *The anti-parasitic effects of nitric oxide.* IUBMB Life, 2003. **55**(10-11): p. 573-8.

129. Thomas, G.R., M. McCrossan, and M.E. Selkirk, *Cytostatic and cytotoxic effects of activated macrophages and nitric oxide donors on Brugia malayi.* Infect Immun, 1997. **65**(7): p. 2732-9.

130. Rockett, K.A., et al., *Killing of Plasmodium falciparum in vitro by nitric oxide derivatives.* Infect Immun, 1991. **59**(9): p. 3280-3.

131. Costa, I.S., et al., *S-nitrosoglutathione (GSNO) is cytotoxic to intracellular amastigotes and promotes healing of topically treated Leishmania major or Leishmania braziliensis skin lesions.* J Antimicrob Chemother, 2013. **68**(11): p. 2561-8.

132. Bergqvist, L., S.E. Strand, and B.R. Persson, *Particle sizing and biokinetics of interstitial lymphoscintigraphic agents.* Semin Nucl Med, 1983. **13**(1): p. 9-19.

133. Oussoren, C., et al., *Lymphatic uptake and biodistribution of liposomes after subcutaneous injection.: II. Influence of liposomal size, lipid composition and lipid dose.* Biochimica et Biophysica Acta (BBA) - Biomembranes, 1997. **1328**(2): p. 261-272.

134. van der Vlies, A.J., et al., *Synthesis of pyridyl disulfide-functionalized nanoparticles for conjugating thiol-containing small molecules, peptides, and proteins.* Bioconjug Chem, 2010. **21**(4): p. 653-62.

135. Saville, B., *A scheme for the colorimetric determination of microgram amounts of thiols.* Analyst, 1958. **83**(993): p. 670-672.

136. Hart, T.W., *Some observations concerning the S-nitroso and S-phenylsulphonyl derivatives of L-cysteine and glutathione.* Tetrahedron Letters, 1985. **26**(16): p. 2013-2016.

137. Michalski, M.L., et al., *The NIH-NIAID Filariasis Research Reagent Resource Center.* PLoS Negl Trop Dis, 2011. **5**(11): p. e1261.

138. Fernandes, D., J.E. Da Silva-Santos, and J. Assreuy, *Nitric oxide-induced inhibition of mouse paw edema: involvement of soluble guanylate cyclase and potassium channels.* Inflamm Res, 2002. **51**(8): p. 377-84.

139. Bryan, S., et al., *The effect of nitric oxide inhibitors and Snitroso-Nacetylpenicillamine on glucose concentration in an animal model.* Journal of Natural Science, Biology, and Medicine, 2011. **2**(1): p. 80-86.

140. Liu, X., et al., *Accelerated reaction of nitric oxide with O2 within the hydrophobic interior of biological membranes.* Proc Natl Acad Sci U S A, 1998. **95**(5): p. 2175-9.

141. Ignarro, L.J., et al., *Oxidation of nitric oxide in aqueous solution to nitrite but not nitrate: comparison with enzymatically formed nitric oxide from L-arginine.* Proc Natl Acad Sci U S A, 1993. **90**(17): p. 8103-7.

142. Kassis, T., et al., *An integrated in vitro imaging platform for characterizing filarial parasite behavior within a multicellular microenvironment.* PLoS Negl Trop Dis, 2014. **8**(11): p. e3305.

143. Smith, V.P., M.E. Selkirk, and K. Gounaris, *Identification and composition of lipid classes in surface and somatic preparations of adult Brugia malayi.* Mol Biochem Parasitol, 1996. **78**(1-2): p. 105-16.

144. Selkirk, M.E. and M.L. Blaxter, *Cuticular proteins of Brugia filarial parasites.* Acta Trop, 1990. **47**(5-6): p. 373-80.

145. Howells, R.E. and S.N. Chen, *Brugia pahangi: feeding and nutrient uptake in vitro and in vivo.* Exp Parasitol, 1981. **51**(1): p. 42-58.

146. Hertz, R., et al., *Proteomic identification of S-nitrosylated proteins in the parasite Entamoeba histolytica by resin-assisted capture: insights into the regulation of the Gal/GalNAc lectin by nitric oxide.* PLoS One, 2014. **9**(3): p. e91518.

147. Siman-Tov, R. and S. Ankri, *Nitric oxide inhibits cysteine proteinases and alcohol dehydrogenase 2 of Entamoeba histolytica.* Parasitol Res, 2003. **89**(2): p. 146-9.

148. Braun, P., et al., *Free amino-acid content of the lymph.* Nature, 1956. **177**(4520): p. 1133-4.

149. Schudel, A., L.F. Sestito, and S.N. Thomas, *Winner of the society for biomaterials young investigator award for the annual meeting of the society for biomaterials, April 11–14, 2018, Atlanta, GA: S-nitrosated poly(propylene sulfide) nanoparticles for enhanced nitric oxide delivery to lymphatic tissues.* Journal of Biomedical Materials Research Part A, 2018: p. n/a-n/a.

150. Laszlo, S., et al., *Early Disappearance of Lymphatics Draining Ischemic Myocardium in the Dog.* Angiology, 1987. **38**(1): p. 73-84.

151. Roozendaal, R., R.E. Mebius, and G. Kraal, *The conduit system of the lymph node.* Int Immunol, 2008. **20**(12): p. 1483-7.

152. Francis, D.M. and S.N. Thomas, *Progress and opportunities for enhancing the delivery and efficacy of checkpoint inhibitors for cancer immunotherapy.* Adv Drug Deliv Rev, 2017. **114**: p. 33-42.

153. Jeanbart, L., et al., *Enhancing efficacy of anticancer vaccines by targeted delivery to tumor-draining lymph nodes.* Cancer Immunol Res, 2014. **2**(5): p. 436-47.

154. Zeng, Q., et al., *Tailoring polymeric hybrid micelles with lymph node targeting ability to improve the potency of cancer vaccines.* Biomaterials, 2017. **122**(Supplement C): p. 105-113.

155. Yang, C., et al., *Tumor-derived exosomes confer antigen-specific immunosuppression in a murine delayed-type hypersensitivity model.* PLoS One, 2011. **6**(8): p. e22517.

156. Chen, S.A., et al., *Plasma and lymph pharmacokinetics of recombinant human interleukin-2 and polyethylene glycol-modified interleukin-2 in pigs.* J Pharmacol Exp Ther, 2000. **293**(1): p. 248-59.

157. Palmer, R.M.J., A.G. Ferrige, and S. Moncada, *Nitric oxide release accounts for the biological activity of endothelium-derived relaxing factor.* Nature, 1987. **327**: p. 524.

158. Kleschyov, A.L., et al., *Does Nitric Oxide Mediate the Vasodilator Activity of Nitroglycerin?* Circulation Research, 2003. **93**(9): p. e104-e112.

159. Taylor, E.L., et al., *Nitric oxide: a key regulator of myeloid inflammatory cell apoptosis.* Cell Death Differ, 2003. **10**(4): p. 418-30.

160. Allen, T.M., C.B. Hansen, and L.S. Guo, *Subcutaneous administration of liposomes: a comparison with the intravenous and intraperitoneal routes of injection.* Biochim Biophys Acta, 1993. **1150**(1): p. 9-16.

161. Kinnunen, H.M. and R.J. Mrsny, *Improving the outcomes of biopharmaceutical delivery via the subcutaneous route by understanding the chemical, physical and physiological properties of the subcutaneous injection site.* J Control Release, 2014. **182**: p. 22-32.

162. Oussoren, C. and G. Storm, *Liposomes to target the lymphatics by subcutaneous administration.* Adv Drug Deliv Rev, 2001. **50**(1-2): p. 143-56.

163. Rohner, N.A. and S.N. Thomas, *Flexible Macromolecule versus Rigid Particle Retention in the Injected Skin and Accumulation in Draining Lymph Nodes Are Differentially Influenced by Hydrodynamic Size.* ACS Biomaterials Science & Engineering, 2017. **3**(2): p. 153-159.

164. Rohner, N.A. and S.N. Thomas, *Melanoma growth effects on molecular clearance from tumors and biodistribution into systemic tissues versus draining lymph nodes.* J Control Release, 2016. **223**: p. 99-108.

165. Kojima, H., et al., *Fluorescent Indicators for Imaging Nitric Oxide Production.* Angew Chem Int Ed Engl, 1999. **38**(21): p. 3209-3212.

166. Brown, A.C., et al., *Molecular interference of fibrin's divalent polymerization mechanism enables modulation of multiscale material properties.* Biomaterials, 2015. **49**: p. 27-36.

167. Phelps, E.A., et al., *Engineered VEGF-releasing PEG-MAL hydrogel for pancreatic islet vascularization.* Drug Deliv Transl Res, 2015. **5**(2): p. 125-36.

168. Nahrevanian, H. and M.J. Dascombe, *Nitric oxide and reactive nitrogen intermediates during lethal and nonlethal strains of murine malaria.* Parasite Immunol, 2001. **23**(9): p. 491-501.

169. Mehta, A., R.S. Verma, and N. Srivastava, *Chlorpyrifos induced alterations in the levels of hydrogen peroxide, nitrate and nitrite in rat brain and liver.* Pesticide Biochemistry and Physiology, 2009. **94**(2): p. 55-59.

170. Kostka, P., B. Xu, and E.H. Skiles, *Degradation of S-nitrosocysteine in vascular tissue homogenates: role of divalent ions.* J Cardiovasc Pharmacol, 1999. **33**(4): p. 665-70.

171. Fukuto, J.M., J.Y. Cho, and C.H. Switzer, *The chemical properties of nitric oxide and related nitrogen oxides,* in *Nitric Oxide*. 2000, Elsevier. p. 23-40.

172. Radi, R., *Peroxynitrite, a stealthy biological oxidant.* J Biol Chem, 2013. **288**(37): p. 26464-72.

173. Beckman, J.S. and W.H. Koppenol, *Nitric oxide, superoxide, and peroxynitrite: the good, the bad, and ugly.* Am J Physiol, 1996. **271**(5 Pt 1): p. C1424-37.

174. Li, C.Q., et al., *Threshold effects of nitric oxide-induced toxicity and cellular responses in wild-type and p53-null human lymphoblastoid cells.* Chem Res Toxicol, 2006. **19**(3): p. 399-406.

175. Andrew, P.S., et al., *Nitric oxide increases fluid extravasation from the splenic circulation of the rat.* Am J Physiol Regul Integr Comp Physiol, 2001. **280**(4): p. R959-67.

176. Saavedra, J.E., et al., *Targeting Nitric Oxide (NO) Delivery in Vivo. Design of a Liver-Selective NO Donor Prodrug That Blocks Tumor Necrosis Factor-α-Induced Apoptosis and Toxicity in the Liver.* Journal of Medicinal Chemistry, 1997. **40**(13): p. 1947-1954.

177. Kourtis, I., *Therapeutic Immunomodulation of the Lymphoid-like Tumor Environment Using Nanoparticulate Formulations*. 2012.

178. Weiler, M., T. Kassis, and J.B. Dixon. *Sensitivity analysis of near-infrared functional lymphatic imaging*. 2012. SPIE.

179. Saul, M.E., et al., *A pharmacological approach to first aid treatment for snakebite.* Nat Med, 2011. **17**(7): p. 809-11.

180. Cals-Grierson, M.M. and A.D. Ormerod, *Nitric oxide function in the skin.* Nitric Oxide, 2004. **10**(4): p. 179-193.

181. F., C.G., *Role of nitric oxide in the regulation of microvascular perfusion in human skin in vivo.* The Journal of Physiology, 1999. **516**(2): p. 549-557.

182. Fukumura, D., et al., *Role of nitric oxide in tumor microcirculation. Blood flow, vascular permeability, and leukocyte-endothelial interactions.* The American Journal of Pathology, 1997. **150**(2): p. 713-725.

183. Ghaffari, A., et al., *Efficacy of gaseous nitric oxide in the treatment of skin and soft tissue infections.* Wound Repair Regen, 2007. **15**(3): p. 368-77.

184. Amadeu, T.P., et al., *S-nitrosoglutathione-containing hydrogel accelerates rat cutaneous wound repair.* J Eur Acad Dermatol Venereol, 2007. **21**(5): p. 629-37.

185. Amadeu, T.P., et al., *Nitric oxide donor improves healing if applied on inflammatory and proliferative phase.* J Surg Res, 2008. **149**(1): p. 84-93.

186. Mowbray, M., et al., *Topically applied nitric oxide induces T-lymphocyte infiltration in human skin, but minimal inflammation.* J Invest Dermatol, 2008. **128**(2): p. 352-60.

187. Ferrini, M.E., et al., *S-nitrosoglutathione reductase inhibition regulates allergen-induced lung inflammation and airway hyperreactivity.* PLoS One, 2013. **8**(7): p. e70351.

188. Jia, L., et al., *Acute and subacute toxicity and efficacy of S-nitrosylated captopril, an ACE inhibitor possessing nitric oxide activities.* Food Chem Toxicol, 2001. **39**(12): p. 1135-43.

189. Gabikian, P., et al., *Prevention of experimental cerebral vasospasm by intracranial delivery of a nitric oxide donor from a controlled-release polymer: toxicity and efficacy studies in rabbits and rats.* Stroke, 2002. **33**(11): p. 2681-6.

190. Bellingan, G.J., et al., *In vivo fate of the inflammatory macrophage during the resolution of inflammation: inflammatory macrophages do not die locally, but emigrate to the draining lymph nodes.* The Journal of Immunology, 1996. **157**(6): p. 2577-2585.

191. Katakai, T., et al., *Lymph Node Fibroblastic Reticular Cells Construct the Stromal Reticulum via Contact with Lymphocytes.* The Journal of Experimental Medicine, 2004. **200**(6): p. 783-795.

192. Gray, E.E. and J.G. Cyster, *Lymph node macrophages.* Journal of innate immunity, 2012. **4**(5-6): p. 424-436.

193. Matsumoto, A. and A.J. Gow, *Membrane transfer of S-nitrosothiols.* Nitric Oxide, 2011. **25**(2): p. 102-7.

194. Rohner, N.A., et al., *Lymph node biophysical remodeling is associated with melanoma lymphatic drainage.* FASEB J, 2015. **29**(11): p. 4512-22.

195. Hubbell, J.A., S.N. Thomas, and M.A. Swartz, *Materials engineering for immunomodulation.* Nature, 2009. **462**(7272): p. 449-460.

196. Babar, I.A., et al., *Nanoparticle-based therapy in an in vivo microRNA-155 (miR-155)-dependent mouse model of lymphoma.* Proceedings of the National Academy of Sciences, 2012. **109**(26): p. E1695-E1704.

197. Cabral, H., et al., *Systemic Targeting of Lymph Node Metastasis through the Blood Vascular System by Using Size-Controlled Nanocarriers.* ACS Nano, 2015. **9**(5): p. 4957-67.

198. Lorenzo-Redondo, R., et al., *Persistent HIV-1 replication maintains the tissue reservoir during therapy.* Nature, 2016. **530**: p. 51.

199. Lee, J.-W., et al., *Peripheral antigen display by lymph node stroma promotes T cell tolerance to intestinal self.* Nature Immunology, 2006. **8**: p. 181.

200. Reddy, S.T., et al., *Exploiting lymphatic transport and complement activation in nanoparticle vaccines.* Nature Biotechnology, 2007. **25**: p. 1159.

201. Chen, J., et al., *Lymphatic-targeted therapy following neoadjuvant chemotherapy: a promising strategy for lymph node-positive breast cancer treatment.* Med Oncol, 2015. **32**(7): p. 184.

202. Bourquin, C., et al., *Targeting CpG Oligonucleotides to the Lymph Node by Nanoparticles Elicits Efficient Antitumoral Immunity.* The Journal of Immunology, 2008. **181**(5): p. 2990-2998.

203. Meng, F., et al., *pH-sensitive polymeric nanoparticles for tumor-targeting doxorubicin delivery: concept and recent advances.* Nanomedicine (Lond), 2014. **9**(3): p. 487-99.

204. Pridgen, E.M., R. Langer, and O.C. Farokhzad, *Biodegradable, polymeric nanoparticle delivery systems for cancer therapy.* Nanomedicine (Lond), 2007. **2**(5): p. 669-80.

205. Colson, Y.L. and M.W. Grinstaff, *Biologically responsive polymeric nanoparticles for drug delivery.* Adv Mater, 2012. **24**(28): p. 3878-86.

206. Higginson, C.J., et al., *Albumin-Oxanorbornadiene Conjugates Formed ex Vivo for the Extended Circulation of Hydrophilic Cargo.* ACS Chem Biol, 2016. **11**(8): p. 2320-7.

207. Higginson, C.J., et al., *Modular degradable hydrogels based on thiol-reactive oxanorbornadiene linkers.* J Am Chem Soc, 2015. **137**(15): p. 4984-7.

208. Kislukhin, A.A., et al., *Degradable conjugates from oxanorbornadiene reagents.* J Am Chem Soc, 2012. **134**(14): p. 6491-7.

209. Hong, V., et al., *Analysis and optimization of copper-catalyzed azide-alkyne cycloaddition for bioconjugation.* Angew Chem Int Ed Engl, 2009. **48**(52): p. 9879-83.

210. Yu, D., et al., *Accessible 5'-end of CpG-containing Phosphorothioate Oligodeoxynucleotides is essential for immunostimulatory activity.* Bioorganic & Medicinal Chemistry Letters, 2000. **10**(23): p. 2585-2588.

211. Hettiaratchi, M.H., Schudel, A.*, Rouse, T., Garcia, A.J., Thomas, S.N., Guldberg, R.E., McDevitt, T.C.. , *A Rapid Method for Determining Protein Diffusion through Hydrogels for Regenerative Medicine Applications. In review.* APL Bioengineering 2018.

212. Goldstein, M.J., et al., *A CpG-loaded tumor cell vaccine induces antitumor CD4(+) T cells that are effective in adoptive therapy for large and established tumors.* Blood, 2011. **117**(1): p. 118-127.

213. Qi, X.-F., et al., *CpG oligodeoxynucleotide induces apoptosis and cell cycle arrest in A20 lymphoma cells via TLR9-mediated pathways.* Molecular Immunology, 2013. **54**(3): p. 327-337.

214. McKenzie, J.A., et al., *The Effect of Topoisomerase I Inhibitors on the Efficacy of T-Cell-Based Cancer Immunotherapy.* J Natl Cancer Inst, 2017.

215. Gadek, T.R., et al., *Generation of an LFA-1 antagonist by the transfer of the ICAM-1 immunoregulatory epitope to a small molecule.* Science, 2002. **295**(5557): p. 1086-9.